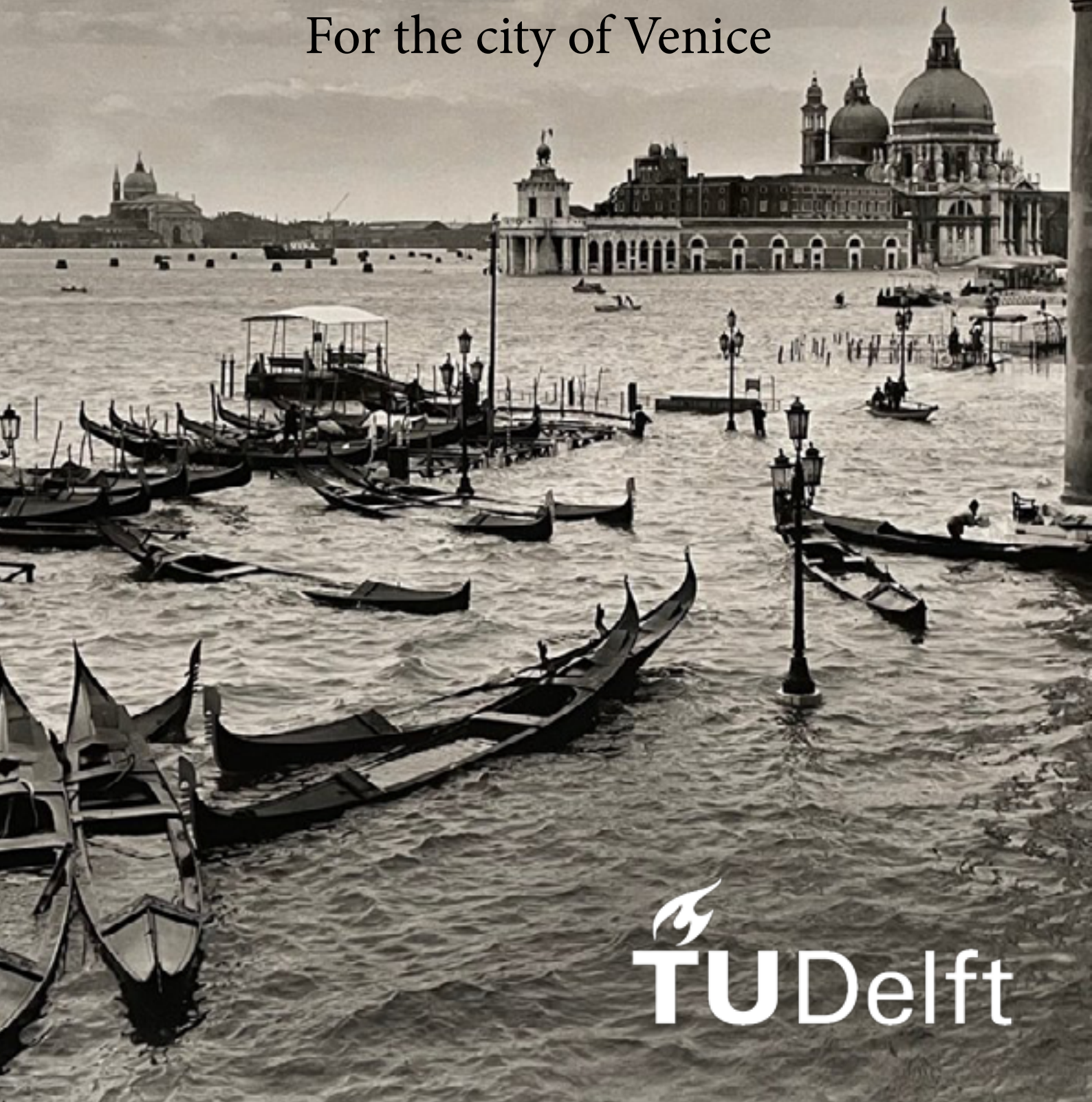# A Bivariate Copula Approach to Extreme Water Level Estimation

For the city of Venice

TUDelft

A Bivariate Copula Approach to Extreme Water Level Estimation

For the city of Venice

Max Draisma

January 11, 2023

Supervisors: Dr ir Alessandro Antonini
Dr ir Elisa Ragno
Dr ir Sofia Caires

Abstract

Understanding the factors that drive extreme water levels is key to an accurate assessment of flood hazard. The city of Venice has always been affected by flooding due to extreme water levels. In this study, we examine the factors driving and influencing extreme water levels in the Venice lagoon, aiming at deriving accurate extreme water level estimates in the Venice lagoon.

Due to the shallowness of the Venice lagoon, extreme water levels are influenced by both atmospheric forcing (surge) and water level of the lagoon (tide and bottom level) and interactions between these two. Furthermore, these extreme water levels have been changing over time due to variations in the bottom level. These variations are reportedly due to local (anthropogenic and natural) subsidence and sea level rise.

In this study we resort to the available long-term water level observations of the Punta della Salute tide-gauge. Given the effects of subsidence and sea level rise in these data, we start by homogenizing the data by removing these trends and jumps from the time-series. Using the homogenized time-series, we study the influence of the dependence between tide and surge components on the extreme water level estimates. Finally, we quantify the effect in the estimates of modelling this dependence in the extreme value models.

To homogenize the data and better understand the underlying trends, a time-series analysis was performed on the time-series of water level observations. Mann-Kendall tests for monotonic trend were performed, followed by an analysis using changepoint detection methods. Changepoint detection was performed using the RHtest and BEAST methods on the Punta della Salute time-series as well as time-series from neighbouring tide-gauge stations. Ultimately trend decomposition using the BEAST method was used to detrend and homogenize the Punta della Salute time-series.

After detrending, the tide and surge components were separated using tidal harmonic analysis and reconstruction. The relationship of these now separated components was quantified during extreme water levels using the Pearson r correlation and the Kendall τ rank correlation.

This relationship between tide and surge was described using copulas to estimate extreme water levels. Different copula variants were evaluated and extreme water level estimates derived using copulas that describe dependence were compared to extreme water level estimates using a copula that describes tide and surge as independent components. Lastly, these were compared to those derived from univariate extreme value analysis to assess the influence of separation of tide and surge components combined with copulas as opposed to a more traditional univariate extreme value analysis.

The main conclusions of this study are as follows.

- The water level observations of the Punta della Salute tide-gauge are indeed affected by jumps and trends due to subsidence and sea level rise. These can be successfully removed using the applied techniques.

- There is a clear dependence between tide and surge in the Venice lagoon, with lower tide levels leading to higher surge levels. The non-inclusion of this dependence (by

assuming independence) in the combined analysis of tide and surge signals to drive total extreme water levels leads to an overestimation of the total water level extremes.

- Extreme water level estimates from the combined analysis of the tidal and surge signal are higher, but compatible with those from the analysis of the total water level signal (without separation of tidal and surge signal). This gives confidence in the combined analysis accounting for the dependence between the signals and allowing for a further application of the models to account for projected climate changes.

Acknowledgements

Contents

<div align="right">

1

</div>

Introduction

The first chapter will describe background situation and the location of the city of Venice; this will be followed by the problem description. Afterwards, the main objective of this thesis will be presented. Finally, the structure of the report is outlined.

1.1. Background

The city of Venice is located in the northwestern Adriatic in the middle of a shallow lagoon. The city was originally built on piles and clusters of low lying islands and has been in a constant struggle with its hostile environment. The fragile equilibrium of the lagoon has been artificially preserved for ages, bringing with it disturbances of biological, ecological, geomorphological and chemical nature [Lionello et al., 2020]. The city is frequently subject to high waters events named "Acqua Alta" (high water). The frequency and severity of Acqua Alta events has drastically increased over the last century [Camuffo et al., 2006] [Cavaleri, 2000] [Gatto and Carbognin, 1981] [Pirazzoli, 1987]. 11 of the 20 highest waters occurred during the last 20 years for the almost 100 year of water level observations. The cause of this increase is due to land subsidence and the impact of the rise in sea level [Carbognin et al., 2010][Zanchettin et al., 2021].

This land subsidence used to originate only from natural consolidation of the sediment and tectonic processes causing land subsidence of a constant rate of 1.3 mm/y over the last millennia [Antonioli et al., 2009], up to the turn of the 20th century, when it fell to 0.4 mm/y [Gatto and Carbognin, 1981]. During the 20th century, groundwater extraction in Venice's mainland port, Porto Marghera, has led to an anthropogenic subsidence in the order of 10 cm over the last century [Emery and Aubrey, 1991]. Groundwater extraction started after the construction of the industrial zone in 1930 and increased after the port expansion in the 1950s. As a result, both the port and the nearby city of Venice started to sink at increased rates. When in 1966 the water reached a height of 194 cm during an extreme Acqua Alta event, extensive damage was done to many cultural sites, and many inhabitants were left homeless. After this extreme storm surge event, measures were taken to prevent future flooding of the city. In the period after the 1966 flood, more funding became available to better understand and predict future Acqua Alta events. In 1969 the Istituto Studio Dinamica Grandi Masse (ISDGM) was founded with the objective of studying causes related to frequent flooding [Cavaleri, 2000], which resulted in the construction of the oceanographic

tower; Piattaforma Acqua Alta, a measurement station off the coast of Venice. Additionally, in this period, due to strong new regulations, groundwater extraction progressively stopped. The restoration of the aquifer caused an uplift after this period equal to 15% of the total subsidence (2 cm) [Gatto and Carbognin, 1981]. After this period of uplift, there was no significant long-term subsidence; however, high rates of subsidence still occur for short periods [Tosi et al., 2013]. These can be attributed to renovation works that cause large loads on the wooden piles and the ongoing consolidation of the soil of the later constructed parts of the city.

While anthropogenic subsidence has come to an end, sea level rise is expected to continue to increase in the coming century, and the natural subsidence of the soil remains. The recently built mobile storm surge barriers (MoSE) constructed between the barrier islands can close the three inlets to the lagoon. This barrier addresses the problem of increased frequency in floods and closes with tides greater than 110 cm. First operated in 2020, the barriers bring an end to extreme events in the near future; bringing an end to one of the longest records of water level observations in the Adriatic coast (1924-2020) for the purpose of extreme value analysis.

1.2. Problem Description

Flooding of coastal regions is recognized as a major threat to people [Lopes and Dias, 2015] and is one of the most frequently occurring disasters in the world [Jonkman, 2005]. The probability of the occurrence of potentially damaging flood events is called flood hazard [Schanze et al., 2006]. Flood hazard assessment is crucial for coastal protection strategies.

Accurate predictions of the combination of factors driving extreme water levels is a key component of assessing and understanding flood hazard [Lyddon et al., 2018], and good quality extreme water level estimates are essential for flood hazard assessment [Batstone et al., 2009] [Arns et al., 2020]. However, extreme water level estimates are always associated with large amounts of uncertainty and this uncertainty further increases in complex coastal regions containing shallow bathymetry. This can partly be contributed to the non-linear interactions between the tides and storm surges. The tide-surge interaction (TSI) is strongest in regions of shallow bathymetry [Mawdsley and Haigh, 2016]. Since Venice is located in the largest Italian estuary with a mean depth of around 0.8-1.1 m [Rapaglia et al., 2010] [Day et al., 1998], non-linear interactions are likely to occur. The non-linear interactions or (TSI) cause lower total water levels in comparison to the case where they are assumed independent [Olbert et al., 2013]. Additionally in light of sea level rise projections [Masson-Delmotte et al., 2021], bottom depth will change affecting this relationship between tide and surge.

Therefore, there is need to investigate tide-surge interactions and incorporate the impact of tide-surge interaction in extreme water level estimation to improve flood hazard assessment for the Venice lagoon.

1.3. Research Objective

The main objective of this thesis will be to

> Quantify the influence of tide-surge interaction on extreme water level estimates and investigate the use of copulas in extreme water level estimation

To this end, the sub-questions formulated below are addressed.

1. How can the (non-)stationarity of a time-series be evaluated?

2. How can the tide and non-tidal components of the water level be separated from one each other?

3. How can the relationship between tide and surge be quantified?

4. How is extreme value analysis performed when tide and storm surge are dependent on one another?

5. What should be the selection criteria of a copula function?

6. How can the the influence of the relationship between tide and non-tidal residual on extreme water level estimations be quantified?

The remainder of this thesis report is divided into 6 chapters. First, the literature review is discussed in which the steps towards answering the research objective are explained. This is followed by a chapter on the exploratory time-series analysis & homogenization. Thereafter the quantification of the dependence and the extreme value analysis using copula functions is performed. After this chapter, the results will be presented followed by the discussion. Lastly we arrive at the conclusion.

2

Literature review

This chapter starts with a case study highlighting the city of Venice and its history of hydraulic interventions and relative sea level rise followed by the data acquisition. Thereafter, the required background information is discussed to understand the underlying processes and methods used in this thesis.

2.1. Case study: Venice lagoon

Venice is located in the northeastern part of the Adriatic Sea. The large lagoon surrounding the low-lying city is connected to the Adriatic by three inlets, the Chioggia, Malamocco and finally the Lido inlet, closest to the city [Robinson et al., 1973]. The city is an iconic place of great cultural and historical importance and has been selected as a UNESCO World Heritage Site since 1987 [WCED, 1987]. The city and its lagoon have a long history of hydraulic interventions. Historically, the surrounding water was always of great military and strategic importance [Pirazzoli, 1987] [Bevilacqua, 2009], so the aim of many of these interventions was to prevent the lagoon from silting up [Gatto and Carbognin, 1981]. Up to the 20th century, any construction that caused deposition was prohibited or strictly regulated [Pirazzoli, 1987]. One of the largest interventions that began in the 15th century [Brambati et al., 2003] [Gatto and Carbognin, 1981] [Lionello et al., 2020] was the redirection of all the major rivers that used to flow into the lagoon. This was done to prevent sedimentation of the lagoon. This stop in sedimentation due to rivers caused natural subsidence to no longer be compensated for by alluvial sediments [Brambati et al., 2003].

More recently, since the 19th century, many more interventions have been carried out, the consequences of which are still being felt today. While the cross-sectional area of the inlets to the lagoon has increased as a result of dredging, the surface area of the lagoon has progressively decreased. The tidal flats have been reclaimed and are now used for the industrial zone, first constructed in 1930 and later expanded in 1953 and the 1960s. Additional land reclamation was for urban development, waste disposal, agriculture, and for the construction of the airport. In this way, the surface area of the lagoon has decreased by 30% since 1830. Furthermore, until the end of the 19th century, the Lido inlet had a depth of 3m and the Malamocco inlet one of 4-5m. During the 20th century, especially once the industrial port, Porto Marghera was established, the depths of the Lido, Malamocco, and Chioggia inlets increased to up to 14 m deep [Pirazzoli, 1987] and breakwaters were built

at the inlets. As a result, there has been a large change in the ratio between the lagoon surface area and the cross-sectional area of the inlets. Consequently, the tidal range and erosion rates have increased due to the deepening of the inlets. The effects of morphological interventions combined with the sea level rise has caused tidal flats and salt marshes to disappear at an increasing rate and have caused extensive damage to flora and fauna [Pirazzoli, 1987]. The man-made changes along with the effects of sea level rise contribute to large amounts of relative sea level rise.

Relative mean sea level change

It is important to make a distinction between relative sea level and absolute sea level. Many records of water level observations before the days of satellite altimetry contain relative sea level observations as opposed to absolute sea level observations. This is because measurement stations themselves are subject to changes in vertical position relative to the sea surface. These changes are caused by many different processes, such as plate tectonic movement, subsidence from aquifer withdrawal, post-glacial rebound, or earthquakes. These processes contribute towards a total vertical land motion which forms the difference between mean sea level and relative mean sea level.

Vertical land motions causing subsidence or uplift of the bottom level of the lagoon impact the measurements obtained from tide-gauges. Figure 2.1 shows how a tide-gauge is fixed to the sea floor. When the sea floor rises or falls, the difference in measurements is recorded by the tide-gauge. Since the second half of the 20$^{\text{th}}$ century, more and more satellite measurements have become available that can help circumvent this problem.
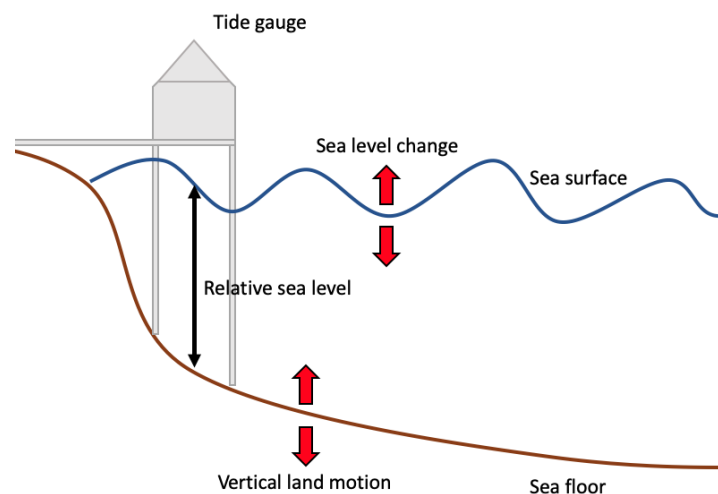
Figure 2.1: Schematic overview of tide-gauge water level measurements.

Vertical land motion (VLM) is a critical contributor to the change in relative mean sea level (RMSL) in the Venice lagoon [Zanchettin et al., 2021]. This vertical land motion can be separated into anthropogenic and natural causes. One of the components of natural VLM is the Glacial Isostatic Adjustment (GIA). GIA is the result of large ice masses that covered large parts of Europe during the last ice age thousands of years ago. These ice masses pressed down to the Earth's surface with extreme loads. The Earth's surface is still rebounding towards isostatic equilibrium, causing either local uplift or subsidence. The influence of

GIA on the change in RMSL in Venice is between -0.2 mm / year (uplift) and +0.5 mm / year (subsidence) [Antonioli et al., 2009]. Other natural causes of ground deformations are plate tectonics, volcanism, and sediment compaction [Wöppelmann and Marcos, 2016]. Sediment compaction played a role after the formation of the lagoon, leading to a total natural land subsidence rate of 1.3 mm/year [Carbognin et al., 2004]. At the turn of the 20th century, this subsidence was still ongoing at 0.9-1.3 mm/y [Zerbini et al., 2017], however during the period 1900-1930, this changed to 0.4 m / y, probably due to a stop in the long-term influence of river diversion that occurred centuries ago [Gatto and Carbognin, 1981].

An even greater contributor to the more frequent acqua alta events is the loss of elevation resulting from man-induced subsidence [Gatto and Carbognin, 1981]. From 1930 and especially during the second half of the 20th, anthropogenic processes began to have a significant effect, resulting in additional land subsidence. This anthropogenic subsidence is due to the very intensive extraction of groundwater in the period of the highest industrial growth after the second world war, causing a drop in the piezometric head of up to 20 m [Gatto and Carbognin, 1981][Zanchettin et al., 2021][Lionello et al., 2020]. Consequently, large amounts of land subsidence were reported over the period 1930-1950, and even larger ones during 1950-1970 attributed to an expansion of the nearby port bringing an increasing groundwater extraction. Since the 1970s, measures have been taken to prevent further groundwater extraction, after which there has been a significant decrease in anthropogenic subsidence [Zerbini et al., 2017]. Levelling measurements in 1973 and 1993 recorded a slowdown in subsidence and a small uplift after restoration of the groundwater level. One of the available time-series of observations comes from a measurement point at Punta Salute in the city of Venice. Since the rising of the Mean Sea Level (MSL) and the subsiding of the tide-gauge influence the relative mean sea level (RMSL), nothing can be said about their independent magnitude. In recent decades, the subsidence in the city has been quasi-stable at 0.25 mm / y on the tide-gauge [Carbognin et al., 2004] [Carbognin et al., 2010]. Today, large-scale subsidence caused by anthropogenic influence has stopped, as confirmed by regional studies in 1993 and 2000 [Carbognin et al., 2005] [Brambati et al., 2003]. Most of the still remaining anthropogenic subsidence caused by renovations is very local and lasts only for short periods of time [Tosi et al., 2013]. No further large-scale anthropogenic subsidence is expected in the future in the city. However, in the MoSE inlets, up to 70mm/y of local settlements occurred [Tosi et al., 2018].

Many authors have found different but comparable numbers for man-induced subsidence during the period of heavy groundwater extraction. In the table below, an overview is given.

The authors seem to agree with an uplift of 2 cm after the closure of the aquifers and a total subsidence over the 20th century in the range of 23-26 cm, of which 9-11 cm is due to anthropogenic influence [Pirazzoli, 1987] [Tosi, 1995] [Brambati et al., 2003] [Tosi et al., 2013] [Cavallaro et al., 2017] [Pirazzoli and Tomasin, 2002].

In addition to the influence of vertical land motions, another factor that influences the relative sea level is the rise of the sea level.

Sea level rise

As mentioned in the previous chapter, it is expected that the anthropogenic subsidence that has occurred in the last century will not continue into the future. Therefore, its contribution to the relative change in sea level should not be considered. This leaves two ongoing

Author(s)	Anthropogenic subsidence	Time Period
[Gatto and Carbognin, 1981]	1 mm/y	1930-1950
	5 mm/y	1950-1970
	-0.5 mm/y	1971-1975
[Carbognin et al., 2004]	2.3 mm/y	1931-1970
	5 mm/y	1952-1968
	14 mm/y	1968-1969
	± 0 mm/y	1993-2000
[Carbognin and Tosi, 1995]	5 mm/y	1950-1970
	-0.5 mm/y	1971-1975
[Tosi et al., 2018]	5 mm/y	2008
[Carbognin et al., 2005]	3.5 mm/y	1930-1973
[Carbognin et al., 2010]	-0.5 mm/y	1971-1975

Table 2.1: Anthropogenic subsidence from literature

processes to take into consideration; SLR and natural VLM. The influences of these two contributors to RSLR will need to be included in the ESL estimates. Natural VLM is simple to include, as it is a very stable contributor to RSLR, determined at a rate of $-0.4 mm/y$. One of the difficulties in accounting for future sea level rise is that there is still great uncertainty in future SLR projections. ICCP has made SLR projections for different climate scenarios [Masson-Delmotte et al., 2021]. The plot below (Figure 2.2) shows the regional SLR projection for different Shared Socioeconomic Pathways (SSP). These SSPs are different potential future scenarios, each with its own projected greenhouse gas emissions and its own sea level rise. Of these potential story-lines, the SSP1-1.9 scenario can be considered to have very low amounts of greenhouse gas emissions, while the opposite was true for the SSP5-8.5 scenarios. Figure 2.2 is specifically for the local SLR in and around Venice. Large confidence intervals indicate the large uncertainties in these projections. One of the reasons is the uncertainty in the total Antarctic contribution towards future SLR.

The projected sea level rise from the figure is much higher than the past global sea level rise rate. The global sea level rise rates of 1901-2010 report a total global sea level rise of 0.19 m on average [Masson-Delmotte et al., 2021] over this period. Local sea level rise for Venice specifically report lower rates of around 1.23 ± 0.13 mm / y during the period 1872-2019 [Zanchettin et al., 2021].

Data acquisition

From the beginning of the 20th century, mechanical tide recorders were developed and became more and more popular as time progressed [Emery and Aubrey, 1991]. These were practical as they did not require a human observer. One such tide-gauge is shown in Figure 2.3, where, using a float and a pulley system, the location of a pen is controlled by the water level, which then marks the paper attached to a rotating recording drum. The stilling well, the construction around the float, stills (filters out) the wave activity [IOC, 2006]. This stilling ensures that long-period processes, such as tides, can be recorded very accurately. This mechanical tide recorder was developed for the Punta della Salute tide-gauge and can be seen in Figure 2.4. The first tide-gauge in Venice was built in 1871 and was lo-
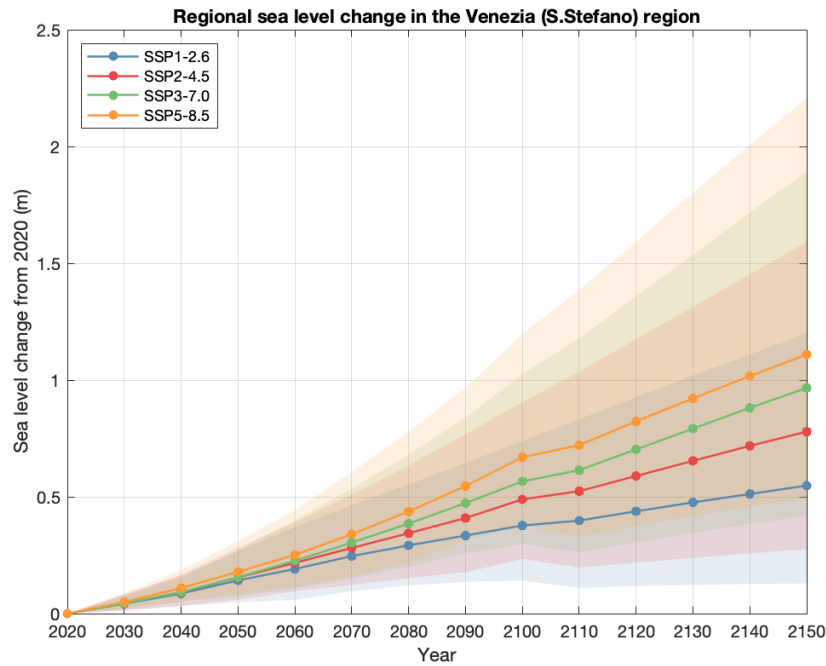
Figure 2.2: Sea level rise estimation for Venice up to 2150.

cated at Campo Santo Stefano, recording only high and low tides. An additional tide-gauge was installed in 1888 at the Venetian Arsenal (Arsenale). Later on in the year 1906 the current Punta della Salute tide-gauge was installed at Saint Mark's Basin and it was not until 1923 that it was relocated to its where it is now in The Giudecca Canal next to Punta della Dogana. Previously, as a reference, Venetians always used the brown-green line made up of algae as the average high tide level named "Comune Marino" (CM) [Carbognin et al., 2010]. Later, the tide-gauge "Zero Mareografico Punta Salute" (ZMPS) became the reference plane, based on the mean tide level between 1885 and 1909 [Zanchettin et al., 2021].

Monthly mean sea-level data are available from San Stefano (Venezia) from 1872 until 1920, but the tide-gauge was moved to a new location in 1911. Furthermore, relative sea level (RSL) observations are available from the Punta Della Salute tide-gauge located in the city centre of Venice, which contains measurements from 1909-2020. Unfortunately, both of these time-series contain large gaps of missing data up to 1924. Therefore, from these 150 years of data, 97 years of RSL measurements were used from 1924 until the end of 2020. Since the newly built storm surge barrier "Modulo Sperimentale Elettromeccanico" (MoSE) began operation in October 2020, data beyond this point are not useful when extreme sea level (ESL) observations are of interest. Starting from 1924, 4 daily tide observations are available from the Punta Della Salute tide-gauge corresponding to high and low tides. From the start of 1983, hourly measurements were available until 2020. These values were interpolated as such to have 15-minute intervals. These data contain mean tide levels (MTL) rather than mean sea level. The difference between the two is caused by shallow-water tidal effects and is reported to be negligible in Venice [Zanchettin et al., 2021]. The difference obtained between the two is reported in MTL-MSL= -0.1 ± 0.1 cm.

Furthermore, 5-minute RSL observations are available from Piattaforma Acqua Alta (1983-2020), a measurement station in the Adriatic Sea located some 15 km from the coast
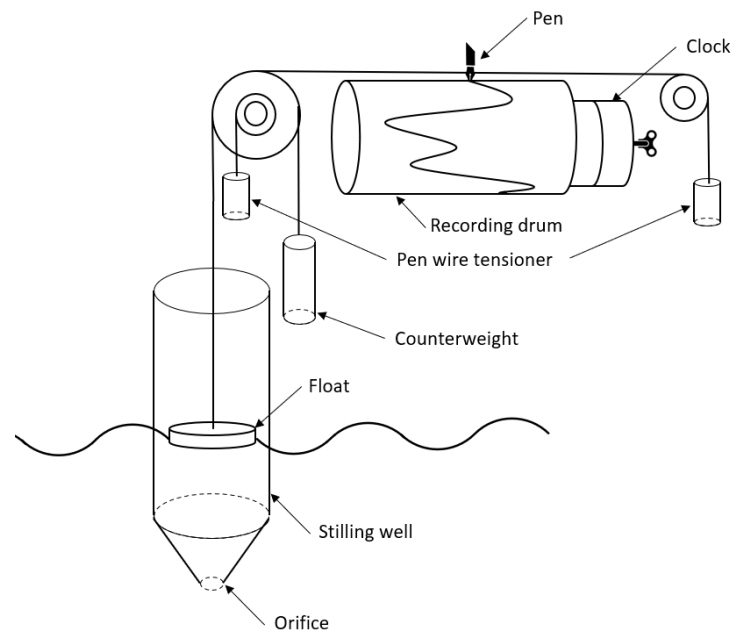
Figure 2.3: Tide-gauge schematic

Figure 2.4: (a) floater gauges resting on top of the water surface inside of the stilling well, (b) recording drum with pen and counterweights.

Figure 2.5: Map of the Northern Adriatic and used tide-gauges

of the Venice lagoon [Cavaleri, 2000] (see also Figure 2.5). This measurement tower was constructed in 1970, resulting from an increased effort to monitor the state of the sea after the disastrous flood of 1966. Long records of monthly tide-gauge data from Marina di Ravenna from 1896 – 1972 (Porto Corsini), Trieste 1875-2021, and Marghera 1989-2020, were available from the Permanent Service of Mean Sea Level (PSMSL) (`https://www.psmsl.org/data`). Higher temporal resolution observations were also obtained from Istituto Superiore per la Protezione e la Ricerca Ambientale (ISPRA) `https://www.venezia.isprambiente.it/index.php` for the Trieste (1988-2009), Marghera(1989-2020) and Marina di Ravenna (1986-2020) time-series. These are observations at half-hour to 5-minute intervals dependent on the year of monitoring. All of these tide-gauges are located in the northern Adriatic within a relatively short distance from each other. Figure 2.5 shows where the tide-gauge stations are located within the northern Adriatic. Long tide-gauges are beneficial for the observations of extreme events.

Extreme events in Venice

Acqua alta events in Venice are due to a combination of processes, most importantly, the combination of tide and storm surge. A storm surge is an abnormal rise in water level due to atmospheric processes (wind, pressure, etc.). Storm surges in Venice are caused by a combination of these atmospheric processes, mainly due to cyclones during the winter period that bring south-eastern winds (Sirocco) or north-eastern winds (Bora) accompanied by low-pressure systems[Umgiesser et al., 2021]. Additionally, Sirocco winds can lead to sieches in the Adriatic due to wind setup with periods of up to 21-23 hours. Tides in the

Adriatic are among the largest in the Mediterranean. During spring tide, the tidal range will reach values of more than 1 m [Umgiesser et al., 2021]. The Venice lagoon is an estuary with shallow bathymetry. This shallow bathymetry is likely to lead to interactions between the tide and storm surge components. The interaction between tide and non-tidal residual is called the Tide-Surge interaction (TSI) and is mainly caused by wind stress, which is more effective in producing storm surges in shallow water. Since surface stress is inversely proportional to depth, this causes an increase in water level, which in turn causes an increase in propagation speed [Santamaria-Aguilar and Vafeidis, 2018].

$$F_s = \frac{\tau_s}{D\rho} \tag{2.1}$$

$$c = \sqrt{gD} \tag{2.2}$$

where τ_s is the wind stress, ρ is the density of the water, and D is the depth of the water. Tide-surge interactions for extreme water levels in shallow regions often lead to peaks of storm surges occurring during low tides. The influence of this interactions will be quantified in this work. To better understand the time-series and to ultimately homogenize the data, first an exploratory data-analysis is performed.

2.2. Exploratory Data Analysis

An exploratory data analysis is an approach in which data sets are analysed in order to summarise their main characteristics, often with the help of statistical graphics and plots. A statistical model can be used, but the main goal of exploratory data analysis is to see what the data can tell us beyond the formal modelling or hypothesis testing task. It is essentially an analysis to better understand the data sets that are being worked on.

One of the main characteristics that the time-series will be analysed for is the presence of trend. The influence of vertical land motions as laid out in the previous section indicates that the observations of the relative mean sea level observations from the Punta della Salute tide-gauge are likely to contain a trend. A trending mean is a violation of stationarity and this stationarity is needed to calculate the statistics that are needed to define extremes [Wang, 2008a]. This is why it is necessary to evaluate the time-series for stationarity. Below the concept of stationarity will be explained and a method will be described to test for a monotonic (always increasing or decreasing) trend.

If the water level at some location is constant in some statistical sense, then the statistical characteristics of the water level are independent of time and this process is said to be stationary [Holthuijsen, 2007]. Stationarity greatly simplifies a process as only the statistical characteristics of a single time step are required to describe the process. Consider a sequence of random variables $X_1, X_2, \ldots$. Then the definition of stationarity is as follows:

Definition 2.2.1 [Coles, 2001, page 25] A random process $X_1, X_2, \ldots$ is said to be stationary if, given any set of integers $\{i_1, \ldots, i_k\}$ and any integer m, the joint distributions of $(X_{i_1}, \ldots, X_{i_k})$ and $(X_{i_{1+m}}, \ldots, X_{i_{k+m}})$ are identical.

The stationarity of a time-series implies that its stochastic properties are homogeneous in time. The opposite then is the non-stationary processes, which are processes that instead have characteristics that systematically change over time [Coles, 2001]. An example of such a non-stationary process is temperature variations throughout the year or over

longer periods of time due to effects of climate change. The two concepts of stationarity and homogeneity are similar. Stationarity refers to a process that is homogeneous in time or time-homogeneous. While homogeneity can refer to some variable being constant with regard to a different variable like space.

Statistical tests can be used to identify (Non-)stationarity in a time-series. In this work, the trend will be evaluated using the non-parametric Mann-Kendall test [Mann, 1945] [Kendall, 1975]. Non-parametric tests have the advantage that they are less sensitive to outliers and can test for trend without specifying whether the trend is linear or not [Wang et al., 2005].

Trend analysis

The Mann-Kendall test (MK) is a statistical test used to determine whether a time-series always increases or always decreases over time. This is called a monotonic trend. Non-parametric tests are tests that do not make assumption about the distribution of the underlying data, for example if the data are independent. The MK test tests the null hypothesis H_0 that a series of observations $x_1, \ldots, x_N$ for observations N come from an independent identically distributed (IID) population. The Mann-Kendall test statistic is given as

$$S = \sum_{i=1}^{N-1} \sum_{j=i+1}^{N} \text{sgn}(x_j - x_i) \tag{2.3}$$

with sgn being the sign function,

$$\text{sgn}(x) = \begin{cases} +1, x > 0 \\ 0, x = 0 \\ -1, x < 0 \end{cases} \tag{2.4}$$

To test the strength of the monotonic relationship between x and y [Kendall, 1938] introduced τ as

$$\tau = \frac{2S}{N(N-1)} \tag{2.5}$$

With the test for significance introduced by [Mann, 1945]. The probability that the test statistic will produce values at least as extreme as the value it produced for your sample is expressed as the p-value. The p-value can be seen as evidence against a null hypothesis. Since positive autocorrelation increases S and consequently the probability of rejecting the null hypothesis [Wang et al., 2005]. When working with a time-series of water level observations, seasonality/autocorrelation is likely present, and so it will need to be accounted for.

Deseasonalization can be performed as [van Belle and Hughes, 1984]: With $\overline{H_{i,j}}$ denoting the monthly mean and $i = 1, \ldots, 12$ denoting the month, and $j = 1, \ldots, k$ the year $1, \ldots, k$,

$$Y_{i,j} = \frac{\overline{H_i} - \overline{H_{i,j}}}{\sigma_{\overline{H_i}}} \tag{2.6}$$

$Y_{i,j}$ are the deseasonalized monthly mean observations. The non-parametric Mann-Kendall (MK) tests can then be run on these deseasonalized monthly observations for significance level $\alpha = 5\%$. This significance level is introduced to avoid rejecting the null hy-

pothesis when it is true. For p values higher than the significance level of 5%, the null hypothesis will be retained, and for other values it will be rejected.

These tests will give an indication if the trends found in the series are statistically significant. In addition to the Mann-Kendall test, the Sen slope estimator can be used to assess the magnitude and sign of the trend [Sen, 1968]. The advantage of Sen's slope is that this method is less sensitive to outliers and missing data than simple linear regression. The magnitude and sign of the trend are of interest, as it allows for comparison of trends during different periods of time. Both the sign of the Sen slope as well as the significance of the MK test can then be applied to different time periods to understand the time-series' behaviour over time. Each individual slope is calculated as

$$Q_i = \frac{x_j - x_i}{j - i}, \quad i = 1, 2, \ldots, N, \tag{2.7}$$

where x_i and x_j are observations at time i and j ($j > i$) [Aditya et al., 2021]. For n observations, there will be $N = n(n-1)/2$ estimates of the slope. With N sorted in ascending order for Q_i, a median value is calculated [Sen, 1968].

When performing regression analysis, autoregressive errors or are a form of serial correlation in the error term. First order autoregressive errors or AR(1) errors can be explained in the following way.

Following [Liu et al., 2020], assuming one has a dependent variable y which has a relationship with k explanatory variables $x_1, \ldots, x_k$ with an AR(1) error process we have:

$$y_t = \beta_0 + \beta_1 x_{t1} + \ldots + \beta_k x_{tk} + u_t \tag{2.8}$$
$$u_t = \rho u_{t-1} + \epsilon_t \tag{2.9}$$

where ϵ_t are uncorrelated random variables ϵ_t has the probability distribution of $N(0, \sigma^2)$ and $|\rho| < 1$ is required for errors to be stationary. This is an example of an autoregressive model. This model represents a time-varying random process which is dependent on its own previous values. In an AR(1) model, the AR model is only dependent on its previous value (not the ones before the previous). Most climatic models exhibit autocorrelation or autoregressive behaviour, as an example one can think of seasonality. A first order autoregressive error, or AR(1) error is then an error at time step ϵ_t which is dependent on the error of the previous time-step ϵ_{t-1}. This can be expressed as

$$\epsilon_t = \rho \epsilon_{t-1} + \omega_t. \tag{2.10}$$

Where now $\omega_t \sim N(0, \sigma^2)$.

The Mann-Kendall monotonic trend test is sensitive to autocorrelation. Autocorrelation can cause an increase of type I errors. Type I errors occur when the null hypothesis is rejected while it is true. This is why variants of the Mann-Kendall tests are also introduced in this work which account for this problem of autocorrelation. One of these methods is the pre-whitening approach. Pre-whitening is a method of identifying a filter for the data which can transform the data into serially independent values (without autocorrelation). Autocorrelation is not a problem in extreme value analysis because in this case extreme events are separated by enough time for them to be serially independent. This is done by a process of declustering. This process will be explained in section 2.3.

Changepoint detection and signal decomposition

Quality control and homogenization of time-series must be performed prior to assessing future change and variability, or when using observations to forecast future scenarios. This quality control as well as the homogenization of the time-series can be done using change-point detection methods. changepoint detection identifies abrupt variation in the process behaviour due to changes in the time-series [Zhang et al., 2022].

To identify changes in a time-series, the RHtestV4 method [Wang, 2008a] and the BEAST method [Zhao et al., 2019] can be used. Examples of changes for a tide-gauge could be changes in measurement techniques, location of tide-gauge, undocumented dredging near/below the gauge, and more. Additionally, the BEAST method allows signal decomposition into a trend, a seasonal component and noise. If a statistically significant change-point is identified at any time t, historical information from recorded events at t can be explored to find a possible cause.

The two methods are explained below; the main difference between the two is that the RHtest detects shifts in mean while the BEAST method detects both shifts in mean and in trend (slope).

RHtest

The RHtestV4 is a software package in R that can be used to detect and adjust for change points (shifts) that could exist in a time-series that may have first-order autoregressive errors [Wang, 2008b]. RHtest was designed to homogenize daily and monthly temperature data, but can also be applied to time-series of different kinds. Homogenization of the time-series is important in preparation of extreme value analysis, which is where the RHtest will be helpful. Furthermore, the changepoint analysis can increase the understanding of the underlying signal.

The RHtest method uses the Penalized Maximum F Test (PMFT) by [Wang et al., 2007] for this which is an extension of the F test. The F test uses an F statistic to compare two statistical models fitted to the time-series to identify which best represents the underlying data. The F-test is performed as follows:

1. Defining the null hypothesis and the alternative hypothesis.

2. Calculate the F value.

3. Find the critical F-value.

4. Compare the F-value with the critical F-value.

5. Consider the p value.

6. Choose whether to reject the null hypothesis.

The F-test compares the fit of two linear models. Specifically for the RHtest, a linear function will be tested against a fit using a piecewise linear function. The penalized maximal F test is an extension of the regular F test. Let ϵ_t be an independent and identically distributed (IID) Gaussian. To identify a sudden change at time $t = k$ in a time-series $\{X_t\}$ with a linear trend β is to test the null hypothesis [Wang et al., 2007].

$$H_0 : X_t = \mu + \beta t + \epsilon, \, t = 1, 2, \ldots, N \tag{2.11}$$

against the alternative hypothesis

$$H_a : \begin{cases} X_t = \mu_1 + \beta t + \epsilon_t, t \le k \\ X_t = \mu_2 + \beta_t + \epsilon_t, k - 1 \le t \le N, \end{cases} \tag{2.12}$$

where $\mu_1 \ne \mu_2$. If the alternative hypothesis H_a is true at a point $t = k$, then the point is called a changepoint and $\Delta = |\mu_1 - \mu_2|$ is the magnitude of the mean change. The maximal in the definition of the PMFT comes from the most probable points of the changepoints associated with F_{max}

$$F_{max} = \max_{1 \le k \le N-1} F_c(k) \tag{2.13}$$

and

$$F_c(k) = \frac{(SSE_0 - SSE_a)}{SSE_a / (N-3)}, \tag{2.14}$$

$$SSE_A = \sum_{t=1}^{k} (X_t - \hat{\mu}_1 - \hat{\beta} t)^2 + \sum_{t=k+1}^{N} (X_t - \hat{\mu}_2 - \hat{\beta} t)^2, \tag{2.15}$$

$$SSE_0 = \sum_{t=1}^{N} (X_t - \hat{\mu}_0 - \hat{\beta}_0 t)^2 \tag{2.16}$$

Here SSE is the abbreviation for the sum of squared estimate of errors. $\hat{\mu}_0$ and $\hat{\beta}_0$ are estimated with constraint $\mu_1 = \mu_2 = \mu$. A changepoint is declared whenever the F_{max} statistic is greater than F_{crit} corresponding to the nominal level of significance α, i.e. the rate at which the null-hypothesis is rejected when true (type I error). α is arbitrary but usually the value of $\alpha = 0.05$ is used (95% confidence interval). If the alternative hypothesis is accepted, the series is divided into two samples at $t = k$ with identical trend but difference in mean $\mu_1 \ne \mu_2$. Since the false alarm rate (FAR), or type I error as above (when a changepoint is mistakenly declared) depends on location k, an empirical penalty factor is applied $P(k)$. Therefore, the penalized maximal F test. This method can be applied to any time-series with a trend and approximately IID Gaussian errors. As advised in [Wang et al., 2007], the time-series should be roughly deseasonalized by subtracting the 12 monthly sample means; this can also be performed by the RHtest itself.

Bayesian change-point detection & time-series decomposition

The Bayesian Estimator of Abrupt change, Seasonal change, and Trend (BEAST) is a Matlab tool which can decompose a 1D time-series into trend components, seasonal components, abrupt changes, and noise [Zhao et al., 2019]. This model can be used grow a better understanding of the data as well as assist with homogenization.

The decomposition of the signal is based on the concept of the Bayesian paradigm. Instead of using the single-best model approach, this framework allows for consideration of many possible models and uses Bayesian Model Averaging (BMA) via Markov Chain Monte Carlo sampling. Using the BMA approximation of non-linear signals and separation of components (trend and periodic) is possible. The changepoints found using BEAST are also indicated by the probability of occurrence calculated by counting the frequency of the sample containing the knot (changepoint) divided by the total number of samples N from the MCMC.

It is based on the assumption that a time-series $G = \{t, y\}$ is composed of these three components:

$$y_i = S(t_i; \Theta S) + T(t_i, \Theta_T) + \epsilon_i \tag{2.17}$$

Here, S and T are the seasonal and trend signals that are parameterised by general linear models and ϵ is the random error that is assumed to be normally distributed with magnitude σ.

Both the seasonal and the trend terms are approximated as piecewise linear functions. The seasonal signal is approximated using a piecewise harmonic function with break points p at timings ξ_k, $k = 1, \ldots, p$. These breakpoints split the time-series into intervals of p + 1 and each of these intervals is then approximated by the piecewise harmonic function in the following form.

$$S(t) = \sum_{l=1}^{L_k} \left[a_{k,l} \cdot \sin\left(\frac{2\pi l t}{P}\right) + b_{k,l} \cdot \cos\left(\frac{2\pi l t}{P}\right) \right] \tag{2.18}$$

L_k is the harmonic order of the corresponding segment k, varies from segment to segment and is assumed to be unknown. P is the period of the seasonal signal, the period used is 12 months for 12 subsequent monthly means. $a_{k,l}$ and $b_{k,l}$ are also segment-specific parameters and are also assumed to be unknown, such as the number of breakpoints p and their timings ξ_k. In the same way, the piecewise linear function approximating the trend is defined as:

$$T(t) = c_j + d_j t \text{ for } \tau_j \leq t < \tau_{j+1}, j = 0, \ldots, m \tag{2.19}$$

Here c_j and d_j are segment-specific parameters, m is the number of change-points with timings τ_j, $j = 1, \ldots, m$. Again, the number of changepoints and their timings are unknown. Note that the notation for the number of change-points and their timings are different for the Seasonal and the Trend function, this is because they may not be the same. The parameters from the Trend and Seasonal signals as defined above are then split into a model structure M containing all changepoints and their timings, β_x then contains all parameter values and its structure is dependent on the Model (more breakpoints means more sections, and thus more parameters are required). The general form of Equation 2.17 then becomes

$$y(t_i) = x_M(t_i)\beta_x + \epsilon_i \tag{2.20}$$

where x_M is the matrix which size depends on M containing parameters of the piecewise harmonic and piecewise linear functions. All of these unknown parameters, as well as the number of breaks and their timings, are then assumed to be random in order to build a Bayesian model for BMA. The posterior probability $p(\beta_M, \sigma^2, M|f)$ is then desired and, by Bayes' theorem, can be described as

$$\underbrace{p(\beta_M, \sigma^2, M|f)}_{\text{Posterior}} = \underbrace{p(f|\beta_M, \sigma^2, M)}_{\text{Likelihood}} \underbrace{\pi(\beta_M, \sigma^2, M)}_{\text{Prior}}$$

The likelihood in this context $p(f|\beta_M, \sigma^2, M)$ is the probability of producing the observations f for parameters β_M, σ^2 and M. The prior $\pi(\beta_M, \sigma^2, M, M)$ can be described as

$$\pi(\beta_M, \sigma^2, M) = \pi(\beta_M, \sigma^2|M)\pi(M) \tag{2.21}$$

These can then be separated into conditional priors $\pi(\beta_M, \sigma^2|M)$ and $\pi(M)$, which are both considered to be flat priors (we have no existing knowledge about the model parameters). However, these can be influenced by user input, for example, the minimum and maximum number of changepoints. Here $\pi(M)$ is the prior of the model structure and $\pi(\beta_M, \sigma^2|M)$ is the prior for the model coefficients. The posterior distribution can then be sampled using Markov chain Monte Carlo (MCMC) sampling using a hybrid reversible jump sampler which allows jumping between different models (as they will have different numbers of changepoints and thus different numbers of parameters). In this way, a chain of posterior samples can be generated that includes different model structures and parameters for every sample. Using these many individual estimates, a Bayesian model average can be made, and a signal can be decomposed into a trend and a seasonal signal, which can then be analyzed for changepoints [Zhao et al., 2019].

A very powerful tool in Bayesian inference is the Monte Carlo Markov chain (MCMC). First, the Monte Carlo method is addressed. Using the Monte Carlo method, one can randomly sample a large amount of data from a distribution and make estimations of the properties of the distribution based on those samples. This can often be easier to calculate, or this method can be used when distribution equations are very complicated properties (e.g. mean, standard deviation) of a distribution directly [van Ravenzwaaij et al., 2018]. The Markov chain is a stochastic model that describes the sequence of events/samples. In this process, the outcome of a given event will affect the outcome of the next event, this is where the 'chain' comes from [van Ravenzwaaij et al., 2018] [Levin et al., 2017]. The first-order Markov chain is defined as [Coles, 2001]

Definition 2.2.2 A random process $X_1, X_2, \ldots$ is a first-order Markov chain if, for every $i = 2, 3, \ldots$, the conditional density function satisfies

$$f(x_i|x_{i-1}, \ldots, x_1) = f(x_i|x_{i-1}) \tag{2.22}$$

An important property of the Markov chain is also that each new sample depends only on the previous sample and on the ones before it. There are different approaches for the Markov chain sequence, like Metropolis-Hastings MCMC and Reversible-jump MCMC as mentioned above, which is a variant of Gibbs sampling (a variant of the Metropolis-Hastings MCMC) that allows simulation of different dimensions.

2.3. Statistical methods

This chapter will outline the statistical methods that are used in this thesis and will explain the concepts behind statistical modeling of extreme values, dependence and the copula function.

Extreme Value Analysis

Extreme value analysis (EVA) is a branch of statistics that describes the unusual. EVA is applied in many fields, for example earthquakes, weather extremes or ocean wave modelling. In this thesis it will be used to estimate extreme sea levels. This section will explain theory essential to extreme value analysis and how EVA can be applied to time-series in order to estimate return values.

Asymptotic theory Asymptotic theory, or large sample theory are methods of assessing behaviour of samples n as the sample size grows to infinity $n \to \infty$. This theory assumes that any sample size will infinitely grow. The asymptotic theory allows for other theorems to be used like the law of large numbers (LLN) and the central limit theorem (CLT).

The law of large numbers states that as a $n \to \infty$, the average of the samples will be the expected value. This can be denoted as

$$\lim_{n \to \infty} \sum_{i=1}^{n} \frac{X_i}{n} = \overline{X} \tag{2.23}$$

Another important law in probability theory is the central limit theorem (CLT).

Theorem 2.3.1 [Coles, 2001, page 27] Let $X_1, X_2, \ldots$, be a sequence of IID random variables with mean μ and finite, positive variance a σ^2. Then,

$$\overline{X}_n = \frac{X_1 + \ldots + X_n}{n}, \tag{2.24}$$

$$\frac{\sqrt{n}(\overline{X}_n - \mu)}{\sigma} \xrightarrow{d} Z \tag{2.25}$$

as $n \to \infty$, where $Z \sim N(0, 1)$.

For a large amount of samples, Equation 2.24 can be written as

$$\overline{X} \dot{\sim} N(\mu, \frac{\sigma}{n}) \tag{2.26}$$

where $\dot{\sim}$ stands for 'is approximately distributed as" [Coles, 2001]. The CLT states that the distribution of sample means are approximately normally distributed, regardless of parent distribution. This implies that statistical methods that work for a normal distribution are also applicable to problems involving other types of distributions.

Extreme value theory provides a framework for extrapolation based on data from observations. If one has a time-series with observations $X_1, X_2, \ldots, X_n$, then

$$M_n = \max(X_1, \ldots, X_n), \tag{2.27}$$

is the maximum of n observations [Coles, 2001]. Since the behaviour of X_i is unknown, finding an exact M_n is not possible. However under asymptotic theory ($n \to \infty$) the approximate behaviour of M_n can be derived by family of models calibrated with observations of M_n [Coles, 2001]. Extreme value analysis provides a family of models to extrapolate from (few) observed extremes to many "unobserved" extremes [Coles, 2001]. Two frequently applied methods of extreme value analysis (EVA) are described in the following two subsection*s.

Annual Maxima The annual maxima (AM) method is a classic method in frequency analysis. It is derived from the block maxima approach which decomposes the data into blocks of equal duration (often 1 year) and takes the maximum value for each period. If the variables are IID, the extremes will converge to a GEV distribution as per the Fisher–Tippett–Gnedenko theorem:

Statement 2.3.1 Let $X_1, X_2, \ldots, X_n$ be a sequence of iid random variables with cumulative distribution function F. Suppose that there exist two sequences of real numbers $a_n > 0$ and $b_n \in \mathbb{R}$ such that the following limits converge to a non-degenerate distribution function:

$$\lim_{n \to \infty} P\left(\frac{\max\{X_1, \ldots, X_n\} - b_n}{a_n} \le x\right) = G(x), \tag{2.28}$$

In this case G belongs to the Gumbel, the Fréchet or the Weibull family [Mood, 1950]. If Equation 2.28 converges that G will assume the GEV as below.

$$G(X) = \exp\left(-\left(1 + \xi\left(\frac{x - \mu}{\sigma}\right)^{-\frac{1}{\xi}}\right), \text{ for } 1 + \xi(x - \mu)/\sigma > 0 \tag{2.29}$$

where ξ is the shape parameter, μ is the location parameter, and σ is the scale parameter. Depending on the shape parameter ξ, governing the tail behaviour of the distribution, the distribution will belong to a different family of extreme value distributions denoted I, II and III. These families are known as the Gumbel, Fréchet, and reversed Weibull extreme value distributions for type I, II, and III, respectively. For $\xi < 0$ and $\xi > 0$, this will mean a type III and II distribution, while for $\xi = 0$ this will lead to the Gumbel family [Coles, 2001] [Caires, 2011]. These three different types of distributions have different shapes and tail behaviour as is highlighted in Figure 2.6. While the Gumbel or type I distribution is unlimited, the type II has got an lower limit and the type III has got an upper limit.

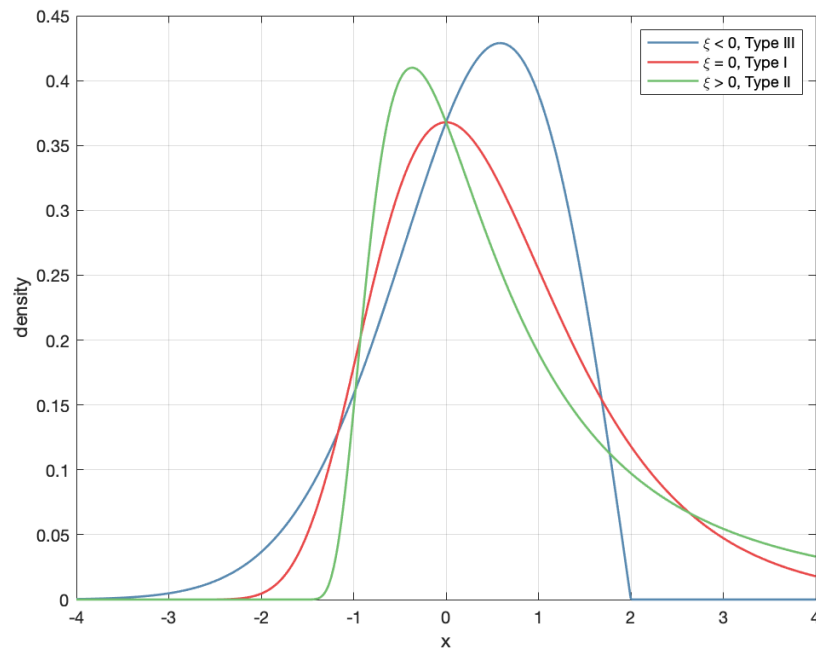Figure 2.6: GEV density plots for different shape parameters for $\mu = 0$ and $\sigma = 1$

From these distributions, the m-year return value can be determined using:

$$Z_m = \begin{cases} \mu - \frac{\sigma}{\xi}\left(1 - \left\{-\log\left(1 - \frac{1}{m}\right)\right\}^{-\xi}\right), & \text{for } \xi \ne 0 \\ \mu - \sigma \log\left\{-\log\left(1 - \frac{1}{m}\right)\right\}, & \text{for } \xi = 0. \end{cases} \tag{2.30}$$

where m is the return period

Peak Over Threshold   Instead of separating observations into years and selecting a maximum for each block, one can also define an event as extreme if it falls above some threshold value [Coles, 2001]. In this way, more data is included, which is especially useful for shorter time-series. This different approach is the peak-over-threshold (POT) method. Using this method, one chooses a threshold for the selection of extremes. All extreme events above this threshold are then included in the analysis. To ensure independent extremes, a d period has to be chosen so as not to include effects from the same event more than once. The declustering period depends on the duration of the storm at the location of interest.

Declustering is a process applied to a time-series to ensure independent observations of extremes. An important assumption in declustering is that two extreme events $X_i > u$ and $X_j > u$ are approximately independent if u is high enough and the time between i and j is high enough. Going back to the temperature example above, if the temperature is high today, this might make it more likely that it is high tomorrow, but not so much over longer time-periods like a month [Coles, 2001].

Definition 2.3.1 [Coles, 2001, page 93] A stationary series $X_1, X_2, \ldots$ is said to satisfy the $D(u_n)$ condition if, for all $i_1 < \ldots < i_p < j_i < \ldots < j_q$ with $j_1 - i_p > l$

$$|\Pr\{X_i \le u_n, \ldots, X_{i_p} \le u_n, X_{j_1} \le u_n, \ldots, X_{j_q} \le u_n\}$$
$$- \Pr\{X_{i_1} \le u_n, \ldots, X_{i_p} \le u_n\} \Pr\{X_{j_1} \ lequ_n, \ldots, X_{j_q} \le u_n\}| \le \alpha(n, l) \tag{2.31}$$

where $\alpha(n, l) \to 0$ for some sequence l_n such that $l_n / n \to 0$ as $n \to \infty$.

The $D(u_n)$ condition makes sure that when variables are far enough apart, the difference in probabilities will will be close enough to zero to not influence the limit laws for extremes (see also section 2.3 on asymptotic theory).

Theorem 2.3.2 [Coles, 2001, page 93] Let $X_1, X_2, \ldots$ be a stationary process and define $M_n = \max\{X_1, X_2, \ldots, X_n\}$. Then if $a_n > 0$ and b_n are sequences of constants such that

$$\Pr\{(M_n - b_n)/a_n \le z\} \to G(z), \tag{2.32}$$

Where G is a distribution function where $D(u_n)$ is satisfied, u_n being $a_n z + b_n$. For every $z \in \mathbb{R}$, G is a member of the GEV family of distributions [Coles, 2001]. This theorem states that the maxima of a stationary series converges provided the $D(u_n)$ condition is satisfied.

A difference between AM and POT is the way extremes are defined. In the AM method, they are defined as block maxima while using POT, extremes are defined as observations that exceed some type of threshold. This difference in approach requires a different model development.

Let $X_1, X_2, \ldots$ be an array of IID random variables from a marginal distribution function H. With a threshold value u, extreme events are observed when $X_i > u$. The stochastic behavior can then be described by the conditional probability

$$Pr(X > u + y | X > u) = \frac{1 - H(u + y)}{1 - H(u)}, y > 0 \tag{2.33}$$

Where for block maxima, the unknown parent distribution is approximated using the GEV, for values above some high threshold, this approximation is performed using the generalized Pareto distribution (GPD) [Coles, 2001]. Using Equation 2.29 for ξ, $\mu > 0$ and $\sigma > 0$, for some high value of u, the distribution function is

$$F(y) = 1 - \left(1 + \frac{\xi y}{\tilde{\sigma}}\right)^{-1/\xi} \tag{2.34}$$

where

$$\tilde{\sigma} = \sigma + \xi(u - \mu) \tag{2.35}$$

where ξ is the shape parameter and σ is the scale parameter. The selection of the threshold for POT plays a very important role, and there are multiple methods to choose this threshold [Caires, 2011]. The sample mean excess function is defined as

$$e_n(u) = \sum_{i \leq n} \frac{(x_i - u) I(u < x_i)}{\sum_{i \leq n} I(u < x_i)}. \tag{2.36}$$

e_n is plotted and termed a mean residual life plot. From the mean residual life plot, one can subjectively assess in the plot above which threshold u the plot shows approximately linear behaviour.

Another procedure is to estimate the model at different thresholds. Above a level u0 at which the asymptotic motivation for the generalized Pareto distribution is valid, estimates of the shape parameter ξ should be approximately constant, while estimates of scale σ should be linear in u [Coles, 2001]. Using this method, one reparameterizes the scale parameter as

$$\sigma^* = \sigma u - \xi u \tag{2.37}$$

where

$$\sigma_u = \sigma_{u_0} + \xi(u - u_0). \tag{2.38}$$

σ^* should remain constant with respect to u [Coles, 2001], and if some u_0 is a valid threshold, then both σ^* and ξ should remain approximately constant above this threshold value.

In the case of interdependence, the assessment using a univariate analysis may not give satisfactory recurrence intervals of extreme events [Sadegh et al., 2017], the bivariate distribution of the two including their dependence can be modeled using a copula [Sklar, 1959]. which will be explained below however first the tide and surge components must be separated and evluated for dependence.

Separation of tide and surge components

In order to separate tidal and surge components of a time-series of water level observations, both analytical methods (Fourier transform/Fast Fourier transform/Wavelet transform) and empirical methods (EMD, EEMD, IF, ALIF) are available. Analytical tidal decomposition methods have the advantage of having a strong mathematical foundation. Most analytical methods have their basis in Fourier transforms or Fast Fourier transforms. The advantage of using empirical methods over analytical methods is that it is better at

processing nonlinear and non-stationary data, and the basis is dictated by data (no prescribed system), which extracts physically meaningful modes. However, many of the empirical methods are highly susceptible to small perturbations and mode and noise mixing [Stallone et al., 2020], additionally, there is no mathematical proof of convergence and their mathematical basis is still lacking [Lin et al., 2009]. With the phases of harmonic constituents are known (these are dependent on the latitude of a time-series), tidal harmonic analysis is preferred for longer time-series where there is good separability of tidal constituents. For shorter time-series empirical methods are worth considering. Therefore, this method was chosen for the decomposition of the tidal signal. Many software packages are available to simplify the process of separating the tide and the NTR on the basis of an analytical approach. These include Delft3D-tide [Deltares, 2021], Task2000, Trappy, T_tide [Pawlowicz et al., 2002] and U_tide [Codiga, 2011]. Many of these methods use the general formula for astronomical tides.

$$H(t) = A_0 + \sum_{i=1}^{k} A_i F_i cos(\omega_i t + (V_0 + u)_i - G_i) \tag{2.39}$$

$H(t)$	water level at time t
A_0	mean water level over a certain period
k	number of relevant constituents
i	index of a constituent
A_i	local tidal amplitude of a constituent
F_i	nodal amplitude factors
$(V_0 + u)_i$	astronomical argument
G_i	improved kappa number (local phase lag)

Due to advantages over other methods and because they use Matlab as their working environment, the T_tide and U_tide were chosen. Both allow for non-uniformly spaced time-series and U_tide also includes the lunar nodal cycle and the lunar apsidal cycle.

The aim of tidal analysis or prediction is to reproduce significant time-stable parameters that at the place of observation describe the tidal regime [Pugh, 1987]. It is assumed that tidal forcing does not change with time and that with a sufficiently long time-series, the true value for each constant is obtained. Tidal harmonic analysis is an analysis that treats tidal observations as the sum of a finite number of harmonic constituents [Pugh, 1987]. Astronomical arguments determine the phases and angular speeds of these constituents. Using tidal harmonic analysis, constituents are selected via an iterative process. By analyzing the diagnostics of the output, constituents can be kept or rejected. This choice can be motivated on the basis of the signal-to-noise ratio of the constituents and on the rate of independence of an included constituent [Codiga, 2011]. The ability to resolve independent constituents is based on the observation duration of the tidal observations. The separability of the constituents is quantified using the Rayleigh criterion, which states that two constituents can be separated if the relative phase difference between the two is at least 2π [Godin G., 1970]. If this criterion is not met, it is difficult to distinguish different sources with relatively close frequencies. Since the time-series used in this thesis is of sufficient length, the Rayleigh criterion is met, meaning separability of constituents is not a problem.

Correlation and dependence modelling

This section will explain the concept of correlation in statistics and how to quantify correlation between variables using statistical tests. Furthermore it will explain how to model dependence using copulas.

Dependence or correlation is the statistical relationship between two random variables. This dependence can be seen as the extend to which two components increase or decrease in harmony [Coles, 2001]. Using correlation tests such as Pearson's correlation coefficient, Kendall's rank correlation τ, and Spearman's rank correlation, dependence can be quantified. These tests give insight on how large the dependence is between both and if they are positively, negatively or not correlated. Here the Pearson's correlation coefficient and the Kendall rank coefficient are explained.

Let $(X_1, Y_1), \ldots, (X_n, Y_n)$ be IID vectors containing observations of tide (X) and storm surge (Y), then the dependence between these variables X and Y can be expressed in Pearson's correlation coefficient [Stepanov, 2015]:

$$\rho_n = \frac{\sum_{i=1}^n (X_i - \overline{X})(Y_i - \overline{X})}{\sqrt{\sum_{i=1}^n (X_i - \overline{X})^2 \sum_{i=1}^n (Y_i - \overline{Y})^2}} \tag{2.40}$$

For Kendall's rank correlation, the concept of concordant pairs and discordant pairs will be explained first. Again, let $(X_1, Y_1), \ldots, (X_n, Y_n)$ be IID, then a pair of observations X_i, Y_i and X_j, Y_j with $i < j$ are concordant if both $X_i > Xj$ and $Y_i > Yj$ or if both $X_i < Xj$ and $Y_i < Yj$. If a pair is not concordant, they are instead discordant [Kendall, 1938]. Then the Kendall τ coefficient is defined as [Nelsen, 2021]:

$$\tau = 1 - \frac{2(\text{number of discordant pairs})}{n(n-1)} \tag{2.41}$$

Both ρ_n and τ will be a number in $[-1, +1]$, where a positive sign indicates a positive relationship between the two variables and vise versa. The further away from 0, the stronger the dependence between the two variables. An example of a positive correlation between two variables are the weight and height of people, taller people often weigh more, hence the positive correlation.

An important difference between the two methods is that the Pearson method is less robust to outliers than rank correlation methods. The Spearman ρ rank correlation is not explained here as the confidence intervals for these ρ are less reliable and less interpretable than confidence intervals for Kendall's τ [Newton et al., 2002]. Furthermore, the Pearson correlation tests for linear relationship where the Kendall correlation tests for a monotonic relationship. Therefore the Kendall τ rank correlation is preferred. The quantified dependence can be described by a copula function.

Modelling of dependence   For specific cases, modelling of dependence can be performed using copulas. Copulas are functions that allow for the separation of multiple marginal distributions and their dependency structure.

Definition 2.3.2 [Haugh, 2016, page 1] A d-dimensional copula, C : $[0,1]^d$: $\rightarrow [0,1]$ is a cumulative distribution function (CDF) with uniform marginals.

According to Sklar's theorem [Sklar, 1959], any number of uniform and univariate marginal distributions can be combined with a copula isolating the dependency structure in a multivariate joint distribution [Haugh, 2016].

Marginal fitting

When fitting a marginal distribution, one can choose to do so using a non-parametric distribution or a parametric one. Non-parametric methods can be advantageous, as they can be used without making assumptions about the underlying distribution of the data. Another advantage is that they can be used when parametric distribution functions cannot describe the data [Bowman and Azzalini, 1999]. However, it may be more difficult to interpret non-parametric models and these models are less sensitive to outliers.

Non-parametric functions   The most simple non-parametric method is the empirical cumulative distribution function (ECDF), which is a step function.

Let $X_1, \ldots, X_n$ be the results of observations n in ascending order with

$$F(x) = P\{X \le x\} \tag{2.42}$$

$F_n(x)$ is known as an empirical distribution function and can be defined as

$$
\begin{aligned}
F_n(x) &= 0, & x &< X_1; \\
F_n(x) &= \frac{k}{n+1}, & X_k &\le x < X_{k+1}, k = 1, 2, \ldots, n-1; \\
F_n(x) &= 1, & X_n &< x
\end{aligned}
$$

Doing so, $nF_n(x)$ represents the total number of values of X that are smaller than or equal to x [Kolmogorov, 1992].

Another non-parametric method is the kernel density estimation (KDE). Kernel density estimation allows for the estimation of a probability density function. Unlike the empirical cumulative density function, the kernel density estimation produces a continuous smooth estimate of the probability function [Węglarczyk, 2018]. Again, let $X_1, \ldots, X_n$ be an IID sample of observations n with an unknown parent distribution function f(x). The kernel estimate $\hat{f}(x)$ of f(x) then allocates each i-th sample observation x_i a function $K(x_i, t$ defined as [Węglarczyk, 2018]:

$$\hat{f}(t) = \frac{1}{n}\sum_{i=1}^{n} K(x_i, t), \quad 0 \le K(x, t) < \infty \quad \text{for} x, t \in \mathbb{R} \tag{2.43}$$

Where

$$\text{for } x \in \mathbb{R} \quad \int_{-\infty}^{\infty} K(x, t)\, dt = 1 \tag{2.44}$$

So that

$$\int_{\infty}^{\infty} \hat{f}(t)\, dt = \frac{1}{n}\sum_{i=1}^{n}\int_{\infty}^{\infty} K(x_i, t)\, dt = 1 \tag{2.45}$$

This kernel smoothens the points as from the empirical cumulative distribution into intervals, an example is shown in Figure 2.7. While this method uses bandwidth it is still

considered a non-parametric method as it does not assume anything about the shape of the resulting distribution, in other words, there is no a priori distribution or model structure. The bandwidth is a free parameter and determines the interval over which the points are smoothened.
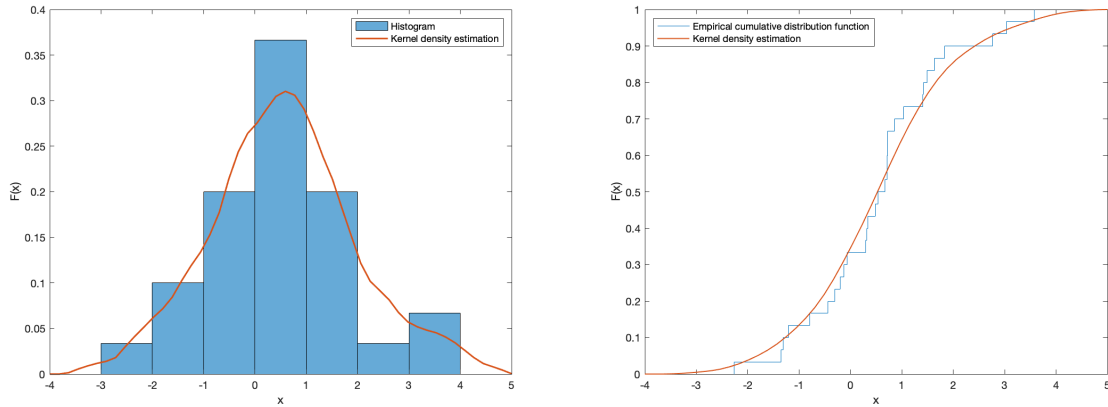
(a) Histogram and KDE of normally distributed data   (b) ECDF and KDE of normally distributed data

Figure 2.7: Example of the empirical cumulative distribution function and smoothing obtained using the kernel density estimation method.

For the kernel density estimation, there are multiple kernel smoother functions available that smooth the data in a different way; examples are the normal, box, triangle and Epanechnikov functions. The different smoothing functions can be seen in Figure 2.8.
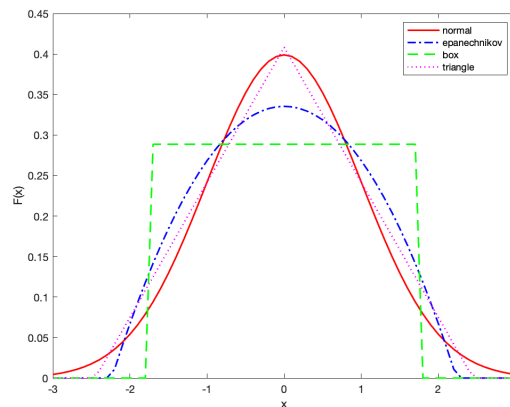

Figure 2.8: Comparison between different kernel smoothing functions.

Parametric functions In the parametric method, one assumes that the true data lie within a family of models. The model can be chosen on physical or empirical grounds. An example, shown before, shows that the AM method is bound to follow a Generalized extreme value distribution, while the Peak-over-Threshold approach follows the Generalized Pareto distribution. However, more often, one looks for a family of models that seem to be consistent with the true observations [Coles, 2001].

Estimation of model parameters is performed using maximum likelihood estimation (MLE). For an unknown parameter θ_0 of the probability density function $f(x;\theta_0)$ where $x_1,\ldots,x_n$ are independent random observations of f, the likelihood function is

$$L(\theta) = \prod_{i=1}^{n} f(x_i;\theta) \tag{2.46}$$

Then the maximum likelihood $\hat{L}$ is the value of θ that maximizes the likelihood function [Coles, 2001] [Edwards, 1972].

Transformation to uniform distribution

The copula method requires the marginal probability distributions of each variable to be uniform, marginals of the tide and non-tidal residual will have to be transformed to a uniform distribution via the probability integral transform.

To transform monotonic increasing continuous cumulative distribution functions into a uniform distribution function, one can use the probability integral transform (PIT). Let $F(x) = P\{\omega : X(\omega) \leq x\}$ define the CDF where X is IID. Then if X has F as its CDF, then the random variable $Y = F(X)$ has for its CDF the uniform distribution function $U(0,1)$ [Casella and Berger, 1990].

Following [Salvadori et al., 2007], for generating observations (x,y) from a pair of random variables (X,Y), with marginals F_X, F_Y and joint distribution F_{XY} and copula **C**. Following Sklar's theorem, one can generate (u,v) from random variables (U,V) uniform on [0,1]x[0,1] and having the same copula **C**. Then using the probability integral transform one can transform (u,v) into (x,y):

$$\begin{cases} x = F_X^{-1}(u) \\ y = F_Y^{-1}(v). \end{cases} \tag{2.47}$$

In this way one can transform to the uniform marginal distribution.

Model selection criteria

Statistical tests such as the Akaike information criterion (AIC) [Akaike, 1974] and log-likelihood allow comparison between different models based on (relative) goodness-of-fit. The log-likelihood function is simply

$$l(\theta) = \log L(\theta) \tag{2.48}$$

with L as in Equation 2.46. The log-likelihood measures the goodness-of-fit for a model and is useful for comparing different model fits. Higher log-likelihood scores will mean a better fit; however, this score is also dependent on the number of model parameters. Therefore, the comparison of log-likelihood scores between two models with a different number of model parameters is not as useful. This is why the Akaike information criterion is also used. The Akaike information criterion (AIC) value is calculated in the following way:

$$AIC = 2k - 2\ln(\hat{L}) \tag{2.49}$$

where $\hat{L}$ is the maximum of the likelihood as in Equation 2.46 [Akaike, 1974]. AIC imposes penalties on functions with a high number of parameters. AIC scores do not inform

about the quality of the fit, but rather about the relative quality compared to other fits. Lower AIC scores will mean a better fit.

Finally, the Bayesian information criterion (BIC) will be explained; this method is related to the AIC but (for $n > 7$) imposes a higher penalty for models including more parameters [Schwarz, 1978]. The BIC value is calculated as follows:

$$BIC = k\ln(n) - 2\ln(\hat{L}) \tag{2.50}$$

where n is the number of observations. Like the AIC, lower scores are preferred over higher ones. When comparing models, the difference in AIC and BIC scores will weigh more heavily than that of the log likelihood because of the inclusion of these penalty terms.

Additionally, statistical tests can be used to evaluate how well a chosen model represents the data. These tests can be parametric like the chi-square or non-parametric like the Kolmogorov-Smirnov test.

Let X be a continuous random variable with distribution function $F(x)$. To evaluate the goodness-of-fit, the following can be tested.

$$H_0 : F(x) = F_0(x) \tag{2.51}$$

where $F_0(x)$ is a specified distribution function of X.

One-sample Kolmogorov-Smirnov test   The one-sample Kolmogorov Smirnov test tests if the population CDF of the observations is the same as the hypothesized distribution function $F(x)$ using the null hypothesis Equation 2.51. The Kolmogorov-Smirnov statistic for $F(x)$ is given as: sample

$$D_n = sup_x|F_n(x) - F(x)| \tag{2.52}$$

with sup_x being the supremum. D_n converges to 0 for $n \to \infty$ if the sample comes from $F(x)$ [Massey, 1951][Slakter, 1965]. The rejection/acceptance of the null hypothesis and the evidence in the form of the p-value is used to determine how well the proposed probability distribution represents the sample data.

Pearson Chi-square test   The Pearson chi-square test tests the same null hypothesis. The difference is that Pearson's chi-square test groups observations into bins and calculates the difference between the calculated and expected counts for each bin [Slakter, 1965].

$$\chi^2 = \sum_{i=1}^{N}(O_i - E_i)^2/E_i \tag{2.53}$$

Here, E_i are the expected counts for $F(x)$ and O_i are the observed counts. For $n \to \infty$, the test statistic follows the chi-square distribution. Again, a p-value can be used to support or reject the null hypothesis.

3

Exploratory Time-Series Analysis & Homogenization

This chapter will focus on the exploratory analysis of the water level observations in Venice with the aim of better understanding the current and past behaviour of the Punta della Salute time-series.

A large difference in the trend of the Punta della Salute time-series as compared to the reported SLR over a similar period [Zanchettin et al., 2021] [Stocker et al., 2013] was found. This chapter serves as a framework to explain the differences between the relative sea level rise as compared to the sea level rise for the Punta della Salute time-series.

The time-series of observations will be evaluated for trend and for changepoints. Using this changepoint analysis, the number of changes and estimates of the timings of each change can be determined. This analysis will be performed using RHtestV4 [Wang, 2008a] and BEAST [Zhao et al., 2019]. The timings of identified changepoints can be linked to historical events, where possible, to confirm their presence and give an indication of their possible cause. Finally, the time-series will be homogenized in preparation for extreme value analysis.

3.1. Trend detection

The Punta della Salute time-series was evaluated for monotonic trend using the Mann-Kendall test and variants of this test [Mann, 1945] [Kendall, 1975]. Since the Mann-Kendall test is not suitable for data that contain seasonality, the time-series was first deseasonalized using Equation 2.6. Following [Masina et al., 2022], multiple variants of the Mann-Kendall tests were used to reduce the uncertainty of the testing methods and to take into account the effects of autocorrellation. The R packages 'modifiedmk' (modified Mann-Kendall) [Patakamuri and O'Brien, 2021] and 'HKprocess' (Hurst-Kolmogorov) [Tyralis, 2016] in R were used to run these tests. These packages contain tests for

1. The original Mann-Kendall **(MK)** trend test [Mann, 1945] [Kendall, 1975] tests the null hypothesis that there is no trend versus the alternative hypothesis that there is a monotonic trend.

2. Mann-Kendall test using the pre-whitening approach **(PW)** [von Storch, 1999], uses the lag-1 autocorrelation coefficient for pre-whitening.

3. Modified Mann-Kendall test for serially correlated data using the [Hamed and Rao, 1998] **(HR)** approach. The input data are detrended and an effective sample size is calculated based on the ranks of significant autocorrelation coefficients

4. The Mann-Kendall test includes the variance correction approach **(PS)** proposed by [Yue and Wang, 2004]. Using this method, the input data is first detrended and an effective sample size is calculated using significant autocorrellation coefficients to address the problem of autocorrelation.

5. Mann-Kendall test under the scaling hypothesis **(HK)** of the data [Hamed, 2008] in which the Hurst exponent is used to measure the long-range dependence / persistence.

These tests were applied over different periods to evaluate the presence of trend over different time-spans and to compare to trends found from literature and reported sea level rise. Alongside tests of monotonic trends, Sen's slopes were calculated over all of these time periods in order to be able to compare their relative slopes. Sen's slope is less sensitive to outliers and the sign of the slope will reveal if statistically significant monotonic trends resulting from the Mann-Kendall tests are upward (subsidence) or downward (uplift). Time-periods evaluated for the Mann-Kendall monotonic trend test and evaluation of Sen's slope were chosen based on the changes in suspected anthropogenic subsidence as from literature [Gatto and Carbognin, 1981] [Carbognin et al., 2004] [Carbognin and Tosi, 1995] [Tosi et al., 2018].

3.2. Changepoint analysis

Statistically significant trends found using MK tests for different periods alongside results from Sen's slope support in identification of past changes in relative sea level within the time-series. To further evaluate the Punta della Salute time-series for (un)documented shifts in relative vertical position, changepoint detection methods can be used. In addition, signal decomposition will be performed to isolate the underlying trend. The analysis of changepoint and trend decomposition will help to understand the temporal pattern of the relative change in mean sea level [Duan et al., 2022]. The changepoint analysis methods used are the RHtestV4 method [Wang, 2008a] and the BEAST method [Zhao et al., 2019] in order to identify undocumented changes and to evaluate the trend.

Both RHtest and BEAST use the term changepoints, however, a distinction has to be made between the two. While RHtests tests for sudden changes of mean only, BEAST tests for abrupt changes, here defined as not only sudden changes but also breakpoints for the trend and seasonal signal to deviate from their previous directories. Both methods of changepoint analysis will be used in this work to compare the results of both methods and their usefulness in exploratory data analysis.

Neighbouring tide-gauge stations of the Punta della Salute station were included in this analysis as well as observations from the Trieste tide-gauge. These were included to be able to attribute identified changepoints to local causes or non-local causes. Here local causes are interpreted as causes for changes in mean/trend that only affect the water level observations of the Marghera, Piattaforma Acqua Alta and Punta della Salute time-series. The

tide-gauge stations of these locations are all within a relatively short distance of one another. If a changepoint is identified in all before-mentioned stations and is also identified in the Trieste water level observations, this is interpreted as a change caused by non-local causes.

To quantify the influence of this anthropogenic subsidence in the Punta della Salute time-series is possible under the assumption of (vertical) stability of the Trieste tide-gauge. Trieste is in a relatively stable area, where vertical land motions are in the range of tenths of mm/y or negligible [Antonioli et al., 2009] [Furlani et al., 2011] [Zerbini et al., 2021] [De Biasio et al., 2020]. Both Venice and Trieste are coastal cities connected to the northern Adriatic and sea level rise rates are assumed to be equal. This assumption is reinforced by a strong Pearson's correlation coefficient for the cross-correlation of sea level anomalies in the northern Adriatic in the range of 0.83 and 0.87 [Bergant et al., 2005]. Furthermore, [Zerbini et al., 2021] indicates a difference of 0.08 ± 0.11 mm/y between the east and west coasts of the Adriatic, based on the averages of the Venice, Marina di Ravenna and Trieste data. Trend decomposition using the BEAST method was applied to the Trieste time-series. With the Trieste tide-gauge as a stable point, this decomposed trend will be similar to the trend in sea level rise. Under the assumption that both the Punta della Salute and Trieste stations experience equal amounts of sea level rise, in this way the trend for Punta della Salute can be separated in SLR and VLM component. This is done by subtracting the decomposed trend from the Trieste tide-series from the decomposed trend of the Punta della Salute time-series.

3.3. Homogenization of the Punta della Salute time-series

The data will need to be homogeneous for extreme value analysis. This is because due to relative sea level rise, the probability of occurrence of extreme events changes over time. In the case of sea level rise, events that were considered extreme in the past may not be considered extreme today. This is why the time-series will need to be converted to some reference point in time. This conversion can be performed using the decomposed trend from the BEAST method, since this trend will contain the total change of the relative position of the city over time. The decomposed trend was subtracted from the time-series of Punta della Salute detrending of the time-series. After this the homogenized time-series was shifted to the mean of the relative sea level observations of 2020. With a homogenized time-series, extreme value analysis can be performed. As trend analysis revealed large differences in Sen's slope for different time-periods, homogenization was performed using the BEAST method as opposed to the RHtest. This is because the RHtest can not approximate the non-linear behaviour when using linear regression to approximate the trend of relative sea level rise.

4

Combined analysis of extreme water levels

This chapter will describe the necessary steps to arrive at an estimation of extreme sea levels from the combination of tide and storm surge components, taking into account the possible dependence between the two. First, the process of separation of the deterministic tide from the stochastic residual will be described. This procedure is performed to evaluate if there is a statistically significant dependence between the two. This dependence will be quantified using statistical tests. This is followed by extreme value analysis using a peak-over-threshold approach for a univariate case to be used as a reference model. Subsequently, a copula approach will be used in order to perform a combined analysis of the tide and surge under influence of dependence. This is done to assess the use of copulas in extreme value analysis. Modelling of dependence between surge and tide via copulas for shallow coastal regions is interesting in light of climate change. Sea level rise affects the bottom depth relative to the sea surface, which changes the relationship between tide and surge in shallow coastal regions.

4.1. Quantification of dependence of tide and surge components

In order to evaluate the dependence between the tide and surge components, these must first be separated from the Punta della Salute time-sreies of water level observations. The astronomical tide is deterministic in nature and can be separated from the sea level to form the non-tidal-residual (NTR). NTR is the sea level contribution caused by meteorological processes such as storm surges and can be described as a stochastic process. Tidal decomposition and projection can be performed using tidal harmonic analysis. A joint probability density function can then be formed from the convolution of the extreme value distribution of the storm surge and the probability density function of the tide [Caires, 2011]. This can only be done under the assumption that the tide and storm surge are independent of each other. This assumption will be investigated, as it may not be likely for shallow coastal regions [Tawn, 1992] [Pugh et al., 1980].

In order to separate the tidal signal from the non-tidal residual (NTR), tidal harmonic analysis was performed on the homogenized Punta della Salute time-series. Tidal harmonic analysis is performed using the Unified tidal analysis and prediction using "UTide"

Matlab functions [Codiga, 2011]. This step is necessary to be able to quantify the dependence between tide and non-tidal residual. Once the tidal analysis and reconstruction was performed. The reconstructed tide was subtracted from the homogenized time-series to calculate the non-tidal residual. With the tidal signal and the non-tidal signal separated, the dependence between the two could be quantified. However, first extreme events had to be selected. While both the annual maxima method and the peak-over-threshold method should have similar results for a time-series of water level observations of this length, the Peak-Over-Threshold (POT) method was chosen.

The threshold selection was performed based on the mean excess plot also known as the mean residual life based on the homogenized observations of the Punta della Salute tide-gauge. With the threshold selected, extreme water levels could now be determined. A declustering period of 48 h was chosen [Tomasicchio et al., 2021] to guarantee the independence (serially independent observations) between consecutive extremes.

To quantify the dependence between tide and surge during extreme events, the separated NTR and tidal signal were evaluated for dependence during the timings of the selected extreme water levels. The dependence was expressed by the Kendall τ rank coefficient and the Pearson r correlation coefficient.

For the univariate reference of extreme sea level estimates, the generalized Pareto distribution was fitted to extreme events using the maximum likelihood method for parameter estimation. Uncertainty was included in the form of adjusted bootstrap confidence intervals [Coles and Simiu, 2003]. m-yr return values were calculated using: [Coles, 2001]

$$z_m = \begin{cases} u + \frac{\sigma}{\xi}[(\zeta_u \cdot m)^\xi - 1] & \text{for } \xi \neq 0 \\ u + \sigma \log(\zeta_u \cdot m), & \text{for } \xi = 0 \end{cases}$$

Where σ and ξ are the scale and shape parameters, ζ_u is described by $\zeta_u = Pr\{x_i > u\}$ with u the POT threshold value and x_i the sea level in cm. The rate of occurrence was included in the ζ_u parameter, Which is

$$\zeta_u = \frac{N}{N_t} \tag{4.1}$$

Where N represents the number of events that exceed the threshold and N_t represents the total number of data during k years [Far et al., 2016]. In this way, the rate of occurrence takes into account the number of average yearly events.

The results of this univariate analysis are used as a reference for the results obtained from the combined analysis of tide and surge. For this combined analysis.

4.2. Combined extreme water level estimation using copula functions

In order to evaluate the use of copulas for the estimation of extreme water levels which take into account dependence between the water level's components of tide and surge, a combined analysis was performed which will be compared to the results of the standard univariate extreme value analysis.

According to Sklar's Theorem [Sklar, 1959] and as stated in Definition 2.3.2, a multivariate distribution can be described using uniform marginal distributions and a copula

describing the dependence. This requires (uniform) marginal distributions to describe the NTR and tide observations.

This is why first the marginal distributions were fit to the tide and surge observations and afterwards be transformed into $U[0,1]$, resulting in uniform marginal distribution. The marginal variables are the separated tide and NTR components of the extreme events of the homogenized Punta della Salute time-series. Different distributions will be evaluated, among the considered distributions are the GEV, generalized Pareto, lognormal, gamma, and Weibull distributions. The parameters of these distributions will be estimated using the maximum likelihood estimation [Coles, 2001]. Non-parametric functions were also tested for the combined analysis however these were not used due to complications further explained in section A.5.

This was followed by model selection using log-likelihood and the Akaike information criterion (AIC) to determine their goodness-of-fit and their relative goodness-of-fit. After the marginal distributions for Tide and NTR were chosen, the distributions were transformed into uniform marginal distributions. This was done using their corresponding inverse cumulative distribution function. The dependence between the two is not altered using this transformation.

In this study, we will be working with the VineCopula package in R as it includes more copula families than are available in Matlab. This package includes 37 different versions (they are listed in section A.3) of Copula variants. The copula functions were fit to the data and then evaluated using the AIC and Bayesian information criterion (BIC). AIC and BIC for copulas are similarly calculated to those of univariate distributions as follows:

$$AIC = -2\sum_{i=1}^{N} ln[c(u_{i,1}, u_{i,2}|\theta] + 2k,$$

where $u_{i,j}$ is the ith element of the jth data vector, $i = 1,\ldots,N$ and $j = 2$ for a bivariate copula. c is the bivariate copula family with parameters θ.

$$BIC = -2\sum_{i=1}^{N} ln[c(u_{i,1}, u_{i,2}|\theta] + ln(N)k$$

Based on AIC and BIC results, four best copula families were selected. First, all available copulas are fitted using maximum likelihood estimation. Then the AIC, BIC and log likelihood scores are computed for the available copula families. Lastly, an independent copula was fitted to the marginals in order to quantify the effect of the tide-surge interaction on extreme water level estimates. Based on the results of the (relative) goodness-of-fit tests, the Gaussian copula, t copula, 90 ° rotated Tawn type 1 copula and the Frank copula were chosen for sampling. Furthermore sampling was done from the independent copula.

Of the four copulas, the Gaussian method was chosen as the best fit (as in Table 5.7). This was based on this copula scoring best on AIC, BIC, and log likelihood. Furthermore, the extreme water level estimates were more in line with the extreme water level observations.

From each of the copulas in Table 5.7, 10^5 samples were taken from the copula space $U[0,1]x[0,1]$. The number of 10^5 was used to guarantee at least 10^4 year of samples for the occurrence interval of $\zeta_u = 2.72$. The inverse cumulative distribution function using the GEV parameters of the respective marginal distributions of NTR and tide was used to transform the samples from their respective uniform marginal distribution to physical quanti-

ties. The new sampled tide and sampled NTR extremes were added together to form a series of sampled extreme water levels. Combinations of the sampled tide and sampled surge level resulted in extremes below the threshold. These values below the chosen threshold of $u = 116cm$ were replaced by resampling. In doing so, these were replaced by a random ESL sample above the threshold value (see also section A.2). Points below threshold were a consequence of sampling from separated series of NTR and tide, allowing for new combinations below the selected ESL threshold.

To the extreme water level samples of the five copula functions, probability distributions were fitted using MLE. Finally, from these distribution functions, return values were calculated and relative differences were computed.

Lastly, an indication of the influence of sea level rise for the extreme water level estimation was made for Venice, under the assumption that the distribution of extremes is independent of SLR. This was done to express the influence of sea level rise on the return values under different SSP scenarios [Masson-Delmotte et al., 2021].

5

Results

This chapter will lay out the results of the performed methods and analysis with the aim to support to answering the main and sub research questions. Firstly the results from the exploratory time-series analysis & homogenization will be presented followed by that of the quantification of the dependence and extreme value analysis.

5.1. Trend analysis of water level observations

The difference in mean water level observations between the year 2021 and 1924 of the Punta della Salute time-series is more than 28 cm. Compared to the effects of global sea level rise over a similar but longer time period (1901-2010), 19 cm of global sea level rise is reported [Stocker et al., 2013]. Table 5.1 shows the results of least squares regression of the Punta della Salute time-series over different time periods of the time-series.

The results of the Mann-Kendall tests and variants of this test evaluated for the deseasonalized Punta della Saluta time-series are shown in Table 5.2. p-values of 5% or lower are indicated in bold with an asterisk, p-values of less than 10% but higher than 5% are indicated in bold. The absence of both indicates a p-value greater than 10%. For this study, a significance level of 5% is chosen. Therefore, values with a p-value of 5% of lower significance signify a statistically significant monotonic trend in the data. The numbers in the table indicate the magnitude of the Sen's slope over their respective period of the deseasonalized monthly means. The Sen's slope gives an indication of the magnitude of the slope. Positive numbers indicate a positive trend signifying an increase in relative sea level while negative numbers indicate a negative trend signifying a decrease in relative sea level.

period	Trend PS	Trend Trieste	Trend PS - Trend Trieste
1930-1949	2.51 mm/y	0.29 mm/y	2.22 mm/y
1950-1969	5.25 mm/y	2.53 mm/y	2.74 mm/y
1970-1975	-3.91 mm/y	-2.66 mm/y	-1.24 mm/y
1976-1988	-0.63 mm/y	-0.15 mm/y	-0.48 mm/y
1989-2022	4.78 mm/y	3.19 mm/y	1.59 mm/y

Table 5.1: Trends of RSL over different periods using ordinary least squares regression.

Period	n	MK	PW	HR	PS	HK
1924-2020	1164	**2.22***	**7.02***	**2.22***	**2.22***	-
1924-1929	72	-0.747	-0.484	-0.747	-0.747	-0.747
1924-1949	312	**2.27***	**1.26***	2.27	**2.27***	2.27
1930-1949	480	0.965	0.353	0.965	**0.965**	0.965
1940-1987	576	**2.29***	**1.29***	**2.29***	**2.29***	**2.29***
1940-1959	480	**2.43***	**1.69***	**2.43***	**2.43***	2.43
1950-1975	552	**2.47***	**1.45***	**2.47***	**2.47***	**2.47***
1950-1969	480	**4.13***	**2.45***	**4.13***	**4.13***	**4.13**
1960-1987	336	**0.746**	0.582	0.746	**0.746***	0.746
1970-2020	612	**2.43***	**1.18***	**2.43***	**2.43***	**2.43***
1970-1987	216	1.30	1.21	1.30	**1.30***	1.30
1970-1975	72	**-8.94***	**-6.47**	**-8.94***	**-8.94***	**-8.94**
1976-1987	144	**2.40**	1.84	2.40	**2.40***	2.40
1988-2020	396	**2.81***	**1.3***	**2.81***	**2.81***	**2.81***

Table 5.2: Sen's slope values $\cdot 10^3$ for deseasonalized Punta Salute over different time periods, n denotes the number of monthly observations included in the statistical tests, numbers in bold denotes a p-value of 10% or less and those with an asterisk denote p-values < 5%.

The different variants of the Mann-Kendall test are denoted **MK** for the standard Mann-Kendall test, **PW** for the pre-whitening approach, **HR** for the Hamed & Rao variance correction approach, **PS** for the Trend-Free Pre-whitening approach and lastly the Mann-Kendall test using the Hurst-Kolmogorov process **HK**.

A common statistically significant monotonic trend was found for 5 of 14 selected periods for all tests. These are for the periods 1924-2021, 1940-1988, 1950-1976, 1950-1970 and 1970-2021, the periods with the largest number of observations. Statistical significance of these tests depends on the length of the period, as well as the variant of the test that is used.

Except for the two periods of 1924-1930 and 1970-1976, all periods have a positive Sen's slope. Sen's slope results indicate that, of the tested periods, the largest positive trend occurs in the period 1950-1970. This means that over the period of 1950-1970, the largest relative sea level rise occurs. The results also indicate negative slopes from 1924-1930 and one in 1970-1976. While it has the lowest number of observations, the monotonic trend in 1970-1976 was determined to be statistically significant by most tests and all tests report p-values below 10%.

The shift in sign of the sen slope for consecutive periods (1950-1970, 1970-1976, 1976-1988) that have statistically significant monotonic trend for multiple tests led to change-point analysis in order to detect changes that may have occurred in the time-series.
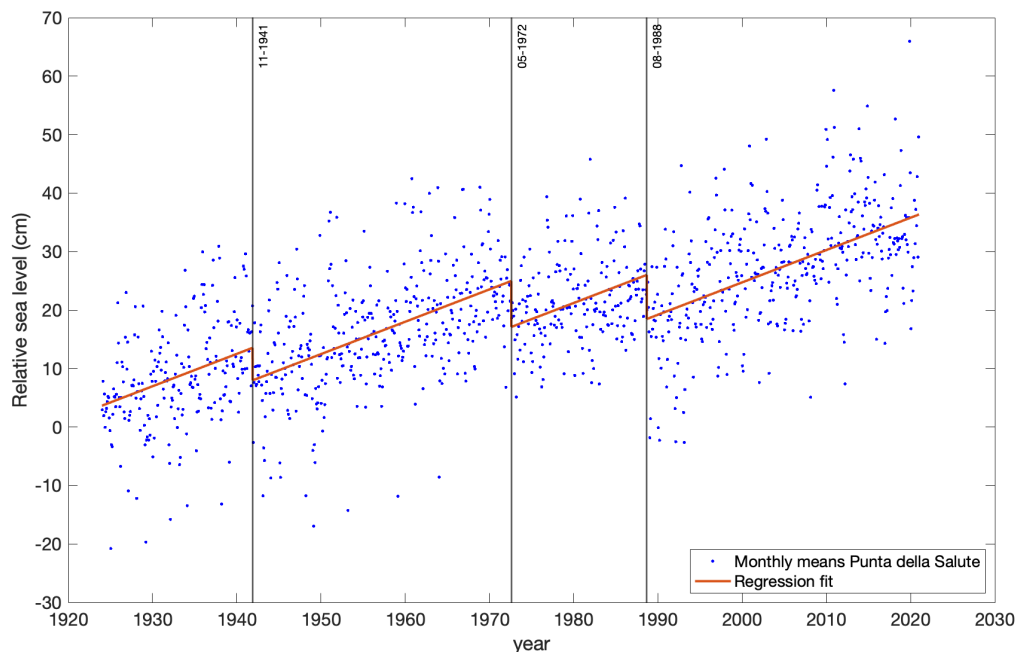
Figure 5.1: RHtest changepoint analysis results of Punta della Salute time-series.

5.2. Changepoint analysis & homogenization

Here, the results of changepoint analysis are reported. Changepoint analysis was performed to identify undocumented changes in the time-series. The time-series of Punta della Salute as well as the neighbouring tide-gauge observations of Trieste, Marghera and Piattaforma Acqua Alta were included in this analysis. First the results of the changepoint analysis performed using the RHtest method are shown, followed by those by the BEAST method. It is important to distinguish the way these two methods test for changepoints. RHtest detects shifts in mean using the penalized maximal F-test (in absence of a reference series) while the BEAST method detects both shifts in mean and trend on the basis of Bayesian model averaging. Lastly the result of the homogenization of the Punta della Salute time-series is shown.

Figure 5.1 show the changepoints resulting from the RHtest method for the Punta della Salute time-series. Three shifts were found using this method in 11-1941, 05-1972 and 08-1988.

Using the RHtest method, the number of identified changepoints and their timings depend on the number of observations. This can be seen from the RHtest result of the Punta della Salute time-series over the same period as that of the Piattaforma Acqua Alta time-series (1983-2021) as in Figure 5.2. The timings of identified changepoints for the time-series of both stations are identical.

Only one changepoint was found resulting from the RHtest on the longer Trieste time-series (1875-2021). This changepoint was found in 2008. Lastly, no changepoints were found for the Marghera time-series (1989-2020).
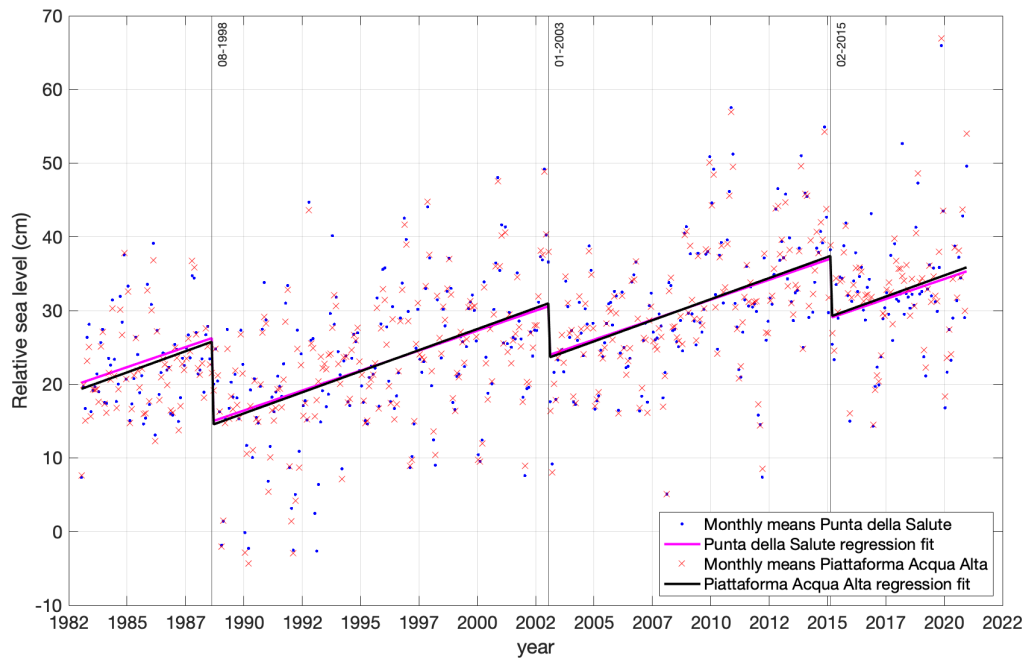
Figure 5.2: RHtest changepoint analysis results of the Punta della Salute and the Piattaforma Acqua Alta time-series when tested over the same time period of 1983-2020.

The same time-series were tested using the Bayesian Estimator of Abrupt change, Seasonal change, and Trend (BEAST) method. This test decomposes a time-series into trend, a seasonal signal and noise. The trend and seasonal signal are then analysed both individually for changepoints. The time-series that were tested are from the tide-gauge stations of Punta della Salute, Trieste, Marghera and Piattaforma Acqua Alta. No changepoints were found for any of these time-series in the (decomposed) seasonal signal. Using Bayesian Model Averaging (BMA) of the BEAST method, the probability of occurrence for every changepoint based on the model result as well as the mean number of changepoints is calculated. To elaborate, if N is the total number of MCMC samples and a chain of trend changepoints $m_{i=1,...,N}^i$ containing the number of changepoints of each MCMC sample then the mean number of changepoints can be denoted $\overline{m} = \sum_{i=1}^{N} m^i / N$ for samples $i,...,N$. In this way, for all time-series the mean number of changepoints containing only the most likely changepoints are shown.

The decomposed trend along with 95% confidence intervals and the mean number of changepoints as from BEAST for Punta della Salute (14) and Trieste (21) are shown in Figure 5.3.

The changepoints identified in the Punta della Salute time-series using the BEAST method are also found in the Trieste time-series except for one changepoint identified in 1968. The decomposed trend from the Punta della Salute time-series shows a steeper slope than that of the Trieste time-series.

The same method was applied to the Marghera and Piattaforma Acqua Alta time-series which can be found in Appendix A. However, no unique changepoints were identified for the Punta della Salute time-series in this way.

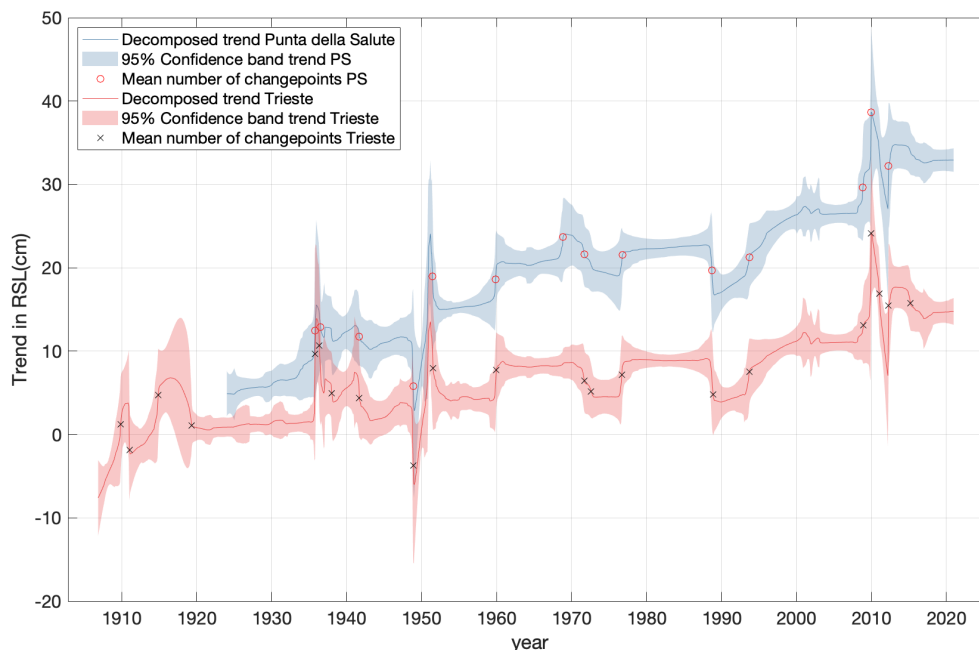Using the BEAST methods, the timings of most changepoints coincide between differ-

Figure 5.3: Changepoints and the decomposed trend along with confidence bands of the Punta della Salute and Trieste time-series resulting from the BEAST method.

ent tide-gauge stations. It was assumed that these changepoints are caused by the same large-scale events. Changepoints that are exclusively identified in the Punta della Salute time-series and in no other time-series are attributed to local causes which only affect the city of Venice. The changepoint in 1968 is unique to the Punta della Salute time-series and is attributed to local causes.

Figure 5.4 shows the relative number of samples that have a negative rate of change at a given time for both the PS and the Trieste time-series. This can be seen as the number of samples with a positive rate-of-change at time t divided by the total number of samples N_t at that time. Indicators of anthropogenic influence can be identified using the slope of the decomposed trends of the Punta della Salute time-series when compared with the Trieste time-series.

In Figure 5.4 the number of samples with negative rate-of change are consequently higher for the Trieste time-series up to 1968. From 1968-1976 more samples report a negative rate-of-change which is a consequence of the period of uplift during this time. From 1993, the number of samples with negative rate-of-change for both time-series are comparable. This result is indicative of the stop of anthropogenic subsidence and agrees with what was found by the regional studies in 1993 and 2000 [Carbognin et al., 2005] [Brambati et al., 2003].

Using trend decomposition in combination with the stable reference point of Trieste, total VLM caused by natural and anthropogenic drivers could be isolated. Due to their different locations, exceptional events of different magnitudes in the eastern and western Adriatic caused large differences in monthly mean RSL. Figure 5.5 shows the difference between the two, which is assumed to be the combination of anthropogenic and natural vertical land motion. The influence of natural VLM is well known and ranges between 0
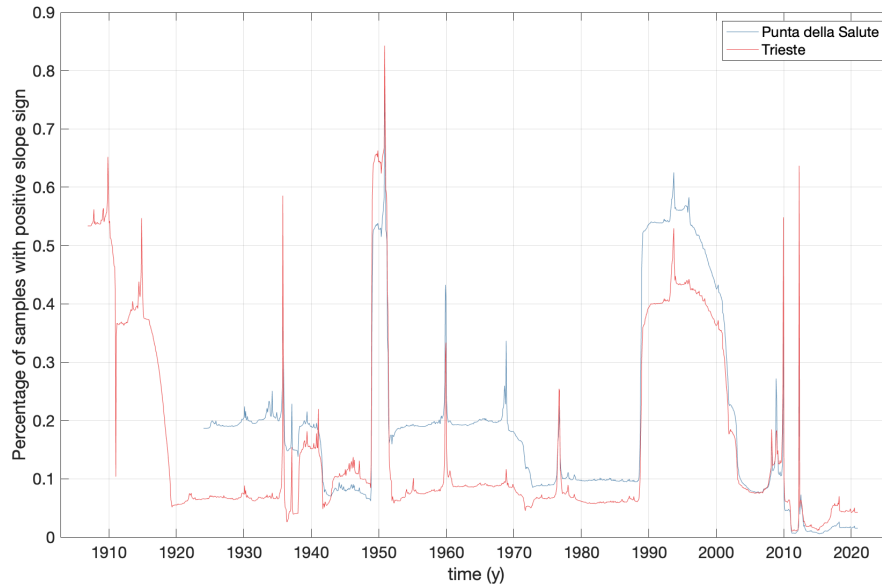
Figure 5.4: Relative rate-of-change over time resulting from the BEAST method for the Punta della Salute and Trieste time-series, higher values indicate a steeper positive slope in RSL.

and 0.5 mm/y [Brambati et al., 2003] [Zanchettin et al., 2021] [Gatto and Carbognin, 1981] [Antonioli et al., 2009] a linear trend of 0.4 mm/y was removed from this residual VLM leaving anthropogenic VLM over time. The total anthropogenic VLM throughout the time-series (1924-2020) was approximately 10 cm, in line with previous estimates by various authors that ranged from 8 to 11 cm [Brambati et al., 2003] [Gatto and Carbognin, 1981] [Carbognin et al., 2005] [Tosi et al., 2013] [Pirazzoli, 1987]. Natural VLM contributed to almost 4 cm during this period.

The difference in trend between PS and Trieste is seen in Figure 5.5. This difference was attributed to be due to VLM. Large shifts in this VLM, pointed out as periods of interest, were investigated.

1. No explanation could be found for this event, both time-series include changepoints during this period. This could be attributed to a more pronounced storm on the east coast like the 2008 storm surge [Međugorac et al., 2015].

2. The large jump happens in 1968 and is caused by the largest anthropogenic subsidence in Venice during this period [Tosi et al., 2002] [Carbognin et al., 2004]. This jump is followed by a negative slope that indicates the uplift period in Venice.

3. This short peak was marked between 06-2008 and 08-2009 is caused by the renovations of Punta della Dogana during this period [Punta della Dogana, 2016]. Punta della Dogana is located right next to the tide-gauge, and experienced large amounts of local anthropogenic subsidence in this period [Tosi et al., 2013].

4. The difference in peak can be attributed to the Bora wind event during the winter of 2012 coinciding with the eastern European cold wave [Davolio et al., 2015] [Mihanović et al., 2013].
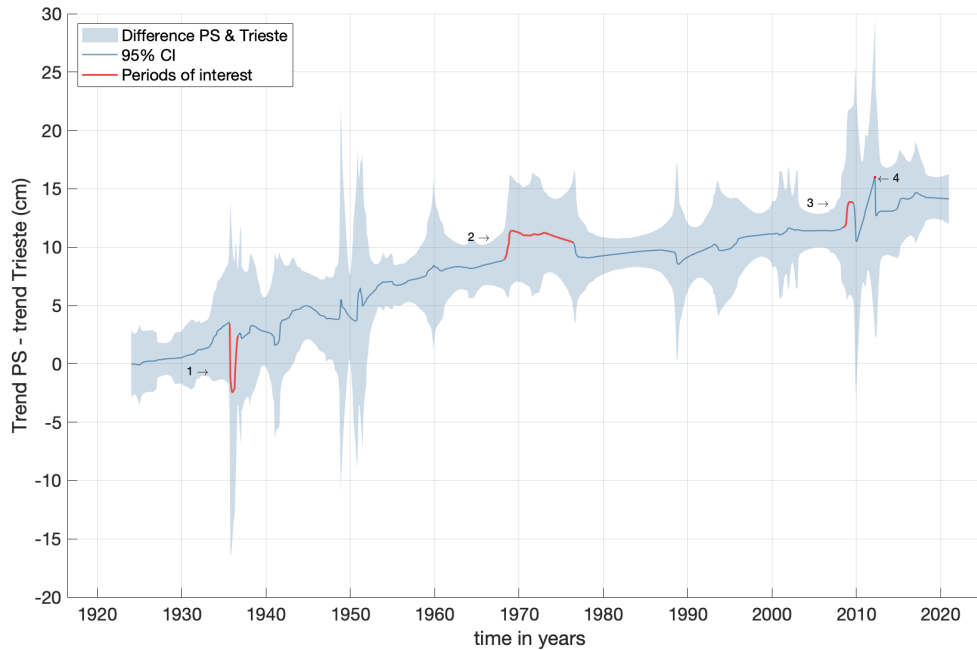
Figure 5.5: The decomposed trend of the Trieste time-series subtracted from the decomposed trend of the Punta della Salute time-series alongside 95% confidence bands. BEAST method was used for the trend decomposition, the blue line is the assumed vertical land motions of the Punta della Salute time-series.

Furthermore, a trend decline for the period 1971 to 1993 [Carbognin et al., 2004] is caused by the increase in sea level that slowly decreased over this period; the same behaviour is observed for the western Mediterranean Sea and Adriatic since 1960 [Tsimplis and Baker, 2000]. During the period of the time-series (1924-2020), the total relative sea level rise was found to be 2.882 mm / y. Of this increase, 1.458 mm / y was caused by VLM and 1.431 mm / y by the rise in sea level.

The BEAST trend decomposition was use for the homogenization of the time-series. The decomposed trend was removed from the relative sea level observations and then shifted to the mean of the relative sea level observations of 2020. Figure 5.6 shows the yearly mean relative sea level observations of Punta della Salute along with the decomposed trend, the mean of the relative sea level observations of 2020 and the new homogenized time-series.
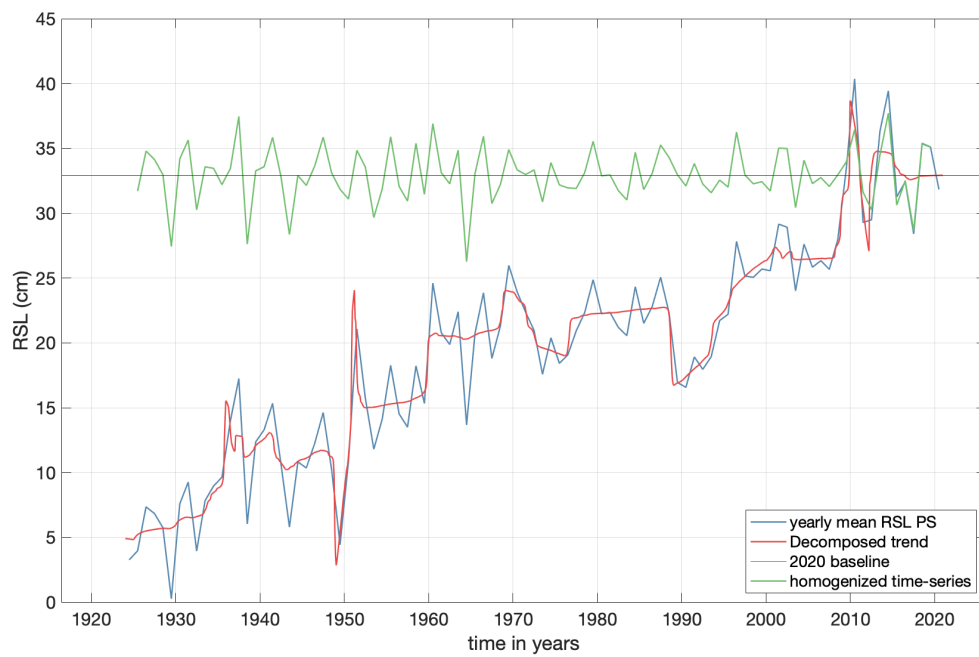
Figure 5.6: Yearly mean relative sea level, decomposed trend from BEAST trend decompoisition, the mean of 2020 relative sea level observations and the homogenized time-series of the Punta della Salute time-series.

5.3. Results of the combined analysis of extreme water levels

This section will show the results of chapter 4, starting with the results of the separation of the tide and the non-tidal component. This is followed by the evaluation of the dependence by the two and the extreme value analysis for the univariate reference case. Lastly, the results of the marginal fitting for the multivariate copula method are shown as well as the return values obtained using this method and a comparison between this method and the univariate reference case is given.

Univariate ESL estimation

For the selection of extreme events, the Peak-Over-Threshold (POT) method was used, the threshold selection was based on the mean excess plot based on the converted time-series as shown in Figure 5.7. The threshold chosen in this way was $u = 116cm$. With the declustering time of 48h, this led to 264 total extreme value observations, leading to a number of $\zeta_u = 2.72$ yearly events on average. Figure 5.8 show the homogenized Punta della Salute time-series along with the threshold and the peaks above this threshold.
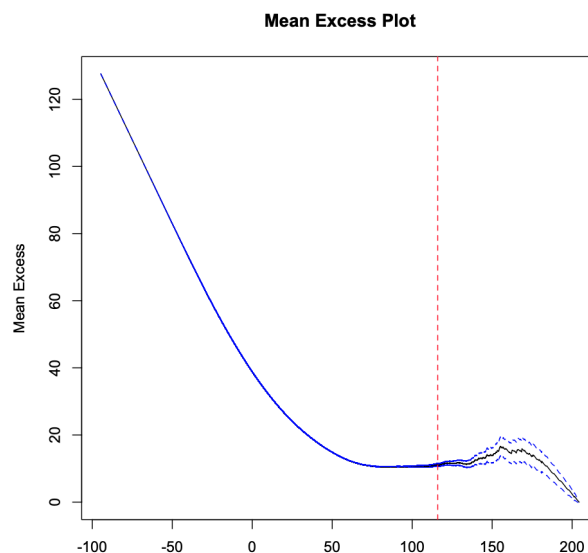

Figure 5.7: Mean excess plot of the homogenized Punta della Salute time-series used for threshold selection with vertical line at u = 116 cm.

For the univariate extreme value analysis, the Generalized Pareto Distribution (GPD) was fit to these extremes using MLE for parameter estimation, including 95% confidence intervals using the adjusted bootstrap method. The result is shown in Figure 5.10 for a return period of up to 10^4 years. This univariate ESL estimation. The values for the $10^2, 10^3$ and 10^4 year return periods and of the corresponding 95% confidence intervals are shown in Table 5.3. GPD parameters from the MLE are $\xi = -0.0046$ and $\sigma = 12.31$. The ESL observation with the highest return period corresponds to that of the 1966 Acqua Alta with a height of 204 cm (after homogenization) and a return period of 97 years.

Tidal harmonic analysis and quantification of dependence

Using tidal harmonic analysis, the Punta della Salute time-series is analysed for tide and the tidal series is reconstructed. The 10 most influential tidal constituents are shown in
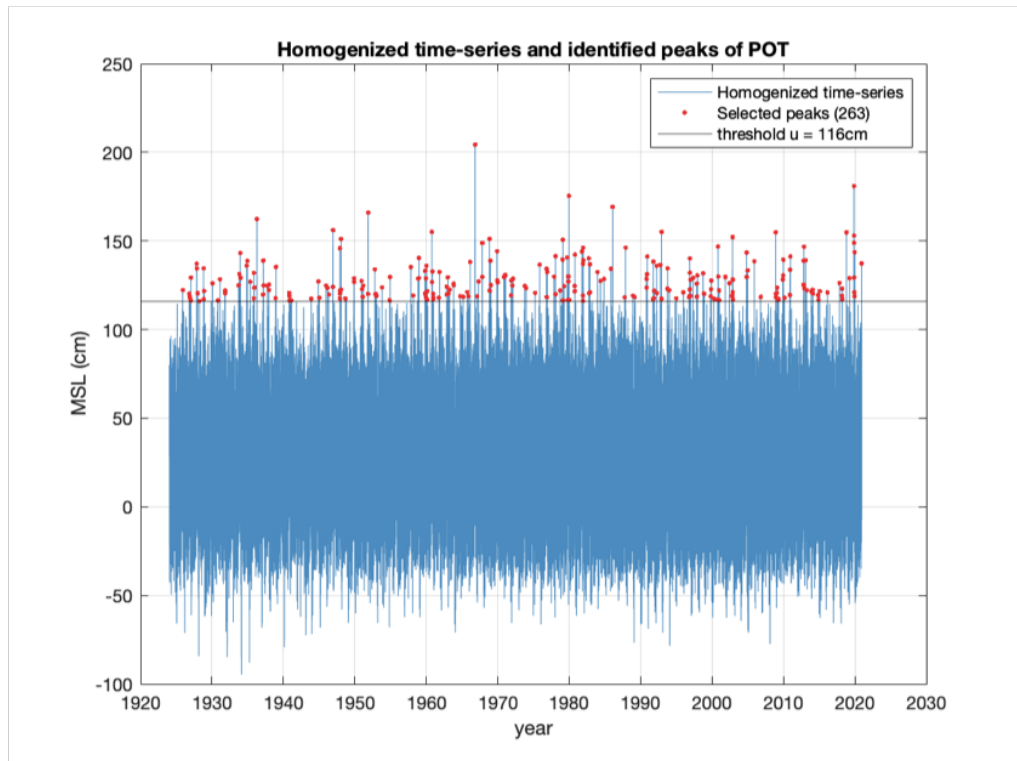
Figure 5.8: Selected peaks higher than threshold of $u = 116cm$ of the homogenized Punta della Salute time-series.
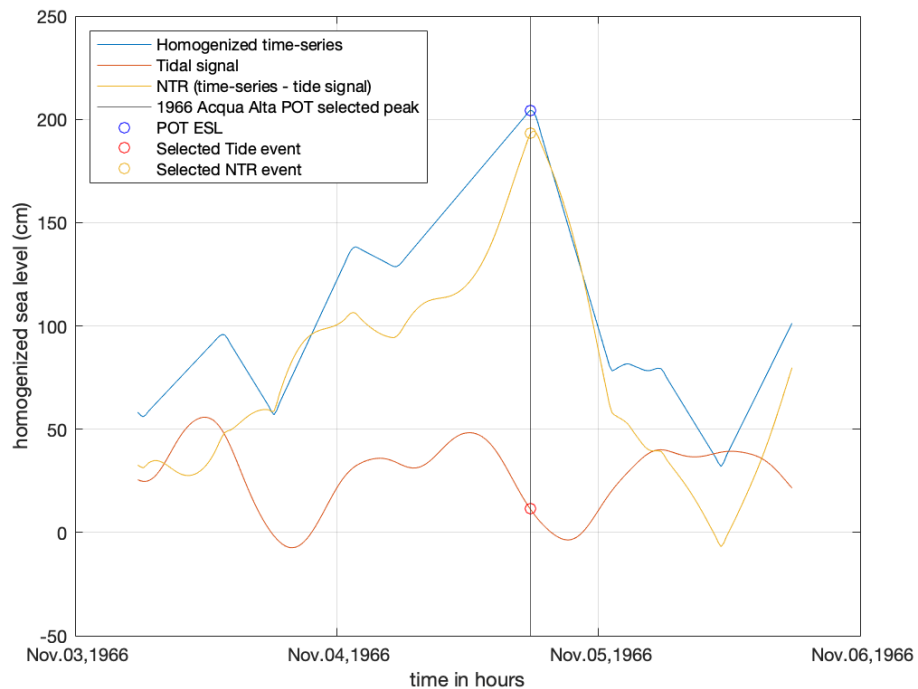

Figure 5.9: Example of the separation of tide and non-tidal residual for extremes of the Punta della Salute time-series.
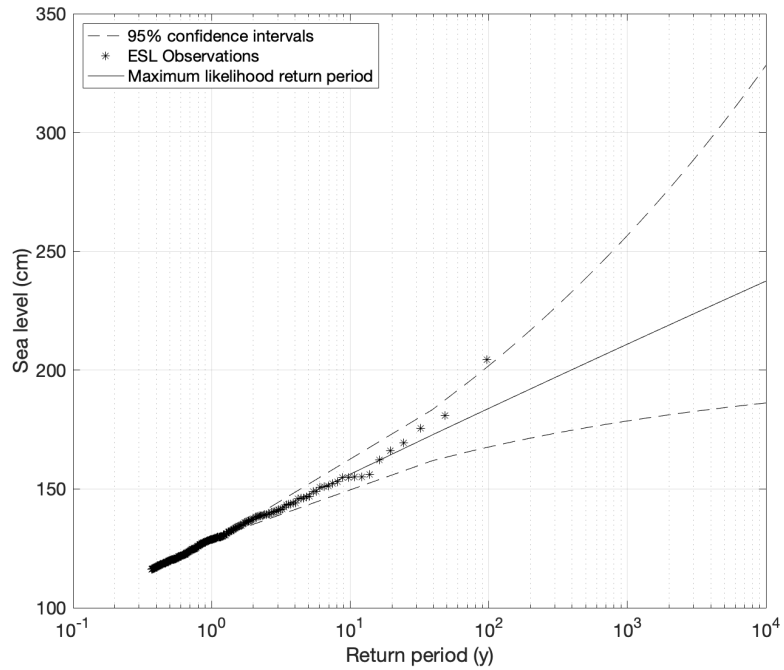
Figure 5.10: Univariate return value plot of the POT-GPD for the homogenized Punta della Salute time-series with threshold $u = 116cm$ including bootstrapped 95% confidence intervals

m-year RP	Return value (cm)	Upper CI (cm)	Lower CI (cm)
100	184.11	204.57	167.82
1000	211.58	263.67	177.85
10000	238.76	330.24	189.68

Table 5.3: Return values of the POT/GPD including 95% confidence intervals

Constituent	Amp (cm)	Phase(°)
M2	21.0	316.0
K1	17.0	92.0
S2	12.2	326.0
P1	5.51	87.9
O1	5.15	78.3
SA	4.08	281.0
K2	3.70	322.0
N2	3.44	315.0
SSA	3.09	112.0
S1	1.96	287.0

Table 5.4: first ten tidal constituents sorted by contribution to tidal amplitude in descending order.

Table 5.4.

After removal of the reconstructed tide from the Punta della Salute time-series, two series were formed, one of the tide and one of the non-tidal residual (NTR). For the evaluation of dependence, only the tide and NTR during extreme events were selected. Figure 5.9 shows how the non-tidal residual and tide events are chosen, the tide and the non-tidal residual (NTR) are separated as in Equation 2.3 and the depdendence was evaluated. A statistically significant correlation between tide and NTR was found to be -0.61 at Punta della Salute with p-value < 0.001 for the Kendall rank correlation. Using the Pearson r correlation this value was found to be -0.81 with a p-value < 0.001. The minus sign of the correlation coefficients indicates a higher number of discordant pairs, meaning that NTR peaks occur more frequently during low tides and high tides more frequently coincide with low NTR. Figure 5.11 shows this influence; the top left and bottom right quadrants contain all discordant pairs.
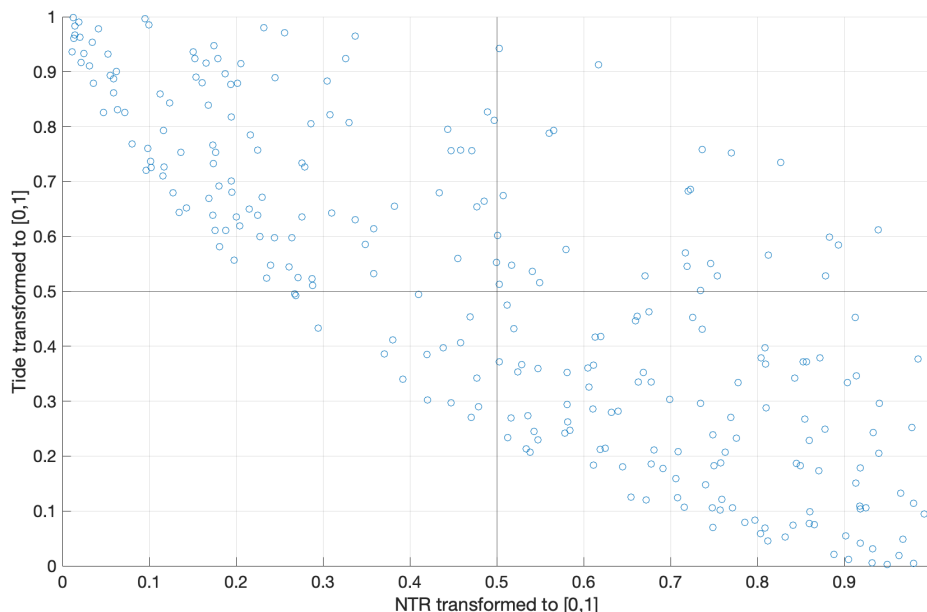
Figure 5.11: Dependence between NTR and tide

Marginal distributions tide and non-tidal residual

In preparation for the copula-based method of extreme value estimation, marginal distributions were evaluated for both tide and non-tidal residual. The results of this evaluation of the NTR can be seen in Figure 5.12. In this plot, the five best-fitting distributions of those that were considered are shown. These five were chosen based on the log likelihood criteria. Parameter estimation was performed using maximum likelihood. Statistical test scores for these distributions can be seen in Table 5.5 which include the log likelihood, Aikake Information Criterion (AIC), Kolmogorov-Smirnov (K-S) test p-values, and the chi-square p-value. The log likelihood measure goodness-of-fit; however, it does not penalise parameter usage, as such a function with more parameters is more likely to generate better log likelihood scores. A lower AIC values means a relative better goodness-of-fit (as compared to other models). For the Kolmogorov-Smirnov test and the chi-square test, higher p-values are considered to be better, a value below 5% means that the null hypothesis that the NTR sample data comes from the listed probability distribution is rejected. The Generalized Extreme Value distribution (GEV) outperformed all other distributions for all tests except the Chi-square goodness-of-fit test, where the null hypothesis is rejected. From Figure 5.12 it can also be seen that it best represents the sample data. The GEV parameters are $\xi = 0.04307$, $\sigma = 13.96$ and $\mu = 64.16$.

The same procedure was applied to the reconstructed tide of the Punta della Salute time-series. The histogram of the tide samples along with the distributions with the highest log likelihood scores are shown in Figure 5.13. Test scores for the distributions are found in Table 5.6. The GEV outperforms other methods in terms of relative goodness-of-fit, goodness-of-fit and p-values for the Kolmogorov-Smirnov test and Chi-square goodness-of-fit test. GEV parameters are $\xi = -0.5394$, $\sigma = 14.02$ and $\mu = 52.58$.
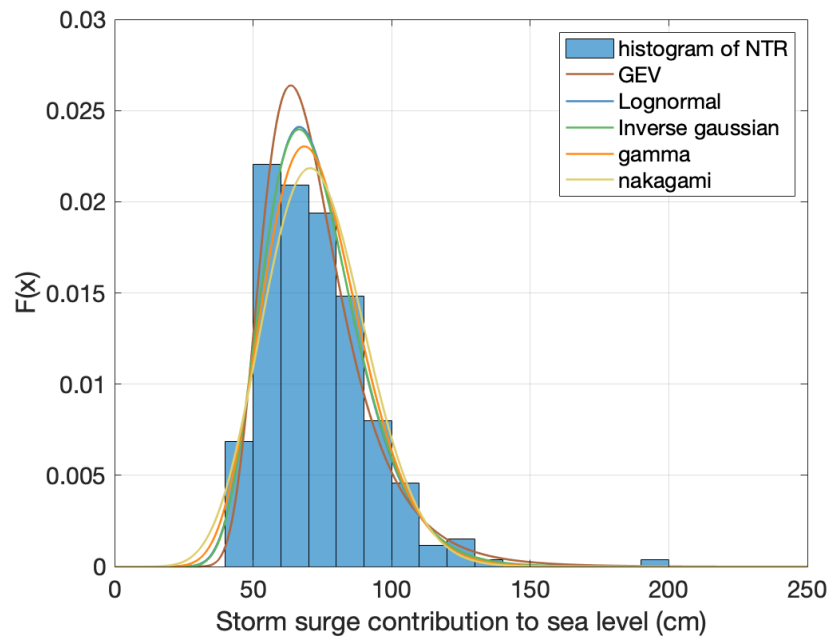
Figure 5.12: Histogram of the NTR data and fit of different families of probability distribution functions to the observed NTR of the Punta della Salute time-series

Family	log likelihood	AIC	K-S p-value	Chi-square p-value
Generalized Extreme Value	-1115	2235	0.7055	0.045
Lognormal	-1118	2241	0.3407	0.24
Inverse Gaussian	-1119	2241	0.3391	0.25
Gamma	-1125	2253	0.2587	0.30
Nakagami	-1134	2272	0.2227	0.25

Table 5.5: Statistical test scores of marginal fits for the non tidal residual.

Family	log likelihood	AIC	K-S p-value	Chi-square p-value
Generalized Extreme Value	-1028	2061	0.945	0.858
Extreme Value	-1032	2067	0.487	0.469
Weibull	-1039	2082	0.459	0.603
t location scale	-1044	2095	0.302	0.0875
logistic	-1045	2095	0.440	0.118

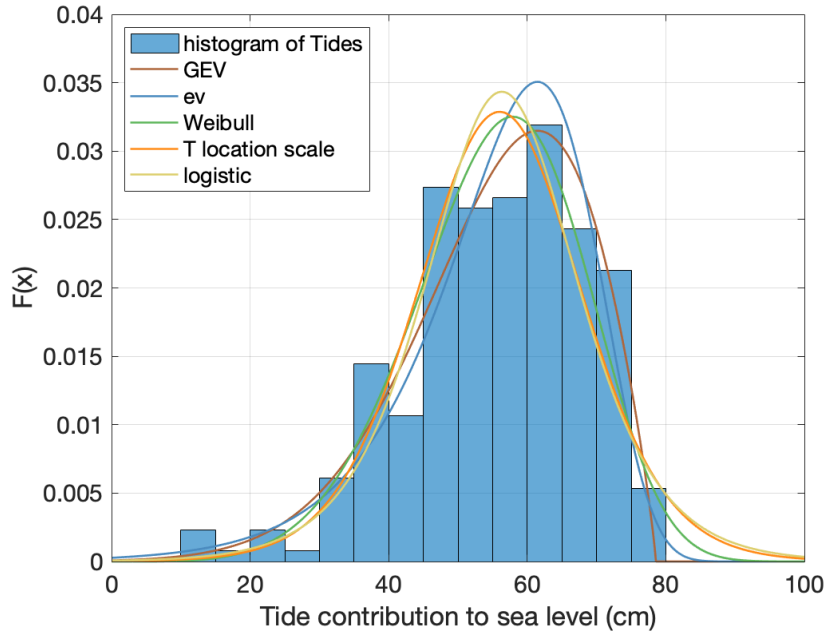Table 5.6: Statistical test scores of marginal fits for the tidal signal.

Figure 5.13: Histogram of the NTR data and fit of different families of probability distribution functions to the observed NTR of the Punta della Salute time-series

Copula Familiy	Log likelihood	AIC	BIC	Kendall τ
Gaussian	137.4	-272.8	-269.23	-0.6
Student t	136.66	-269.32	-262.18	-0.59
90° Rotated Tawn type 1	130.95	-257.89	-250.75	-0.53
Frank	129.49	-256.98	-253.41	-0.6

Table 5.7: Log likelihood, Aikake Information Criterion, Kolmogorov-Smirnov and the Chi-square goodness-of-fit scores for distribution MLE fits to the non-tidal residual's contribution to water level of extreme events.

Results of the combined analysis of tide and surge

The results of the criteria for the copula functions are shown in Table 5.7. This table shows the log likelihood, AIC, Bayesian Information Criterion (BIC), and lastly the Kendall τ rank correlation coefficient. From the copula families tested, the Gaussian and Student t copulas showed similar results in goodness-of-fit and AIC & BIC scores. While the Kendall τ rank correlation coefficient of the Gaussian, Student t and Frank copula closely resemble the calculated dependence of -0.61, the 90° rotated Tawn type 1 copula reports a correlation coefficient of -0.53. The kernel estimation of the copula density along with the copula density plots of the four copulas described above can be found in section A.1.

Figure 5.14 and Figure 5.15 show the copula isolines of the Gaussian copula and the Rotated Tawn type 1 copula in addition to the isolines of the independent copula and observational data. Isolines are lines containing points that share common probabilities [Lucey et al., 2022]. Large differences can be observed between the independent copula and the dependent copulas, but also between the dependent copulas. While they share the same correlation, the difference between the density of the Gaussian copula and the Frank
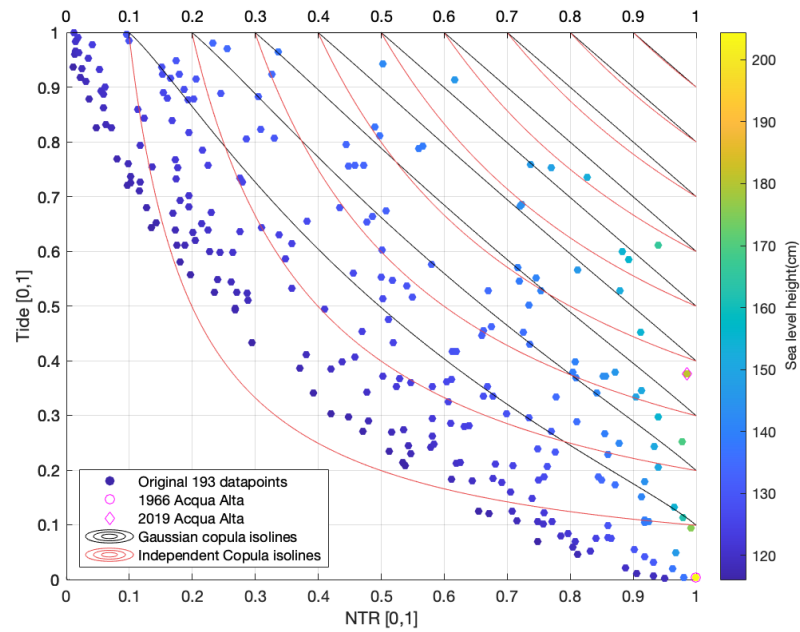
Figure 5.14: Observed data and isolines from the Gaussian copula and independent copula

Family	log likelihood	AIC
Generalized Extreme Value	-3.606e+05	7.212e+05
Lognormal	-3.744e+05	7.489e+05
Inverse Gaussian	-3.745e+05	7.490e+05
Gamma	-3.763e+05	7.527e+05
Nakagami	-3.785e+05	7.569e+05
Generalized Pareto	-3.641e+05	7.281e+05

Table 5.8: Statistical test scores of distribution fits to the sampled extreme water level samples resulting from the combined analysis of tide and surge.

copula can be seen from the difference in isolines (e.g. see the 0.4 isolines). Furthermore, in the plots the 2 most extreme events have been highlighted, which are the 1966 and 2019 acqua alta. Lastly, it shows that the occurrences of the highest extreme water levels are caused by storm surge as opposed to tide.

Figure 5.16 show the fit of the probability distribution to the sampled extreme water level. These sampled extreme water levels are the combination of the sampled tide and sampled non-tidal residual using the Gaussian copula function. Generated extreme water level samples below the threshold were resampled and Table 5.8 show the log likelihood and AIC scores for the six probability distributions with highest log likelihood scores. These distributions were fitted using MLE.

The result is the return value plot in Figure 5.17, which shows the return values using sampled data from the five different copulas along with the results of the univariate fit. The independent copula and the Tawn copula report large return values compared to the univariate case. The 100, 1000 and 10000 year return values and their confidence intervals are shown in Table 5.9.
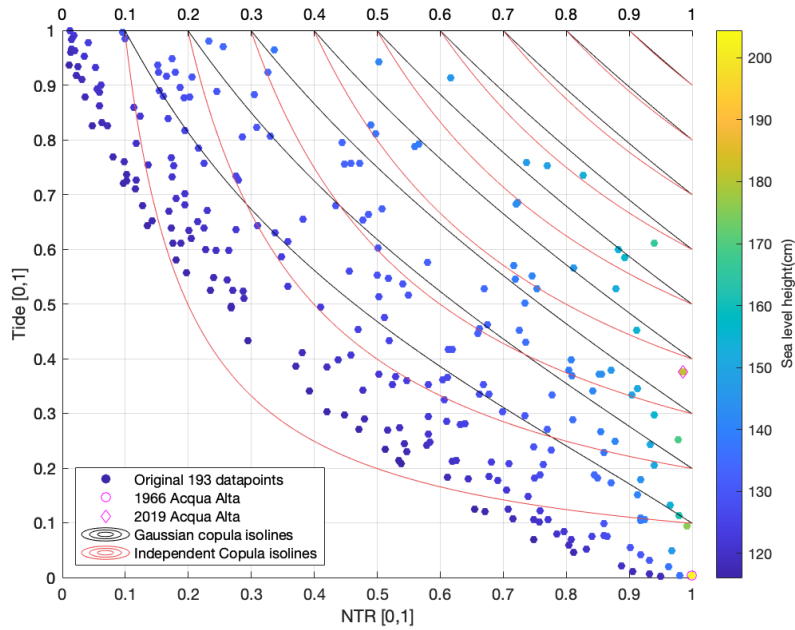
Figure 5.15: Observed data and isolines from the 90°Rotated Tawn type 1 copula and independent copula
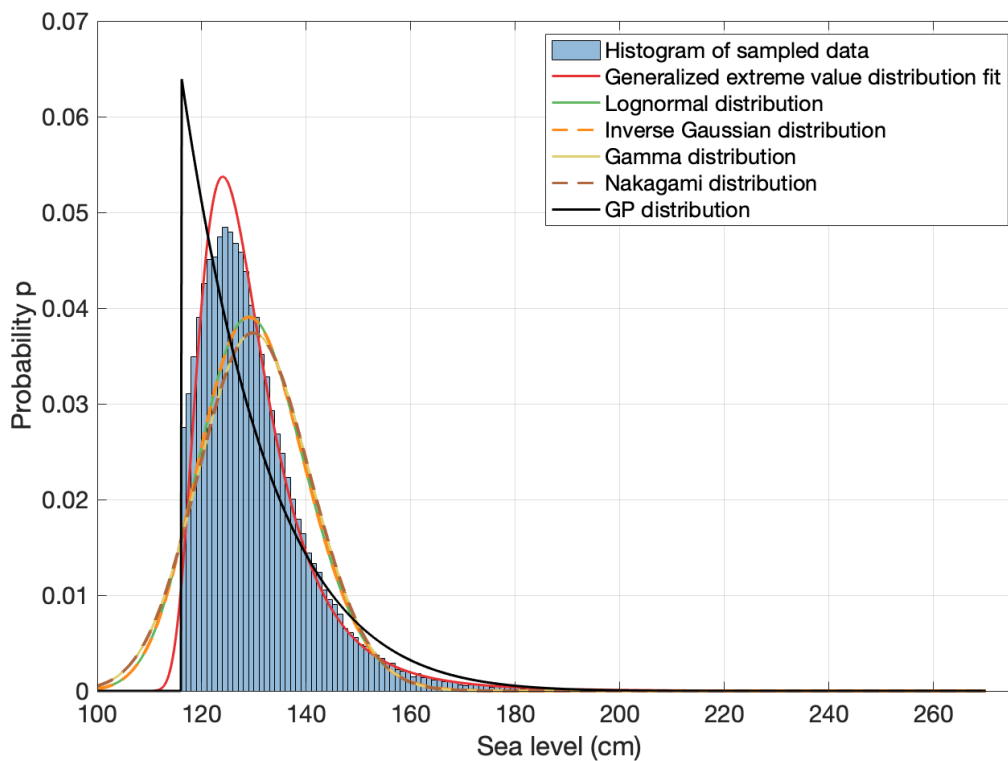

Figure 5.16: Histogram of extreme water level samples from the combined analysis of tide and surge using the Gaussian copula and probability distribution function fits using MLE.
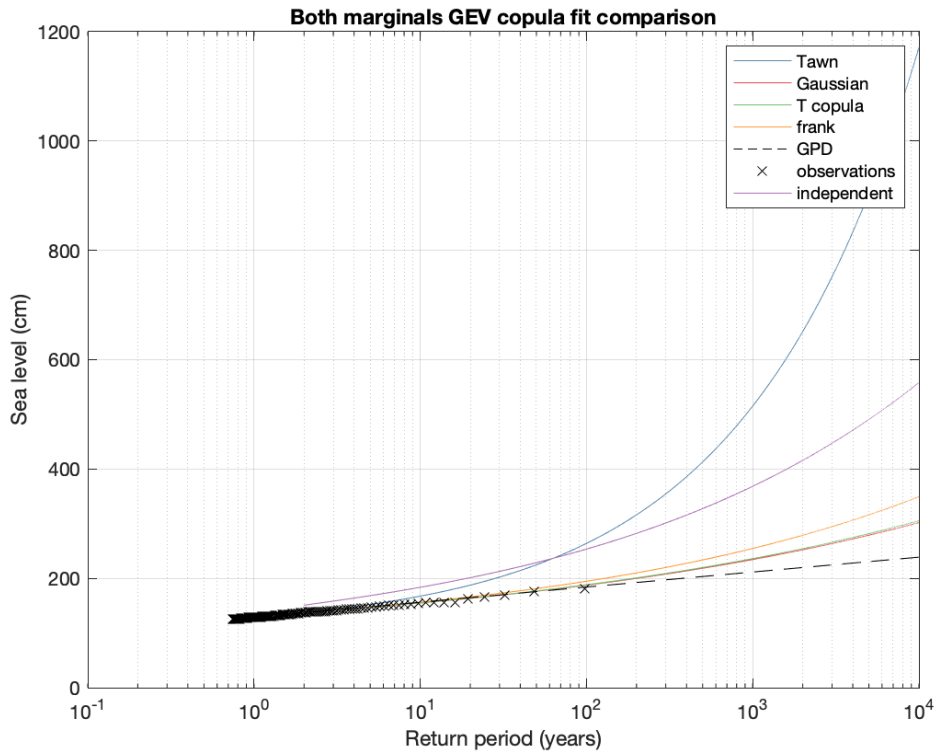
Figure 5.17: Return values for Punta della Salute resulting from the POT-GPD and from the combined analysis using the dependent Gaussian copula and the independent copula along with 95% confidence bands and extreme water level observations.

Method	m-year RP	Return value (cm)	Upper CI (cm)	Lower CI (cm)
Univariate GPD	100	184.11	204.57	167.82
	1000	211.58	263.67	177.85
	10000	238.76	330.24	189.68
Gaussian copula	100	187.57	209.94	172.29
	1000	234.44	301.38	195.69
	10000	301.95	467.09	222.05
T copula	100	188.27	213.09	172.48
	1000	236.09	306.63	195.98
	10000	305.40	475.92	222.65
Tawn copula	100	263.94	322.93	223.86
	1000	515.16	819.08	344.06
	10000	1171.15	2476.80	581.11
Frank copula	100	194.67	228.39	176.54
	1000	254.71	348.52	207.05
	10000	349.39	580.04	244.87
Independent copula	100	253.55	316.23	218.90
	1000	368.41	574.05	272.65
	10000	558.03	1130.79	340.90

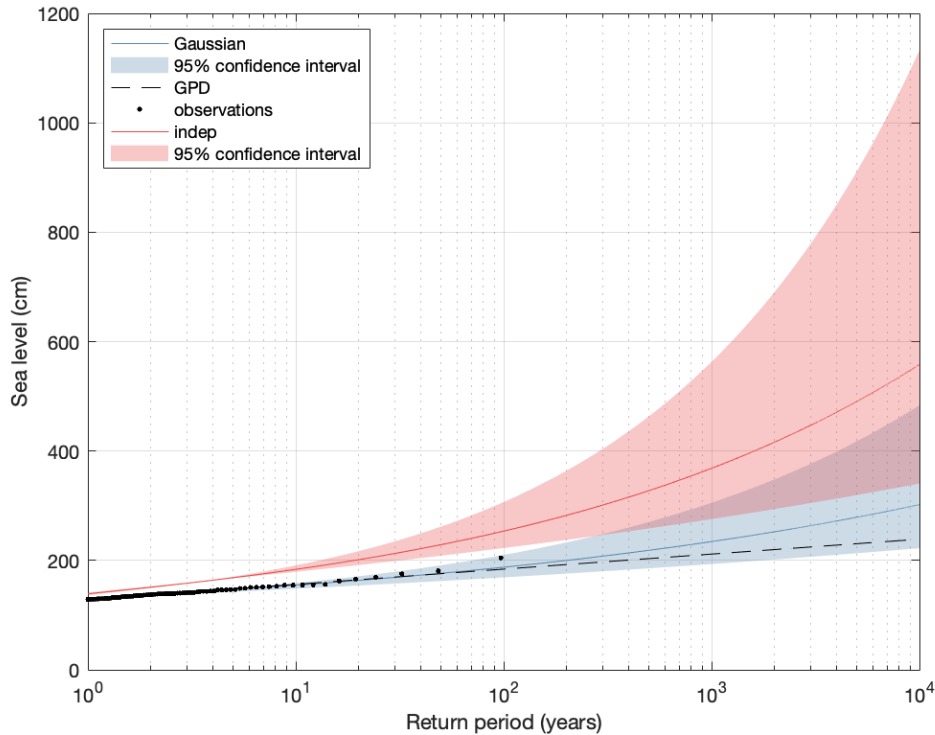Table 5.9: m-year return values for different approaches

Figure 5.18: Return value plot as result from bivariate copulas and univariate GPD.

The Gaussian copula and the Frank copula use a correlation coefficient of $\tau - 0.6$, more representative of the found correlation of -0.61. The T copula reported a correlation coefficient of $\tau = -0.59$, while the 90° rotated Tawn type 1 copula used $\tau = -0.52$. A comparison between the return values resulting from the independent copula, the Gaussian copula, and the univariate GPD return values is represented in Figure 5.18. The influence of dependence on return values is represented in the higher return values for the independent copula.

The relative difference between the POT-GPD return values to those resulting from the combined analysis using the Gaussian copula are found in Table 5.10 along with those of the combined analysis from the independent copula relative to those from the Gaussian copula. Relative difference between the 100 and 1000-year return period of the GPD-POT

Method	m-year RP	Return value (cm))
	100	-0.018
Univariate GPD	1000	-0.098
	10000	-0.21
	100	0.35
Independent copula	1000	0.57
	10000	0.85

Table 5.10: relative difference for m-year return values for the univariate GPD and the independent copula relative to that of the Gaussian copula method.

approach and the results from the combined analysis using the Gaussian copula are smaller than 10%. This difference gets larger for the 10000-year return values. This is a result of the difference in tail between the two distribution functions. The GPD parameters are $\xi = -0.0046$ and $\sigma = 12.31$ and for the GEV fit to the Gaussian copula samples are $\xi = -0.160$, $\sigma = 6.93$ and $\mu = 125$.

Lastly the influence of the projected sea level rise on return values is shown in Figure 5.19. This figure indicates how the current 100-year return value changes over time due to the effects of SLR for different SSP scenarios. The difference in height between a 100-year return level and a 200-year return level is 6 cm. This means that after 6cm of SLR, what is now considered a 200-year return-level will be expected to occur on average once every 100 years instead. Depending on the SSP scenario, the SLR in 2100 will be in the range of 14 to 119 cm. This indicates the large influence a relatively small amount of relative sea level rise has on the average rate of occurrence of extreme water level events.
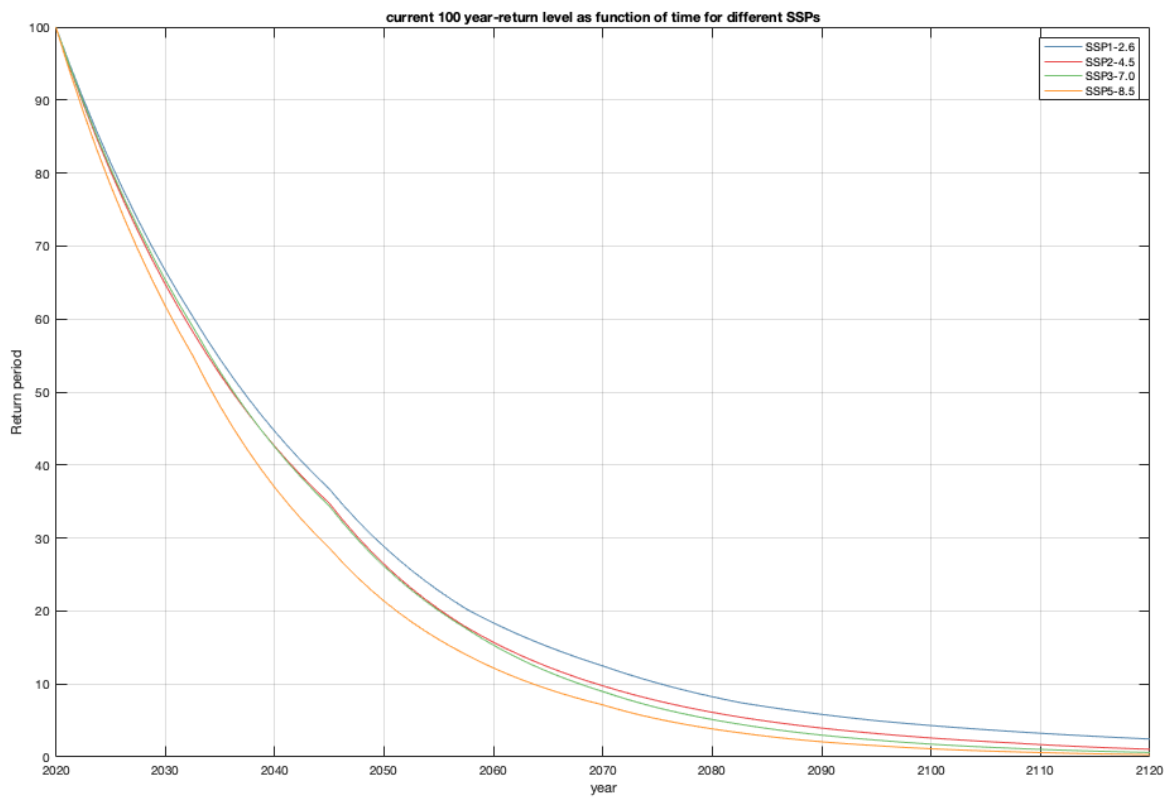

Figure 5.19: Return period as function of time

6

Discussion and Recommendations

This thesis presents an estimation of extreme water levels for Venice, including a new approach to account for trends in water level time-series using a Bayesian algorithm for signal decomposition. In addition, the use of copulas functions to describe the dependence between storm surge and tide was evaluated for a combined extreme value analysis was evaluated. This chapter will underline and discuss the results of this method.

The modelling of this tide-surge relationship for shallow coastal regions is valuable in the light of climate change. That is because this relationship will change for many (shallow) coastal regions in the future due to a changing bottom depth caused by sea level rise affecting the impact of non-linear interactions. This relationship between tide and surge affects extreme water levels and for many shallow coastal regions this interaction results in lower extreme water levels. Therefore, successfully describing this relationship can increase the accuracy of extreme water level estimation to benefit flood hazard assessment.

The investigation into the use of copulas for a combined analysis including dependence between tide and surge is a step towards a combined analysis taking into account temporal variation of the dependence.

6.1. Exploratory analysis

Large differences of mean water level between the start and the end of the Punta della Salute time-series were reported. These were higher than the average global sea level rise over a longer period spanning these measurements.

A potential explanation for this difference is the effects of anthropogenic subsidence. Based on these large differences a trend analysis using the Mann-Kendall monotonic trend test was performed, which allowed for the evaluation of (non-)stationarity over different periods in time. The results of these tests reported a statistically significant trend over most of the longer periods of time. The Sen slope calculated during these periods gives indications of the periods during which the trend was relatively the largest. These results indicate the greatest subsidence during the period 1950-1969 and the greatest uplift during 1970-1975. The non-stationarity and the subsidence and uplift during these periods agree with what is known from the literature.

During 1950-1969, the most severe period of subsidence was reported in Venice; the cause of this subsidence was groundwater withdrawal for the port close to the city. This

was followed by a period of uplift starting in 1970-1975, during which the aquifers below the city were actively being restored.

This shift between slopes led to further investigation using changepoint analysis methods; RHtest and BEAST. Both methods were considered in order to compare and evaluate their use in the exploratory analysis of the time-series.

Both methods found changepoints in the Punta della Salute time-series which could be attributed to anthropogenic subsidence. The 05-1972 changepoint found by the RHtest coincides with the largest consistent downward slope in the decomposed trend of the time-series. All the changepoints found using the RHtest method were also found by applying the BEAST method to the same time-series. More changepoints were identified using the BEAST method, as this method detects shifts in mean and trend as opposed to only the mean by the RHtest. Additionally, changepoint analysis using BEAST (combined with reference time-series of Marghera, Piattaforma Acqua Alta and Trieste) allowed for the separation of local- and large-scale events attributed to sudden shifts or changes in trend and seasonality.

The changepoint analysis using the BEAST method revealed a very large overlap of changepoints between all considered time-series (Punta della Salute, Marghera, Piattaforma Acqua Alta and Trieste). The overlap in changepoints indicates that mainly large-scale events have affected the time-series. Similarly, unique changepoints can be linked to local-scale events. In this way, unique changepoints could be attributed to local-scale events such as construction works next to the tide-gauge. Using this method, the influence of recorded events was confirmed to be present in the time-series data. Furthermore the 1968 changepoint which was attributed to local causes can be tied to the period of the largest (anthropogenic) subsidence of 14 mm / y [Tosi et al., 2002][Carbognin et al., 2004]. Using the changepoint analysis especially large-scale events can be captured. More changepoints attributed to local events were expected considering the long history of anthropogenic intervention in and near the city of Venice as outlined in the literature study. This is most likely due to atmospheric effects causing larger and more sudden changes in water level observations as compared to anthropogenic subsidence.

Under the assumption of an equal amount of sea level rise between the Trieste and Punta della Salute time-series, the influence of vertical land motion was isolated. The resulting trend of Vertical Land Motion for the city of Venice shows behaviour that agrees with literature regarding upward and downward slopes during certain time frames. Changepoint analysis provides useful information, especially in combination with trend decomposition and the use of reference series. Information about past events may help form a better understanding of the time-series and forecast future behaviour. The separation of VLM and sea level rise using trend decomposition using this method may be interesting for conducting research on the rise of global sea level. Since for this type of research, long-term tide-gauge observations are used as a primary source of information. At the moment, mostly tide-gauges that are located in areas of relatively stable land motion are used [Zervas et al., 2013]. The isolation of the vertical land motion component using reference series may increase the number of tide-gauge stations available for research on global sea level change.

The trend decomposition using the BEAST method was used to homogenize the time-series data. Many methods make use of a 19-year-centered running mean that is used to account for the metonic cycle and the lunar nodal cycle [Pirazzoli and Tomasin, 2002]

[Ferrarin et al., 2022]. Regression, moving mean and filtering all are problematic in dealing with non-linear non-stationary data [Wu et al., 2007]. The difference between the decomposed trend and the moving mean, in particular, is that the decomposed trend is much less smooth than a 19-year moving average. This is also where large differences between BEAST and RHtest can be observed. RHtest uses linear regression in between changepoints to approximate trend over the entire time-series. However, when a trend is non-linear this approximation does not represent the true trend accurately. A comparison between the two changepoint analysis methods indicates that the BEAST method is more suited when approximating time-series containing non-linear behaviour and may therefore be beneficial for time-series homogenization.

While the Bayesian ensemble algorithm BEAST brings forward interesting results in changepoints analysis and signal decomposition, a form of caution must be taken in interpreting their results. While some timings of change-points as analyzed by RHtest and BEAST were linked to historical events, their timings may be coincidental. This highlights one of the difficulties in using changepoint analysis methods, which is the validation of the result. In this study, BEAST was used to correct for anthropogenic vertical land motion and the decomposed trend was used, in which trends from the literature and recorded extreme events were recognized. While such a decomposed trend may agree with expected values, it may not represent the true trend.

6.2. Combined Analysis of Tide and Surge

In shallow coastal regions, interdependence between tide and storm surge is likely, and this relationship was quantified for the Punta della Salute time-series. A negative dependence between tide and storm surge was found to be -0.61, comparable to the dependence found elsewhere [Ferrarin et al., 2022]. When considering the plot of isolines, the 1966 acqua alta follows the reported negative dependence. This acqua alta was a combination of one of the lowest tides in our ESL observations combined with the highest storm surges on record. The 2019 event shows a very different behaviour. Although this acqua alta is still paired with one of the highest storm surges on record, it occurred along with a relatively high tide. Interestingly, the negative dependence is less evident for the most exceptional extreme events. This was an unexpected finding and could not be explained. This could be further explored by performing research on how tide-surge interactions affect the maximum extreme water levels in shallow coastal regions. The shapes of the chosen copula functions were consistent with the tide and NTR samples. However, the difference in results for other copula selection methods, such as the inference function of margins (IFM) method [Wainwright, 2005] [Pons et al., 2021] and the semiparametric method (SP) [Kim et al., 2007] were not included in this analysis and may be interesting to investigate in the future.

Using the peak-over-threshold (POT) method for the selection of extreme events and the separation of tide and surge components of these extremes in the combined analysis resulted in sampled extreme water levels below the threshold. This is a result of new combinations from the marginal distributions of tide and surge that allowed combinations below the threshold value and is also shown in section A.2. This problem was solved by removing values below the threshold and by resampling from the samples above this threshold. Using this approach combined with the use of the GEV for both marginal distributions, the

GEV was chosen to best resemble the sampled extreme water levels as opposed to the expected generalized Pareto distribution. The problem with generating new samples below the threshold was unexpected; investigation into using the Annual Maxima method for the selection of extremes as opposed to the POT method is therefore recommended, as this circumvents this problem.

Although the AIC and BIC scores of the copula were quite similar, large differences were found in the return value estimates. The Tawn copula reported as the third-best copula fit generated exceptionally large return values, exceeding the independent copula. This emphasizes the importance of the copula selection process. These large differences may be attributed in part to its difference in Kendall τ correlation, compared to the other copulas considered. A large difference could be seen between the independent and dependent copulas. This was to be expected, as for the independent copula, any tide can occur during any storm surge.

The return value plot of the combined analysis of the Gaussian copula function suggests that this model is appropriate for the observations. It also shows that these are compatible with those of the univariate analysis.

In this study it was assumed that the distribution of extremes are independent on sea level rise. However, SLR causes a redistribution of the ocean's mass to change the location of amphidromic points, altering tidal characteristics. Additionally, climate change also affects local storminess, leading to different storm surge behavior over time. This increase in storminess may be even more important to include in the Adriatic, as it can also lead to different behavior of Sieches in the basin (Adriatic). Lastly, SLR will influence the bottom depth and therefore also the non-linear interactions between tide and surge. Temporal variation of these two components as well as the dependence should be accounted for to improve accuracy of extreme water level estimation.

To further improve the accuracy of the combined analysis using copula functions, this non-stationarity should be accounted for in the analysis. In a combined analysis one can work with time-dependent marginal distributions in order to account for non-stationarity in the tidal and surge components. These marginal distributions contain time dependent location and/or scale parameters $\mu(t)$, $\sigma(t)$.

Additionally, an approach may be to include the temporal variation of the dependence between the tide and surge components. A time-varying copula function can be used to describe the temporal variation of dependence between tide and surge as the affects of non-linear interactions change due to a changing bathymetry.

Lastly, in this study, tide-gauge observations from 1924-2020 were used. The San Stefano tide-gauge began operation in 1872 within a relatively short distance (1km) of the currently used tide-gauge Punta della Salute. It is recommended to investigate the inclusion of the observations of this tide-gauge to the Punta della Salute observations to increase the length of the observational period. This may increase accuracy of extreme water level estimation and is especially useful when considering a non-stationary analysis in the future, as this method of analysis increases the level of uncertainty.

7

Conclusion

This final chapter explains the outcome of the proposed research objective. In addition, the sub-questions are answered as stated in chapter 1. The main objective of this thesis was to:

Quantify the influence of tide-surge interaction on extreme sea level estimates and investigate the use of copulas in extreme sea level estimation as compared to extreme sea level estimation using a univariate approach.

The main conclusions of this report are as follows.

- The dependence between storm surge and tide is statistically significant and quantified. The Pearson r correlation coefficient reports a value -0.81 and the Kendall τ correlation reports a value of -0.61. This negative dependence means that, during extreme events, the highest storm surges are more likely to occur during low tide. The non-linear (tide-surge) interactions in the shallow lagoon result in a lowering of the extreme sea level. This is confirmed from the combined analysis of tide and surge using a copula functions. From this combined analysis it can be seen that higher return values are reported using a copula function that excludes this dependence.

- Extreme water level estimates from the combined analysis of the tidal and surge signal using the copula function report higher return values than those resulting from the univariate analysis. These two methods are compatible considering the small relative difference in the return values between the two. This gives confidence in the combined analysis, which accounts for the dependence between the tide and surge water level components. This is a promising approach for the integration of tide-surge dependence in extreme water level estimation. As this work focused only on a stationary approach, in the light of climate change opportunities to consider are adapting this method for the inclusion of non-stationarity.

- Trend analysis of the Punta della Salute time-series report statistically significant monotonic trend over the entire period of observations. When comparing the mean sea level between 1924 and 2021, a relative sea level rise of 2.882 mm/y is found. This rate is much higher than both reported global sea level rise of 1.743 mm/y and the relative sea level rise for Venice of 1.23 ± 0.13 mm/y. Under an assumption of equal sea level rise between Venice and Trieste and using the changepoint analysis and trend decomposition allowed for separation of the vertical land motion from

the relative sea level rise. By doing so, this study finds a sea level rise rate of 1.431 mm/y. 1.458 mm/y could be attributed to vertical land motion over this same period, of which 1.058 was caused by anthropogenic subsidence assuming the constant rate of 0.4 mm/y resulting from natural processes. This leads to a total anthropogenic subsidence of 10.26 cm. Long-term anthropogenic subsidence is no longer present, however short-term effects of human-induced effects are still occurring and can be traced back in the time-series.

Lastly, the sub-questions are answered below.

1. How can the (non-)stationarity of a time-series be evaluated?

   Non-stationarity can be evaluated using trend analysis like the non-parametric Mann-Kendall (MK) test. In the case were a statistical significant monotonic trend is found there is a temporal change in mean. Alternatively, one can test for stationarity using the two common tests; Augmented Dickey-Fuller test (ADF Test) and Kwiatkowski-Phillips-Schmidt-Shin test (KPSS test)

2. How can the tide and non-tidal components of the water level be separated from each other?

   The separation of these two components is based on the deterministic nature of the tide. Using harmonic analysis, a Fourier series approach, the phases and amplitudes of tidal constituents can be determined and the tide can be reconstructed. In this thesis, 64 tidal constituents are considered and tidal reconstruction is performed using U_tide. Removing the (reconstructed) tidal signal from the signal of water level observations separates the time-series into a tidal and a non-tidal signal (or non-tidal residual).

3. How can the relationship between tide and surge be quantified?

   The correlation is the degree to which two variables are linearly related. The three most comment methods to quantify the relationship between two variables, are the Pearson r correlation coefficient, the Spearman ρ rank correlation coefficient and the Kendall τ rank correlation. These methods all quantify correlation; however, they quantify correlation in a different way. Pearson's correlation measures the strength of the linear relationship between two variables. The Spearman rank correlation and the Kendall rank correlation measure the strength of monotonic relationship between variables.

4. How is extreme value analysis performed when tide and storm surge depend on each other?

   In this work, this was performed using the POT method to select extremes water level observations. Marginal distributions were fit to the tide and surge water level components of these extreme water level observations. After transforming both distributions into uniform marginal distributions, a suitable copula function will need to be found to describe the dependence between the two. Using the copula function and uniform marginal distributions, new tide and surge samples can be generated. Extreme sea level estimates are calculated using the combination of these samples to generate samples of extremes.

5. What should be the selection criteria of a copula function?

   Copula sampling should be based on (relative) goodness-of-fit criteria like the AIC, BIC and log likelihood scores and also on how well the dependence parameter of the copula function represents the true correlation coefficient between the observations.

6. How can the influence of the relationship between tide and non-tidal residual on extreme water level estimations be quantified?

   A comparison can be made between extreme water level estimation resulting from a copula with a dependence parameter $\neq 0$ and the results from extreme water level estimation using the independent copula. The difference between the return values is due to the impact of the tide-surge interactions on the water level.

Supplementary Material

Additional changepoint analysis results

The results of the Beast method for the Punta della Salute time-series and the Marghera time-series are shown in Figure A.1. Results from the Trend decomposition show similar behaviour of trend between Punta della Salute and Marghera. The changepoint identified using in 09-1993 in the Punta della Salute is not found in the similar time-series of the Marghera station, however this changepoint was found in the Trieste time-series.
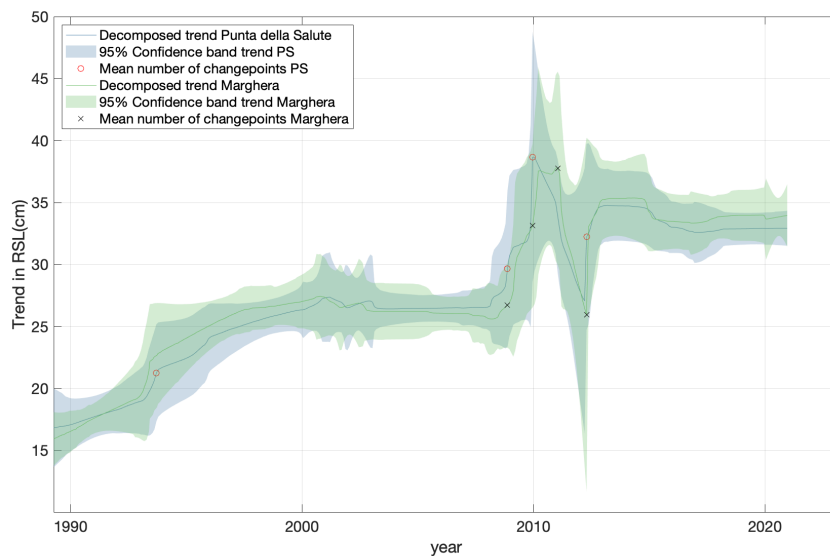

Figure A.1: Changepoints and the decomposed trend and its confidence band of the Punta della Salute and Marghera time-series

and for the Punta della Salute and Piattaforma Acqua Alta (PFAA) results of the BEAST trend decomposition and changepoint analysis is shown in Figure A.2. More changepoints are found in the PFAA time-series than in that of the Punta della Salute time-series. The difference is due to the more extreme conditions at these measurement stations as compared

Figure A.2: Changepoints and the decomposed trend and its confidence band of the Punta della Salute and Piattaforma Acqua Alta time-series

to that of Punta della Salute of which the tide-gauge is located in the shallow Venice lagoon. This can also be seen in the decomposed trend of the PFAA time-series which shows the same local maxima and minima that of the Punta della Salute time-series but in this time-series these are more extreme.

Lastly the RHtest results are shown for the Trieste and Marghera time-series in Figure A.3 and Figure A.4
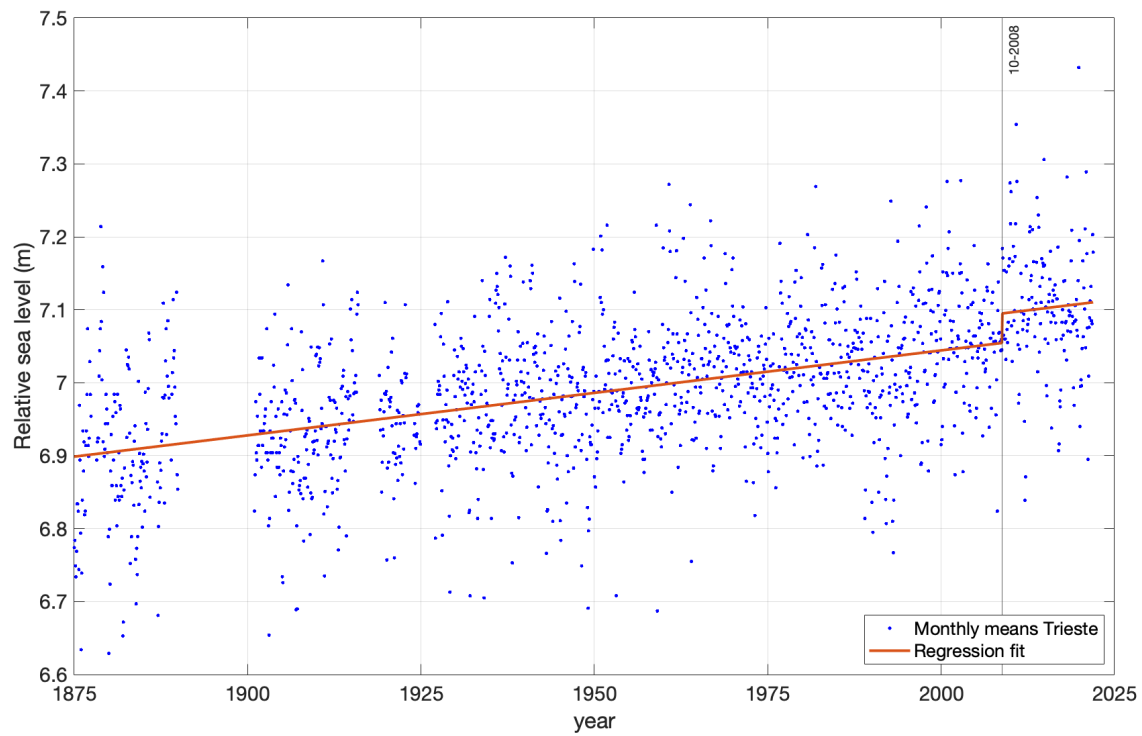
Figure A.3: RHtest changepoint analysis results of the Trieste time-series.
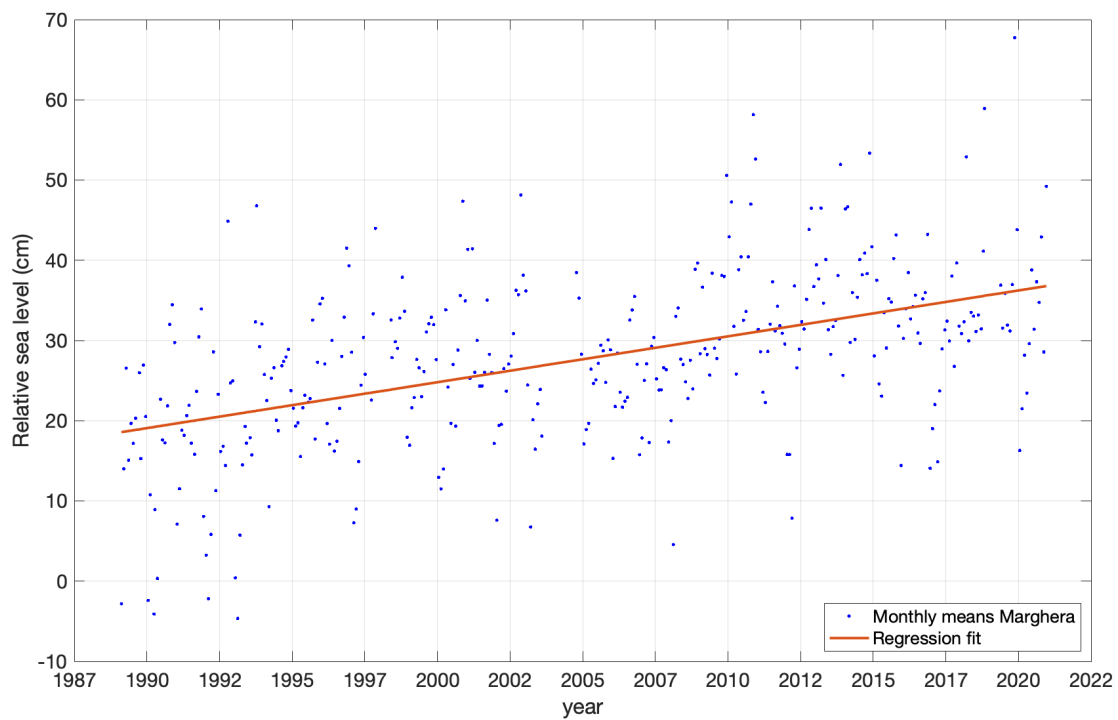

Figure A.4: RHtest changepoint analysis results of the Marghera time-series.
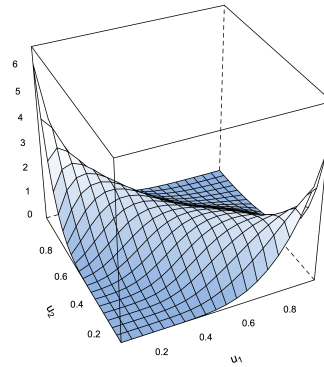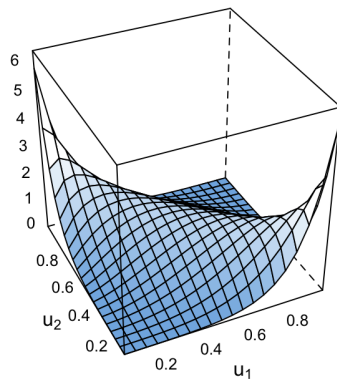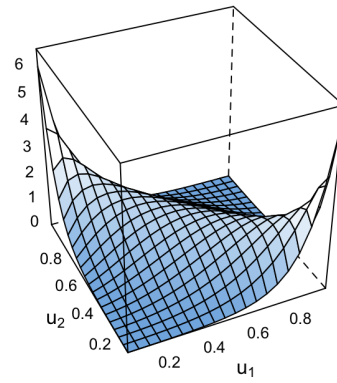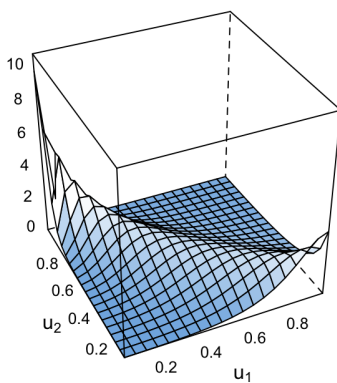
A.1. Copula densities

Figure A.5: Kernel estimate of bivariate copula density of transformed observations where u_1 and u_2 are NTR and tide transformed to $U[0,1]$.
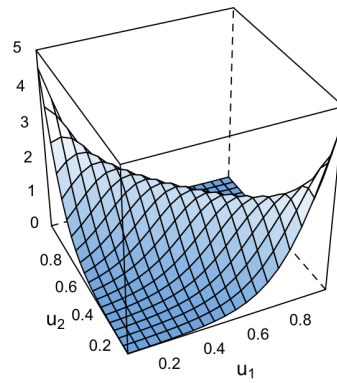

(a) Gaussian Copula fit p = -0.81

(b) student t Copula fit p1 = -0.88, p2 = 30

(c) Tawn type 1 rotated 90°, p1 = -3.12, p2 = 0.71

(d) Frank copula fit, p1 = -7.81

Figure A.6: Density plots of the four best copula fits where u_1 and u_2 are NTR and tide transformed to $U[0,1]$.

A.2. Sampled extremes below threshold

The figures below show the extremes resulting from the combination of the sampled tide and surge from the Gaussian copula function Figure A.7 and the independent copula function Figure A.8. For sampling from dependent copula, 10% of the combination of generated tide and surge are below the threshold value of $u = 116cm$, for the independent copula 30% was below this threshold value.
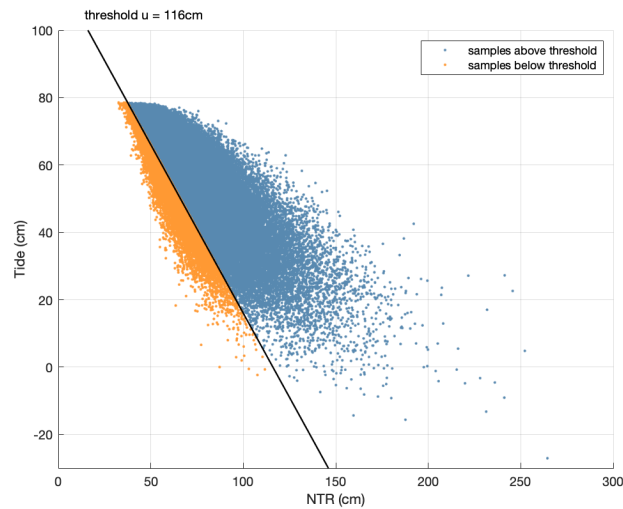
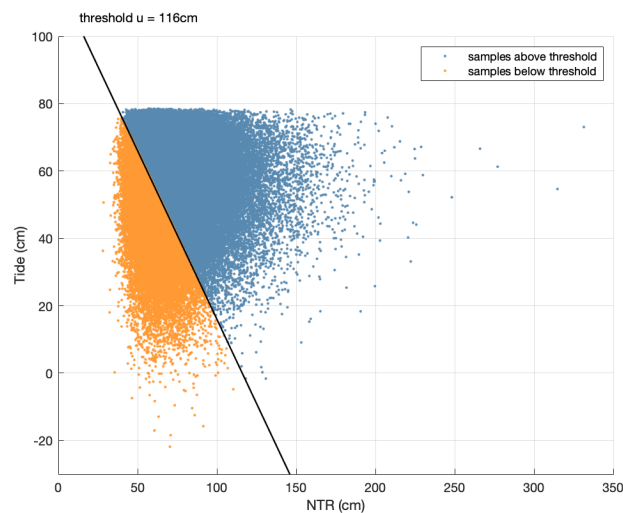Figure A.7: Generated Gaussian copula samples with indicated POT threshold

Figure A.8: Generated independent copula samples with indicated POT threshold

A.3. VineCopula copula families

Via the VineCopula, many different multivariate copula families can be fit to marginal distribution functions. Below is the list of all multivariate copula families which are included in VineCopula. Only copulas able to capture negative dependence were tested for fit.

- independence copula
- Gaussian copula
- Student t copula (t-copula)
- Clayton copula
- Gumbel copula
- Frank copula
- Joe copula
- BB1 copula
- BB6 copula
- BB7 copula
- BB8 copula
- rotated Clayton copula (180 degrees; survival Clayton")
- rotated Gumbel copulavival Gumbel")
- rotated Joe copula (180 degrees; survival Joe")
- rotated BB1 copula (180 degreevival BB1")
- rotated BB6 copula (180 degrees; survival BB6")
- rotated BB7 copula (180 degreevival BB7")
- rotated BB8 copula (180 degrees; "survival BB8")
- rotated Clayton copula (90 degrees)
- rotated Gumbel copula (90 degrees)
- rotated Joe copula (90 degrees)
- rotated BB1 copula (90 degrees)
- rotated BB6 copula (90 degrees)
- rotated BB7 copula (90 degrees)
- rotated BB8 copula (90 degrees)
- rotated Clayton copula (270 degrees)
- rotated Gumbel copula (270 degrees)
- rotated Joe copula (270 degrees)
- rotated BB1 copula (270 degrees)
- rotated BB6 copula (270 degrees)
- rotated BB7 copula (270 degrees)
- rotated BB8 copula (270 degrees)
- Tawn type 1 copula
- rotated Tawn type 1 copula (180 degrees)
- rotated Tawn type 1 copula (90 degrees)
- rotated Tawn type 1 copula (270 degrees)
- Tawn type 2 copula
- rotated Tawn type 2 copula (180 degrees)
- rotated Tawn type 2 copula (90 degrees)
- rotated Tawn type 2 copula (270 degrees)

A.4. Tidal regime

Form factors were used to determine the tidal regime at the Punta della Salute tide-gauge, determined by the K_1, O_1, M_2 and S_2 constituents [Van Der Stock, 1897] [Courtier, 1938]. These constituents were calculated for this tide-gauge by the tidal harmonic analysis and reconstruction.

$$F = \frac{K_1 + O_1}{M_2 + S_2} \tag{A.1}$$

Four types of tidal regimes are classified. For the constituents in Table 5.4, Equation A.4 finds $0.25 < F < 2$, which is indicative of a mixed semi-diurnal regime. A mixed semi-diurnal regime is characterized by two daily high waters (HWs) and two daily low waters (LWs) of different heights.

A.5. Complications parametric methods

Using the kernel density estimator and the empirical cumulative distribution function, complications were encountered for different reasons. Using the empirical cumulative distribution function (ecdf), the sampling was performed as follows.

- An empirical cumulative distribution was made.

- The distribution was transformed to $U[0,1]$.

- VineCopula package was used to find copula functions for the dependence structure of the uniform marginal distributions.

- Samples were transformed back to physical quantities using the quantile function.

The quantile function can be used as the inverse cumulative distribution function of the ecdf and allows transformation from probability of occurrence to physical quantities. The problem encountered originates from the linear interpolation used by the quantile function. As the ecdf is a step-wise function, linear interpolation is used in order to be able to generate points in between observations. This interpolation was performed as follows.

$$y = f(x) = y_1 + \frac{x - x_1}{x_2 - x_1}(y_2 - y_1), \tag{A.2}$$

where $f(x)$ is the value of interest with x between two points x_1, x_2 for known data points (x_1, y_1), (x_2, y_2) where $y_1 = f(x_1)$ and $y_2 = f(x_2)$. The linear interpolation will cause problems at the outer edges, as there is no next point to perform the linear interpolation. The result was that for all probabilities in $[1 - \frac{1}{2n}, 1]$ that are transformed using the quantile function, the same value equal to the highest extreme observed is assigned. The same holds for the interval $[0, \frac{1}{2n}]$. As a consequence, there will be clustering of the maxima and minimum observed extremes. In Figure A.9a this clustering is shown for the highest NTR value.

Using the kernel density estimator lead to complications when sampling non-tidal residual due to the large difference between the highest observed NTR (193cm) and the second highest NTR (138cm). This resulted in a lack of observations between these highest NTR events; this is highlighted in Figure A.9b
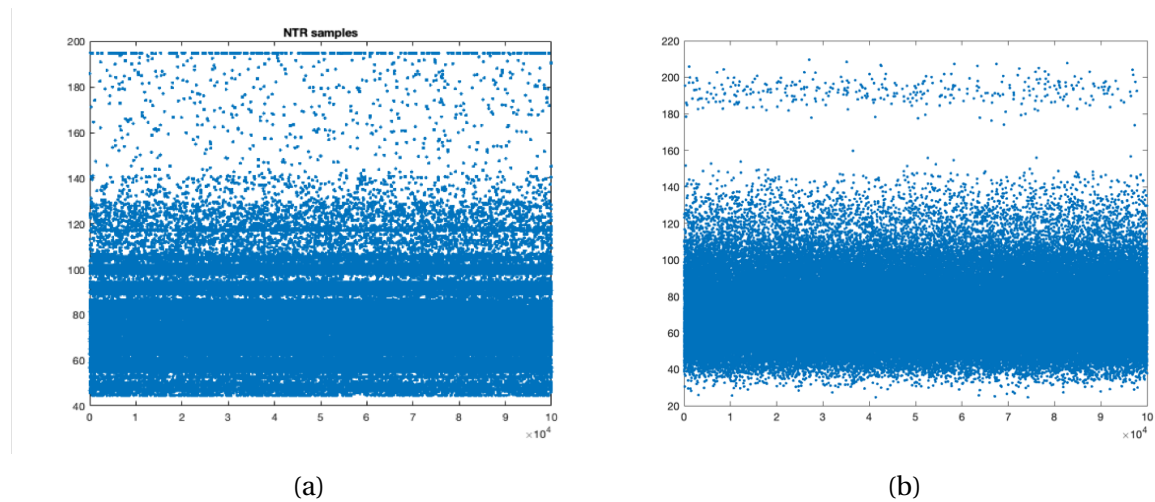
Figure A.9: Copula samples of contribution to sea level (cm) of non-tidal residual using the (a) ecdf as marginals and (b) KDE for marginals

A.6. Verification of seasonal decomposition of the BEAST method

The accuracy of seasonal decomposition using the BEAST method was tested by comparing the decomposed seasonal signal as per beast and comparing it with results from a stable seasonal filter. This stable seasonal filter is applied to the monthly RSL observations and composed of the means per month (e.g. mean of all January means) after detrending using a 13-term moving average [Brockwell and Springer, 2002]. This seasonal filter is then centered around 0 and compared to the decomposed seasonal signal resulting from the BEAST method. The difference in results from both methods can be seen in Figure A.10a. Following this procedure, trend decomposition was performed by BEAST after removing seasonal trend using BEAST trend decomposition and by deseasonalization using the stable filter. These results can be found in Figure A.10b.
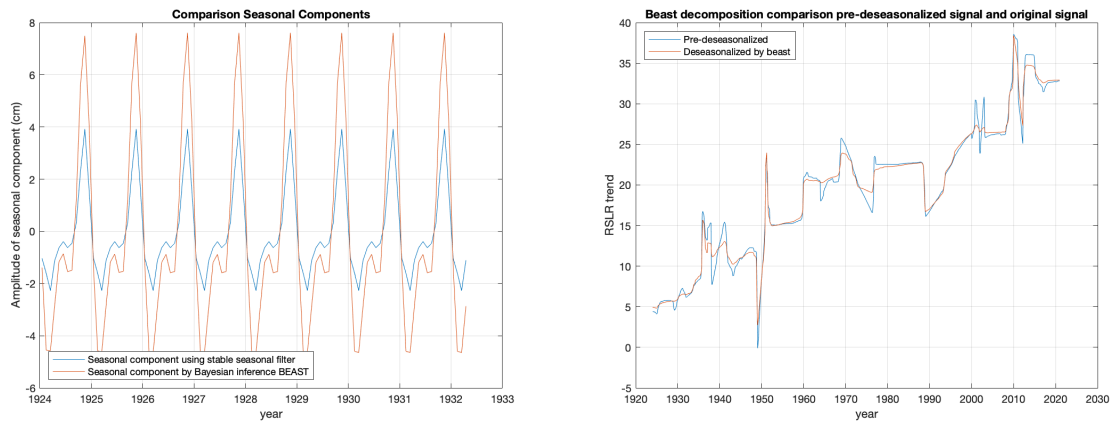
(a) Comparison between stable filter and the piece-wise harmonic function resulting from BEAST

(b) Comparison between decomposed trends for pre-deseasonalized signal and unaltered signal

Figure A.10: Verification of decomposition using the BEAST method

One of the problems of MCMC sampling is that subsequent samples are correlated. This is because each subsequent sample is based on the current sample. To prevent autocorrelation in the sampling process, a thinning factor was applied. A thinning factor reduces the amount of correlation by thinning out the Markov Chain. The sensitivity to thinning factors of 1, 3, 5, 10 was tested, meaning when sampling 1, 3, 5 or 10 samples are discarded before taking a next sample. Furthermore, the user defined input for minimum and maximum number of changepoints from which sampling is performed was varied. With the minimum set to 0, sensitivity to the maximum number of changepoints was investigated. Decomposition was performed for a maximum number of 10, 20, 30, 40, 50 and 100 changepoints.

Bibliography

[Aditya et al., 2021] Aditya, F., Gusmayanti, E., and Sudrajat, J. (2021). Rainfall trend analysis using Mann-Kendall and Sen's slope estimator test in West Kalimantan. In IOP Conference Series: Earth and Environmental Science, volume 893. IOP Publishing Ltd.

[Akaike, 1974] Akaike, H. (1974). A new look at the statistical model identification. IEEE Transactions on Automatic Control, 19(6):716–723.

[Antonioli et al., 2009] Antonioli, F., Ferranti, L., Fontana, A., Amorosi, A., Bondesan, A., Braitenberg, C., Dutton, A., Fontolan, G., Furlani, S., Lambeck, K., Mastronuzzi, G., Monaco, C., Spada, G., and Stocchi, P. (2009). Holocene relative sea-level changes and vertical movements along the Italian and Istrian coastlines. Quaternary International, 206(1-2):102–133.

[Arns et al., 2020] Arns, A., Wahl, T., Wolff, C., Vafeidis, A. T., Haigh, I. D., Woodworth, P., Niehüser, S., and Jensen, J. (2020). Non-linear interaction modulates global extreme sea levels, coastal flood exposure, and impacts. Nature Communications, 11(1).

[Batstone et al., 2009] Batstone, C., Lawless, M., Horburgh, K., Blackman, D., and Tawn, J. (2009). Calculating Extreme Sea Level Probabilities Around Complex Coastlines: A Best Practice Approach. Technical report.

[Bergant et al., 2005] Bergant, K., Sušnik, M., Strojan, I., and Shaw, A. G. (2005). Sea level variability at Adriatic coast and its relationship to atmospheric forcing. Annales Geophysicae, 23(6):1997–2010.

[Bevilacqua, 2009] Bevilacqua, P. (2009). Venice and the Water: A Model for Our Planet. Polar Bear & Company.

[Bowman and Azzalini, 1999] Bowman, A. W. and Azzalini, A. (1999). Applied Smoothing Techniques for Data Analysis: The Kernel Approach with S-PLUS Illustrations. Journal of the American Statistical Association, 94(447):982.

[Brambati et al., 2003] Brambati, A., Carbognin, L., Quaia, T., Teatini, P., and Tosi, L. (2003). The Lagoon of Venice: Geological setting, evolution and land subsidence. Episodes, 26(3):264–265.

[Brockwell and Springer, 2002] Brockwell, P. J. and Springer, R. A. D. (2002). Introduction to Time Series and Forecasting, Second Edition. Technical report.

[Caires, 2011] Caires, S. (2011). Extreme value analysis: Still water level. JCOMM Technical Report, 58.

[Camuffo et al., 2006] Camuffo, D., Colacino, M., Enzi, S., Cocheo, C., Pagan, E., and Sturaro, G. (2006). Extreme events in Italy from documentary sources: Venice as a case study(*). 29.

[Carbognin et al., 2010] Carbognin, L., Teatini, P., Tomasin, A., and Tosi, L. (2010). Global change and relative sea level rise at Venice: What impact in term of flooding. Climate Dynamics, 35(6):1055–1063.

[Carbognin et al., 2004] Carbognin, L., Teatini, P., and Tosi, L. (2004). Eustacy and land subsidence in the Venice Lagoon at the beginning of the new millennium. Journal of Marine Systems, 51(1-4 SPEC. ISS.):345–353.

[Carbognin et al., 2005] Carbognin, L., Teatini, P., and Tosi, L. (2005). Land Subsidence in the Venetian area: known and recent aspects. Giornale di Geologia Applicata, 1:5–11.

[Carbognin and Tosi, 1995] Carbognin, L. and Tosi, L. (1995). Land subsidence and degradation of the Venice littoral zone, Italy. Technical Report 234.

[Casella and Berger, 1990] Casella, G. and Berger, R. L. (1990). Statistical inference, volume 1. Duxbury Press.

[Cavaleri, 2000] Cavaleri, L. (2000). The oceanographic tower Acqua Alta-activity and prediction of sea states at Venice. Technical report.

[Cavallaro et al., 2017] Cavallaro, L., Iuppa, C., and Foti, E. (2017). Effect of partial use of venice flood barriers. Journal of Marine Science and Engineering, 5(4).

[Codiga, 2011] Codiga, D. L. (2011). Unified tidal analysis and prediction using the UTide Matlab functions.

[Coles, 2001] Coles, S. . (2001). An introduction to statistical modeling of extreme values. Springer, London.

[Coles and Simiu, 2003] Coles, S. and Simiu, E. (2003). Estimating Uncertainty in the Extreme Value Analysis of Data Generated by a Hurricane Simulation Model.

[Courtier, 1938] Courtier, A. (1938). Classification of tides in four types. Technical report, Service Hydrographique de la Marine, Paris.

[Davolio et al., 2015] Davolio, S., Stocchi, P., Benetazzo, A., Bohm, E., Riminucci, F., Ravaioli, M., Li, X. M., and Carniel, S. (2015). Exceptional Bora outbreak in winter 2012: Validation and analysis of high-resolution atmospheric model simulations in the northern Adriatic area. Dynamics of Atmospheres and Oceans, 71:1–20.

[Day et al., 1998] Day, J. W., Scarton, F., Rismondo, A., and Are, D. (1998). Rapid Deterioration of a Salt Marsh in Venice Lagoon, Italy. Technical Report 2.

[De Biasio et al., 2020] De Biasio, F., Baldin, G., and Vignudelli, S. (2020). Revisiting vertical land motion and sea level trends in the northeastern adriatic sea using satellite altimetry and tide gauge data. Journal of Marine Science and Engineering, 8(11):1–24.

[Deltares, 2021] Deltares (2021). Delft3D 3D/2D modelling suite for integral water solutions User Manual TIDE. Technical report, Deltares, Delft.

[Duan et al., 2022] Duan, G., Gong, H., Chen, B., Li, X., Pan, X., Shi, M., and Zhang, H. (2022). Spatiotemporal heterogeneity of land subsidence in Beijing. Scientific reports, 12(1):15120.

[Edwards, 1972] Edwards, A. W. F. (1972). Likelihood. University Press.

[Emery and Aubrey, 1991] Emery, K. O. and Aubrey, D. G. (1991). Sea Levels, Land Levels, and Tide Gauges. Springer New York.

[Far et al., 2016] Far, S. S., Khairi, A., and Wahab, A. (2016). Evaluation of Peaks-Over-Threshold Method.

[Ferrarin et al., 2022] Ferrarin, C., Lionello, P., Orlić, M., Raicich, F., and Salvadori, G. (2022). Venice as a paradigm of coastal flooding under multiple compound drivers. Scientific Reports, 12(1).

[Furlani et al., 2011] Furlani, S., Biolchi, S., Cucchi, F., Antonioli, F., Busetti, M., and Melis, R. (2011). Tectonic effects on Late Holocene sea level changes in the Gulf of Trieste (NE Adriatic Sea, Italy). Quaternary International, 232(1-2):144–157.

[Gatto and Carbognin, 1981] Gatto, P. and Carbognin, L. (1981). The lagoon of venice: Natural environmental trend and man-induced modification. Hydrological Sciences Bulletin, 26(4):379–391.

[Godin G., 1970] Godin G. (1970). The resolution of tidal constituents. Technical report, Oceanographic Research Department of Energy, Mines and Resources, Ottawa.

[Hamed, 2008] Hamed, K. H. (2008). Trend detection in hydrologic data: The Mann-Kendall trend test under the scaling hypothesis. Journal of Hydrology, 349(3-4):350–363.

[Hamed and Rao, 1998] Hamed, K. H. and Rao, A. R. (1998). Hydrology A modified Mann-Kendall trend test for autocorrelated data. Technical report.

[Haugh, 2016] Haugh, M. (2016). IEOR E4602: Quantitative Risk Management. Technical report.

[Holthuijsen, 2007] Holthuijsen, L. H. (2007). Waves in Oceanic and Coastal Waters. Cambridge University Press.

[IOC, 2006] IOC (2006). Manual on sea level measurement and interpretation, v. IV: An Update to 2006; IOC. Manuals and guides; Vol.:14; 2006. Technical report.

[Jonkman, 2005] Jonkman, S. N. (2005). Global Perspectives on Loss of Human Life Caused by Floods. Technical report.

[Kendall, 1975] Kendall, M. (1975). Rank correlation methods. Charles Griffin, London, 4th edition.

[Kendall, 1938] Kendall, M. G. (1938). A new measure of rank correlation. Biometrika, 30(1-2):81–93.

[Kim et al., 2007] Kim, G., Silvapulle, M. J., and Silvapulle, P. (2007). Comparison of semi-parametric and parametric methods for estimating copulas. Computational Statistics and Data Analysis, 51(6):2836–2850.

[Kolmogorov, 1992] Kolmogorov, A. (1992). On the Empirical Determination of a Distribution Function. pages 106–113.

[Levin et al., 2017] Levin, D. A., Peres, Y., and Wilmer, E. L. (2017). Markov Chains and Mixing Times, second edition. Technical report.

[Lin et al., 2009] Lin, L., Wang, Y., and Zhou, H. (2009). Iterative Filtering as an alternative algorithm for Empirical Mode Decomposition. Technical report.

[Lionello et al., 2020] Lionello, P., Nicholls, R., Umgiesser, G., and Zanchettin, D. (2020). Introduction to the special issue Venice flooding and sea level: past evolution, present issues and future projections. Natural Hazards and Earth System Sciences Discussions, pages 1–12.

[Liu et al., 2020] Liu, T., Liu, S., and Shi, L. (2020). Time Series Analysis Using SAS Enterprise Guide SPRINGER BRIEFS IN STATISTICS. Technical report.

[Lopes and Dias, 2015] Lopes, C. L. and Dias, J. M. (2015). Assessment of flood hazard during extreme sea levels in a tidally dominated lagoon. Natural Hazards, 77(2):1345–1364.

[Lucey et al., 2022] Lucey, J. T. D., Gallien, T. W., and Gallien, T. (2022). Characterizing multivariate coastal flooding events in a semi-arid region: The implications of copula choice, sampling, and infrastructure. Technical report.

[Lyddon et al., 2018] Lyddon, C., Brown, J. M., Leonardi, N., and Plater, A. J. (2018). Flood Hazard Assessment for a Hyper-Tidal Estuary as a Function of Tide-Surge-Morphology Interaction. Estuaries and Coasts, 41(6):1565–1586.

[Mann, 1945] Mann, H. B. (1945). Nonparametric Tests Against Trend. Econometrica, 13(3):245–259.

[Masina et al., 2022] Masina, M., D'Ayala, D., and Antonini, A. (2022). Variations in monthly maximum gust speed at St Mary's, Isles of Scilly (UK). Earth and Space Science.

[Massey, 1951] Massey, F. J. (1951). The Kolmogorov-Smirnov Test for Goodness of Fit. Journal of the American Statistical Association, 46(253):68–78.

[Masson-Delmotte et al., 2021] Masson-Delmotte, V., P. Zhai, A. Pirani, S. L. Connors, C. Péan, S. Berger, N. Caud, Y. Chen, L. Goldfarb, M. I. Gomis, M. Huang, K. Leitzell, E. Lonnoy, J.B.R. Matthews, T. K. Maycock, T. Waterfield, O. Yelekçi, R. Yu, and B. Zhou (2021). The Physical Science Basis Summary for Policymakers Working Group I contribution to the Sixth Assessment Report of the Intergovernmental Panel on Climate Change. Technical report.

[Mawdsley and Haigh, 2016] Mawdsley, R. J. and Haigh, I. D. (2016). Spatial and temporal variability and long-term trends in skew surges globally. Frontiers in Marine Science, 3(MAR).

[Međugorac et al., 2015] Međugorac, I., Pasarić, M., and Orlić, M. (2015). Severe flooding along the eastern Adriatic coast: the case of 1 December 2008. Ocean Dynamics, 65(6):817–830.

[Mihanović et al., 2013] Mihanović, H., Vilibić, I., Carniel, S., Tudor, M., Russo, A., Bergamasco, A., Bubić, N., Ljubešić, Z., Viličić, D., Boldrin, A., Malačič, V., Celio, M., Comici, C., and Raicich, F. (2013). Exceptional dense water formation on the adriatic shelf in the winter of 2012. Ocean Science, 9(3):561–572.

[Mood, 1950] Mood, A. (1950). Introduction to the theory of statistics. Technical report.

[Nelsen, 2021] Nelsen, R. (2021). Kendall tau metric.

[Newton et al., 2002] Newton, E. H. J., Cox, N. J., Baum, C., College, B., Bellocco, R., Institutet, K., Clayton, D., Garrett, J. M., Gregory, A., Hardin, J., Jenkins, S., Lauritsen, J., Long, J. S., Lumley, T., Pagano, M., Rabe-Hesketh, S., Royston, J. P., Ryan, P., Weesie, J., and Wooldridge, J. (2002). Parameters behind nonparametric statistics:
}Kendall's tau, Somers' D and median
}differences. Technical report.

[Olbert et al., 2013] Olbert, A. I., Nash, S., Cunnane, C., and Hartnett, M. (2013). Tide-surge interactions and their effects on total sea levels in Irish coastal waters. Ocean Dynamics, 63(6):599–614.

[Patakamuri and O'Brien, 2021] Patakamuri, S. and O'Brien, N. (2021). Modified Versions of Mann Kendall and Spearman's Rho Trend Tests. R package version 1.6. CRAN. Retrieved from https://CRAN.R-project.org/package=modifiedmk.

[Pawlowicz et al., 2002] Pawlowicz, R., Beardsley, B., and Lentz, S. (2002). Classical tidal harmonic analysis including error estimates in MATLAB using T TIDE $. Technical report.

[Pirazzoli, 1987] Pirazzoli, P. (1987). Recent Sea-Level Changes and Related Engineering Problems in the Lagoon of Venice (Italy). Technical report.

[Pirazzoli and Tomasin, 2002] Pirazzoli, P. A. and Tomasin, A. (2002). Recent Evolution of Surge-Related Events in the Northern Adriatic Area. Technical Report 3.

[Pons et al., 2021] Pons, A., Cristobal-Fransi, E., Vintrò, C., Rius, J., Querol, O., and Vilaplana, J. (2021). An Application of the IFM Method for the Risk Assessment of Financial Instruments. Computational Economics.

[Pugh, 1987] Pugh, D. (1987). Tides, surges, and mean sea-level. J. Wiley.

[Pugh et al., 1980] Pugh, D. T., Mlnstp, P., and Vassie, J. M. (1980). Applications of the joint probability method for extreme sea level computations. Technical Report 2.

[Punta della Dogana, 2016] Punta della Dogana (2016). Punta della Dogana.

[Rapaglia et al., 2010] Rapaglia, J., Ferrarin, C., Zaggia, L., Moore, W. S., Umgiesser, G., Garcia-Solsona, E., Garcia-Orellana, J., and Masqué, P. (2010). Investigation of residence time and groundwater flux in Venice Lagoon: Comparing radium isotope and hydrodynamical models. Journal of Environmental Radioactivity, 101(7):571–581.

[Robinson et al., 1973] Robinson, A. R., Tomasin, A., and Artegiani, A. (1973). Flooding of Venice : Phenomenology and prediction of the Adriatic storm surge. Technical report.

[Sadegh et al., 2017] Sadegh, M., Ragno, E., and AghaKouchak, A. (2017). Multivariate Copula Analysis Toolbox (MvCAT): Describing dependence and underlying uncertainty using a Bayesian framework. Water Resources Research, 53(6):5166–5183.

[Salvadori et al., 2007] Salvadori, G., De Michele, C., Nathabandu, T. K., and Rosso, R. (2007). Extremes in Nature. Technical report.

[Santamaria-Aguilar and Vafeidis, 2018] Santamaria-Aguilar, S. and Vafeidis, A. T. (2018). Are Extreme Skew Surges Independent of High Water Levels in a Mixed Semidiurnal Tidal Regime? Journal of Geophysical Research: Oceans, 123(12):8877–8886.

[Schanze et al., 2006] Schanze, J., Zeman, E., and Marsalek, J. (2006). Flood Risk Management. Technical report, Ostrov.

[Schwarz, 1978] Schwarz, G. (1978). Estimating the Dimension of a Model. The Annals of Statistics, 6(2).

[Sen, 1968] Sen, P. K. (1968). Estimates of the Regression Coefficient Based on Kendall's Tau. Journal of the American Statistical Association, 63(324):1379–1389.

[Sklar, 1959] Sklar, A. (1959). Fonctions de Répartition à n Dimensions et Leurs Marges. Publications de l'Institut Statistique de l'Université de Paris, 8:229–231.

[Slakter, 1965] Slakter, M. J. (1965). A Comparison of the Pearson Chi-Square and Kolmogorov Goodness-of-Fit Tests with Respect to Validity. Journal of the American Statistical Association, 60(311):854–858.

[Stallone et al., 2020] Stallone, A., Cicone, A., and Materassi, M. (2020). New insights and best practices for the successful use of Empirical Mode Decomposition, Iterative Filtering and derived algorithms. Scientific Reports, 10(1).

[Stepanov, 2015] Stepanov, A. (2015). On the Kendall Correlation Coefficient.

[Stocker et al., 2013] Stocker, T., D. Qin, G.-K. Plattner, M. Tignor, S.K. Allen, J. Boschung, A. Nauels, Y. Xia, V. Bex, and P.M. Midgley (eds.) (2013). Climate Change 2013: The Physical Science Basis. Contribution of Working Group I to the Fifth Assessment Report of the Intergovernmental Panel on Climate Change. Technical report, IPCC, Cambridge.

[Tawn, 1992] Tawn, J. A. (1992). Estimating Probabilities of Extreme Sea-Levels. Technical Report 1.

[Tomasicchio et al., 2021] Tomasicchio, G. R., Salvadori, G., Lusito, L., Francone, A., Saponieri, A., Leone, E., and De Bartolo, S. (2021). A Statistical Analysis of the Occurrences of Critical Waves and Water Levels for the Management of the Operativity of the MoSE System in the Venice Lagoon. Stochastic Environmental Research and Risk Assessment.

[Tosi, 1995] Tosi, L. (1995). Analysis of actual land subsidence in Venice and its hinterland (Italy) Interreg ITA-SLO TRETAMARA View project Coastal system changes over the Anthropocene: Natural Vs Induced drivers in China and Italy View project. Technical report.

[Tosi et al., 2002] Tosi, L., Carbognin, L., Teatini, P., Strozzi, T., and Wegmüller, U. (2002). Evidence of the present relative land stability of Venice, Italy, from land, sea, and space observations. Geophysical Research Letters, 29(12):3–1.

[Tosi et al., 2018] Tosi, L., Da Lio, C., Teatini, P., and Strozzi, T. (2018). Land subsidence in coastal environments: Knowledge advance in the Venice coastland by TerraSAR-X PSI. Remote Sensing, 10(8).

[Tosi et al., 2013] Tosi, L., Teatini, P., and Strozzi, T. (2013). Natural versus anthropogenic subsidence of Venice. Scientific Reports, 3.

[Tsimplis and Baker, 2000] Tsimplis, M. N. and Baker, T. F. (2000). Sea level drop in the Mediterranean Sea: An indicator of deep water salinity and temperature changes? Geophysical Research Letters, 27(12):1731–1734.

[Tyralis, 2016] Tyralis, H. (2016). HKprocess: Hurst-Kolmogorov Process. R package version 0.1-1. CRAN. Retrieved from https://cran.r-project. org/web/packages/HKprocess/index.html.

[Umgiesser et al., 2021] Umgiesser, G., Bajo, M., Ferrarin, C., Cucco, A., Lionello, P., Zanchettin, D., Papa, A., Tosoni, A., Ferla, M., Coraci, E., Morucci, S., Crosato, F., Bonometto, A., Valentini, A., Orlic, M., Haigh, I. D., Woge Nielsen, J., Bertin, X., Bustorff Fortunato, A., Pérez Gómez, B., Alvarez Fanjul, E., Jourdan, D., Pasquet, A., Mourre, B., Tintoré, J., and Nicholls, R. J. (2021). The prediction of floods in Venice: methods, models and uncertainty.

[van Belle and Hughes, 1984] van Belle, G. and Hughes, J. P. (1984). Nonparametric Tests for Trend in Water Quality. Water Resources Research, 20(1):127–136.

[Van Der Stock, 1897] Van Der Stock, J. (1897). Tides and Tidal Streams in the Indian Archipelago, Batavia.

[van Ravenzwaaij et al., 2018] van Ravenzwaaij, D., Cassey, P., and Brown, S. D. (2018). A simple introduction to Markov Chain Monte–Carlo sampling. Psychonomic Bulletin and Review, 25(1):143–154.

[von Storch, 1999] von Storch, H. (1999). Misuses of Statistical Analysis in Climate Research. Analysis of Climate Variability, pages 11–26.

[Wainwright, 2005] Wainwright, J. T. (2005). Quantitative Risk Management. Technical report.

[Wang et al., 2005] Wang, W., Van Gelder, P. H. A. J. M., and Vrijling, J. K. (2005). Trend and stationarity analysis for streamflow processes of rivers in Western Europe in the 20th century. Technical report.

[Wang, 2008a] Wang, X. L. (2008a). Penalized maximal F test for detecting undocumented mean shift without trend change. Journal of Atmospheric and Oceanic Technology, 25(3):368–384.

[Wang, 2008b] Wang, X. L. (2008b). Penalized maximal F test for detecting undocumented mean shift without trend change. Journal of Atmospheric and Oceanic Technology, 25(3):368–384.

[Wang et al., 2007] Wang, X. L., Wen, Q. H., and Wu, Y. (2007). Penalized maximal t test for detecting undocumented mean change in climate data series. Journal of Applied Meteorology and Climatology, 46(6):916–931.

[WCED, 1987] WCED (1987). Our common future.

[Węglarczyk, 2018] Węglarczyk, S. (2018). Kernel density estimation and its application. ITM Web of Conferences, 23:00037.

[Wöppelmann and Marcos, 2016] Wöppelmann, G. and Marcos, M. (2016). Vertical land motion as a key to understanding sea level change and variability.

[Wu et al., 2007] Wu, Z., Huang, N. E., Long, S. R., and Peng, C.-K. (2007). On the trend, detrending, and variability of nonlinear and nonstationary time series. Technical report.

[Yue and Wang, 2004] Yue, S. and Wang, C. (2004). The Mann-Kendall Test Modified by Effective Sample Size to Detect Trend in Serially Correlated Hydrological Series. Technical report.

[Zanchettin et al., 2021] Zanchettin, D., Bruni, S., Raicich, F., Lionello, P., Adloff, F., Androsov, A., Antonioli, F., Artale, V., Carminati, E., Ferrarin, C., Fofonova, V., Nicholls, R. J., Rubinetti, S., Rubino, A., Sannino, G., Spada, G., Thiéblemont, R., Tsimplis, M., Umgiesser, G., Vignudelli, S., Wöppelmann, G., and Zerbini, S. (2021). Sea-level rise in Venice: Historic and future trends (review article).

[Zerbini et al., 2021] Zerbini, S., Bruni, S., and Raicich, F. (2021). Tide gauge data archaeology provides natural subsidence rates along the coasts of the Po Plain and of the Veneto-Friuli Plain, Italy. Geophysical Journal International, 225(1):253–260.

[Zerbini et al., 2017] Zerbini, S., Raicich, F., Prati, C. M., Bruni, S., Del Conte, S., Errico, M., and Santi, E. (2017). Sea-level change in the Northern Mediterranean Sea from long-period tide gauge time series.

[Zervas et al., 2013] Zervas, C., Gill, S., and Sweet, W. (2013). Estimating Vertical Land Motion from Long-Term Tide Gauge Records National Ocean Service Center for Operational Oceanographic Products and Services. Technical report.

[Zhang et al., 2022] Zhang, H., Jeffrey, S., and Carter, J. (2022). Change point detection and trend analysis for time series. Chinese Journal of Chemical Physics, 35(2):399–406.

[Zhao et al., 2019] Zhao, K., Wulder, M. A., Hu, T., Bright, R., Wu, Q., Qin, H., Li, Y., Toman, E., Mallick, B., Zhang, X., and Brown, M. (2019). Detecting change-point, trend, and seasonality in satellite time series data to track abrupt changes and nonlinear dynamics: A Bayesian ensemble algorithm. Remote Sensing of Environment, 232.